Title
Genetic Interactions Involving Components of the Endosomal Protein Trafficking Machinery

Author
Rodriguez-Fernandez, Imilce de los Angeles

Publication Date
2012

Peer reviewed|Thesis/dissertation

UNIVERSITY OF CALIFORNIA

Los Angeles

Genetic Interactions Involving Components of the Endosomal Protein Trafficking Machinery

A dissertation submitted in partial satisfaction of the

requirements for the degree Doctor of Philosophy

in Human Genetics

by

Imilce de los Angeles Rodriguez-Fernandez

2012

ABSTRACT OF THE DISSERTATION

Physical and Genetic Interactions Involving Components of the

Endosomal Protein Trafficking Machinery

by

Imilce de los Angeles Rodriguez-Fernandez

Doctor of Philosophy in Human Genetics

University of California, Los Angeles, 2012

Professor Esteban C. Dell'Angelica, Chair

The goal of this dissertation is to better understand the endosomal protein trafficking machinery; focusing on the role of the biogenesis of lysosome-related organelles complex-1 (BLOC-1), Adaptor Protein-3 (AP-3), and Rabaptin-5-associated exchange factor for Rab5 (Rabex-5). BLOC-1 is a stable protein complex implicated in protein trafficking between endosomes and lysosome-related organelles (LRO). Mutations in three subunits of BLOC-1 cause Hermansky-Pudlak syndrome (HPS) types 7, 8 and 9, and two of its subunits have been tentatively associated to schizophrenia. A data-mining approach was developed to prioritize over 100 candidate-binding partners for fly and human BLOC-1. The top candidate in the ranking was the Rab GTPase Rab11. Experiments done in *Drosophila melanogaster* revealed a synthetic lethal genetic interaction between Rab11 and Rab32/38; the later encoded by the gene *lightoid*. AP-3

is a stable heterotretameric complex also involved in trafficking between endosomes and LROs. Mutations in one subunit of AP-3 results in HPS type 2. Homologues of AP-3 genes in *Drosophila melanogaster* are involved in pigment granule biogenesis. A large-scale screening was conducted to identify genetic modifier of AP-3 function in the fly eye. Deletions in two regions in chromosome 2 and two regions in chromosome 3 modified the AP-3 mutant g^2 eye pigment color in heterozygous form. Further experiments demonstrated that *Gap69C* and *Atg2* are genetic modifiers of AP-3. Rabex-5 is a guanine nucleotide exchange factor of Rab5, a Rab GTPase important in the early endosome trafficking. To understand Rabex-5 physiological function a reverse genetic approach was undertaken to generate a mutant form of the Rabex-5 encoding gene, *Rbx5*. Homozygous loss-of-function ($Rbx5^{ex1}$) mutant flies displayed a "giant larvae" phenotype and did not survive to adulthood. Mutant larval tissues including the brain and wing imaginal discs displayed growth abnormalities. Rescue experiments suggested that $Rbx5^{ex1}$ adult lethality was due to affecting Rab5 function.

The dissertation of Imilce de los Angeles Rodriguez-Fernandez is approved.

Janet S. Sinsheimer

David E. Krantz

Karen Reue

Esteban C. Dell'Angelica, Committee Chair

University of California, Los Angeles

2012

Para Mamá, Papá y David

TABLE OF CONTENTS

LIST OF TABLES AND FIGURES

Chapter 1

Chapter 2

Chapter 3

Chapter 4

LIST OF ABBREVIATIONS

AP-3:	Adaptor Protein-3
BLOC-1:	Biogenesis of lysosome-related organelles complex-1
Dk:	Deficiency kit
Dpn:	Deadpan
GAP:	GTPase-activating protein
GEF:	Guanine nucleotide exchange factor
GMR:	*glass* multimer reporter
GTP:	guanosine triphosphate
LROs:	lysosome-related organelles
Hoechst:	trihydrochloride, trihydrate
HPS:	Hermansky-Pudlak Syndrome
PBS:	phosphate-buffered saline
PBST:	PBS with 0.4% Triton X-100
Rabex-5:	Rabaptin-5-associated exchange factor for Rab5
Rbx5:	*Rabex-5* gene
NE:	neuroepithelium

NB: neuroblasts

SNARE: soluble *N*-ethylmaleimide-sensitive factor attachment protein receptor

TM6: *TM6B, p^{Xp} Tb^{1}* (*Drosophila* balancer chromosome)

UAS: upstream activation system

Ub: ubiquitin

ACKNOWLEDGEMENTS

During my doctoral studies, I was very lucky to be surrounded by great people, from which I learned a lot and were always there for me, making this thesis possible.

I would like to thank my thesis advisor, Esteban Dell'Angelica for being a great mentor and role-model. He was always willing to teach me new concepts and answer all of my questions, no matter how busy he was. This dissertation would not have been possible without all his support, guidance and motivation. I will always be thankful.

Also, I would like to thank my committee members, Janet S. Sinsheimer, David E. Krantz and Karen Reue, for all their advice and support throughout the years. For always being available to discuss any questions or concerns; and for making me feel part of their own research group.

Many thanks to Julian Martinez-Agosto for all his help during the project presented on Chapter 4, without his constant advice and insight this project would not have been possible. He was always willing to help and teach me new techniques and concepts. Also many thanks to Volker Hartenstein, for his collaboration on the project presented in Chapter 4, I will always be thankful on the training I got and for his many advices.

I would also like to thanks my current and former lab mates, Veronica T. Cheli, Ramin Nazarian, Julia T. Garcia, Diego Hoyle and Frank Lee, for making every day in the lab fun and for all their help. Special thanks to Veronica and Ramin, for their patience, support and motivation while training me, and for the many interesting conversations and jokes.

Many thanks to my family in Puerto Rico, for their love and always being there for me, and for making me feel like I never left. Special thanks to my mom, dad, brothers and sister, for letting me follow my goals in life and for being supportive. Thanks to my in-laws for loving me as a daughter and for their constant support.

I am extremely grateful to my husband, David Hermina, for his love, outstanding support and motivation every day of my doctoral studies. Without him this dissertation would not have been possible.

I want to thank many of the friends I made along the way. Thanks to my "second family" in LA and to all my friends in the Gonda Building, for making my doctoral studies a lot of fun. Thanks to my best friend Desiree Cotto for being an example of dedication, courage and ambition.

Chapter 2 is a reprint of the article: "A Data-mining Approach to rank candidate protein-binding partners – The case of biogenesis of lysosome-related organelles complex-1 (BLOC-1)" by Imilce A. Rodriguez-Fernandez and Esteban C. Dell'Angelica, *J Inherit Metab Dis* 32: 190-203 reproduced with permission from the Society for the Study of Inborn Errors of Metabolism (SSIEM) and Springer. The final publication of this reprint is available at springerlink.com.

This research was supported by the National Institute of Health UCLA Human Genetics Genomic Analysis Training Program (GATP) pre-doctoral training grant, and by the UCLA Dissertation Year fellowship.

VITA

2002-2004	Started B.Sc. in Biology University of Puerto Rico, Ponce Campus Ponce, Puerto Rico
2003-2004	Honor Student Award Department of Biology University of Puerto Rico, Ponce Campus Ponce, Puerto Rico
2004-2006	B.Sc., Microbiology Magna Cum Laude University of Puerto Rico, Mayaguez Campus Mayaguez, Puerto Rico
2007-2011	Pre-doctoral training grant UCLA Human Genetics Genomic Analysis Training Program (GATP)
Winter 2008	Teaching Assistant, Cell and Molecular Biology Laboratory Department of Molecular, Cell and Developmental Biology University of California, Los Angeles
2009	Honorable Mention Status FORD Foundation Diversity Pre-doctoral Fellowships Program, National Academies
Fall 2009	Teaching Assistant, Introduction to Cell Biology Department of Molecular, Cell and Developmental Biology University of California, Los Angeles
2011	Honorable Mention Status FORD Foundation Diversity Dissertation Year Fellowships Program, National Academies
2012	UCLA Dissertation Year Fellowship

PUBLICATIONS

Rodriguez-Fernandez IA, Dell'Angelica EC (2009) A data-mining approach to rank candidate protein-binding partners-The case of biogenesis of lysosome-related organelles complex-1 (BLOC-1). *J Inherit Metab Dis* 32: 190-203.

Ghiani CA*, Starcevic M***, Rodriguez-Fernandez IA**, Nazarian R, Cheli VT, Chan LN, Malvar JS, de Vellis J, Sabatti C, Dell'Angelica EC (2010) The dysbindin-containing complex (BLOC-1) in brain: developmental regulation, interaction with SNARE proteins, and role in neurite outgrowth. *Mol Psychiatry* 15: 204-215. *Equally contributing authors.

Beck JR, **Rodriguez-Fernandez IA**, de Leon JC, Huynh M, Carruthers VB, Morrissette NS, Bradley PJ (2010) A Novel Family of Toxoplasma IMC Proteins Display a Hierarchical Organization and Function in Coordinating Parasite Division. *PLoS Pathog* 6(9): e1001094.

Hoyle DJ, **Rodriguez-Fernandez IA**, Dell'Angelica EC (2011) Functional interactions between OCA2 and the protein complexes BLOC-1, BLOC-2 and AP-3 inferred from epistatic analyses of mouse coat pigmentation. *Pigment Cell and Melanoma Res* 24(2):275-81.

Arboleda VA, Lee H, Parnaik R, Fleming A, Banerjee A, Ferraz-de-Souza B, Délot EC, **Rodriguez-Fernandez IA**, Braslavsky D, Bergadá I, Dell'angelica EC, Nelson SF, Martinez-Agosto JA, Achermann JC, Vilain E. (2012) Mutations in the PCNA-binding domain of CDKN1C cause IMAGe syndrome. *Nature Genet* 44:788-792.

SELECTED PRESENTATIONS

Rodriguez-Fernandez IA, Cheli VT, Dell'Angelica EC. "A data-mining approach to prioritize candidate binding partners of Biogenesis of Lysosome-related Organelles Complex-1 (BLOC-1)". Annual American Society for Cell Biology (ASCB) Meeting. December 13-17, 2008. San Francisco, CA.

Rodriguez-Fernandez IA, Cheli VT, Hoyle DJ and Dell'Angelica EC. "Screening for genetic modifiers of AP-3, a protein complex involved in intracellular protein trafficking and implicated in Hermansky-Pudlak syndrome". 53rd Annual Drosophila Research Conference. March 7-11, 2012. Chicago, IL.

CHAPTER 1

INTRODUCTION

Endosomal protein trafficking

Endocytosis is the process used by eukaryotic cells to internalize portions of the plasma membrane, containing ligand-bound receptors and other proteins, in the form of a vesicle. The cargo within the vesicle is then delivered to a membrane-bound organelle known as early endosomes [1]. Two mechanisms for endocytosis have been described based on the presence and requirement of the scaffolding protein, clathrin. Clathrin-mediated endocytosis is the best characterized type of internalization (Figure 1.1). At the plasma membrane, this process involves the interaction of a receptor intracellular domain with an adaptor protein (i.e. AP-2) that in turn associates with clathrin, forming what is known as a clathrin-coated vesicle (or clathrin-coated vesicle pit). This vesicle is pinched-off the plasma membrane by the protein dynamin, transported by motor proteins and then docked and fused to an aceptor membrane by the action of SNARE (soluble *N*-ethylmaleimide-sensitive factor attachment protein receptor) proteins [2,3]. Non-clathrin-mediated endocytosis is not well understood and in some cases requires the presence of certain microdomains at the plasma membrane known as lipid rafts [1]

Regardless of the type of endocytosis used by the cell, vesicles are transported to early endosomes. In a scenario where signal attenuation at the plasma membrane is needed, a ligand-bound receptor is transported to the late endosome and multivesicular body and finally reaches the lysosome, where it gets degraded. If along this route the receptor is needed again, then from the early endosome gets recycled back to the plasma membrane [1]. Early and late endosomes, multivesicular bodies and lysosomes can be identified in a cell based on their difference in protein composition and, in the case of lysosomes, their acidic luminal pH [4]. Of particular importance is the role of molecular switches belonging to the large family of small GTPases known as Rabs [5]. When active these proteins “label” the membrane of organelles to coordinate

the events involved in the docking and fusion of vesicles. The endosomal protein trafficking results in a highly complex, intertwined network, owing to the constellation of proteins involved at each step. Many of the trafficking routes and machineries are starting to be elucidated.

Recent evidence suggests that endosomal protein trafficking plays a more central role in cell signaling than previously anticipated (reviewed in [1,6,7,8]). The canonical view of the relationship between signaling and endosomal protein trafficking is by signal attenuation of receptors sent to the lysosome for degradation. Interestingly, it has been shown that, at least for EGFR, signaling can propagate even after internalization from a compartment termed as the "signaling endosome" [7]. Thus, not only the endosomal-lysosomal system serves as avenue for trafficking it can also be view as a signaling platform [7]. Mutations in genes encoding endocytic proteins have been identified in human cancer [9,10]. Similar findings have been made, in the fruit fly *Drosophila melanogaster*, where mutations in endocytic genes (termed as endocytic tumor suppressors) resulted in tissue growth abnormalities and adult lethality (reviewed in [11]).

Additional disorders can arise when mutations affect a gene encoding a protein involved in the activity of lysosomes such as when affecting the sphingolipidose β-Glucosidase A (Gaucher disease) or the integral membrane protein LAMP2 (Danon disease) [12] . Similarly, affecting the protein complexes involved in the biogenesis of related compartments known as lysosome-related organelles (LROs) result in a disorder called Hermasky-Pudlak Syndrome (HPS) [12,13]. The identification and study of such human disorders or relevant animal models has provided insight on how the biogenesis of these organelles may occur. Model organisms are important for the implementation of strategies such as forward and reverse genetics, including genetic screenings and epistasis analyses. Information gathered from these strategies may help

elucidate the functions of many genes and their role together in the biogenesis of lysosomes and LROs.

Lysosome-related organelles

LROs comprise a group of heterogenous organelles that provide certain cell types the capacity of performing specialized functions. As their name implies, LROs share some characteristic with lysosomes, such as acidic luminal pH and common membrane proteins [13,14]. In mammalian cells, at least ten different LROs have been identified [4,13]. Some relevant examples of mammalian LROs are: the melanosomes, which synthesize and store the pigment melanin, the platelet dense granules, which are important for platelet aggregation, and the lamellar bodies of type II alveolar epithelial cells, which are important for the storage and secretion of pulmonary surfactant [13]. Interestingly, the melanosomes and platelet dense granules co-exist with conventional lysosomes while other LROs appear to have replaced lysosomes [4]. This suggests that the endosomal protein trafficking machinery for the biogenesis of LROs and lysosome may be shared. These specialized organelles are not unique to mammals. The worm, *Caenorhabditis elegans,* utilizes a type of LRO called the gut granule for fat storage [15]. The fruit fly, *Drosophila melanogaster,* has pigment granules, found inside the pigment cells of each individual unit of the compound eye [16].

Knowledge gained from studying diseases that affect LROs biogenesis, such as Hermasky-Pudlak syndrome (HPS), have helped decipher part of the molecular mechanism for the formation of these organelles [17]. HPS is a rare, Mendelian autosomal disorder characterized by oculocutaneos albinism (resulting from abnormal melanosomes), bleeding

diathesis (caused by absence of platelet dense granules) and, in some patients, pulmonary fibrosis (due to abnormal lamellar bodies) [18,19]. Each HPS type is defined based on the gene found to be mutated. Thus far, there are nine types of HPS with mutations in genes encoding subunits of at least four different protein complexes, known as biogenesis of lysosome-related organelles complex (BLOC)-1, -2, -3 and adaptor protein (AP)-3 [17,20]. Owing to the scope of this dissertation, the role of BLOC-1 and AP-3 in LROs biogenesis is further described.

BLOC-1

BLOC-1 is a stable cytosolic complex composed of eight different subunits, known as dysbindin, pallidin, muted, cappuccino, snapin, BLOC subunit 1 (BLOS1), BLOS2 and BLOS3 (Figure 1.2). Mutations in three human genes encoding the proteins dysbindin, BLOS3 and pallidin result in HPS types 7, 8 and 9, respectively [17,20]. A role of BLOC-1 in the biogenesis of LROs was first proposed based on the coat color phenotype of pallid and muted mice strain, which carry a mutation in the gene encoding pallidin and muted, respectively. These mice strains displayed similar characteristics in abnormal melanosomes and platelet dense granules observed for HPS patients [21]. Five more BLOC-1 deficient mice strains displaying the similar phenotypes have been described (see Table 1.1) (reviewed in [22]). Murine mutations in genes encoding subunits of the other complexes mutated in HPS, BLOC-2, -3 and AP-3, have been studied. Epistasis analyses of double and triple mutant mice deficient in AP-3, BLOC-1, AP-3, BLOC-2 and/or BLOC-3 suggested that, at least for pigmentation, the three BLOCs do not work in a linear pathway and that the interaction between AP-3 and BLOC-1 suggested that these complexes act at least in independent of each other [23,24]. However, BLOC-1 was found to

interact biochemically with AP-3 and BLOC-2 [24]. BLOC-1 is required for sorting of tyrosinase-related protein 1 (Tyrp1), a protein important for melanin biosynthesis, from the early endosome to the melanosome [25]. Another study tested for genetic interactions between alleles resulting in mutations in BLOC-1 and OCA2 (also known as P protein), a protein mutated in oculocutaneous albinism type 2 in humans and found to localize to melanosomes. The findings of this study suggested that OCA2 may require BLOC-1 to exert its biological function [26]. Orthologs of each subunit of BLOC-1 have been found in *Drosophila melanogaster* and *blos1* mutant flies displayed eye pigmentation defects demonstrating a conserved role of BLOC-1 in the biogenesis of fly pigment granules [27].

Two of BLOC-1 subunits, dysbindin and BLOS3, have been tentatively associated to schizophrenia (discussed in [28]). In the brain, BLOC-1 was found to interact with two SNARE proteins, SNAP-25 and Syntaxin-13, which are key regulators of the fusion of intracellular membranes [29]. In addition, BLOC-1 was shown to be important for neurite outgrowth of primary hippocampal neurons suggesting a novel role in neurodevelopment [29]. In flies, BLOC-1 deficiency resulted in abnormal glutamatergic transmission and behavior [27].

The identification of binding partners could lead to a better understanding of the molecular mechanisms in which BLOC-1 is involved. Efforts have been made, particularly through large-scale studies of protein-protein interaction, to identify binding partners of BLOC-1 (reviewed in [30]). Large-scale strategies particularly when the yeast two-hybrid system is used can result in many false-positives. Hundreds of potential binding candidates for human and fly BLOC-1 have been published, making follow-up studies virtually impractical. To address this issue, Chapter 2 of this dissertation discusses the development of a data-mining approach to prioritize candidate binding partners found in the literature for human and fly BLOC-1.

AP-3

AP-3 is a conserved and stable heterotetrameric complex that mediates intracellular protein trafficking to lysosomes in fibroblasts and to LROs in specialized cells (Figure 1.2) [31]. In addition, AP-3 is structurally and functionally related to AP-1, AP-2 and AP-4, which are adaptor complexes involved in intracellular protein trafficking events. The role of AP-3 in the biogenesis of lysosomes and LROs emerged from the efforts of many laboratories using distinct animal models with AP-3 mutations, and from the discovery that mutations in the β3A subunit of AP-3 results in HPS type 2 [31,32,33]. In mice, defects in AP-3 result in two strains called pearl and mocha (Table 1.1) [34,35]. The phenotype displayed in these mice (i.e. hypopigmentation of coat color and eyes), resembles the clinical characteristics of HPS patients. In *Drosophila melanogaster,* four eye pigmentation mutants, *garnet, carmine*, *orange* and *ruby* result from mutations in the gene encoding the δ, μ3, σ3 and β3 subunit of AP-3, respectively (Table1.1) [36,37,38].

Adaptor protein complexes participate in coat assembly and cargo selection, which are important for intracellular protein trafficking across the different membrane-bound compartments. Cargo selection by all AP complexes is achieved by tyrosine- and dileucine-based sorting signals found in the cytoplasmic tail of receptors[39]. AP-3 have been identified to play a role in the transport of tyrosinase (a melanin precursor), to melanosomes in a possible redundant pathway with AP-1 [40]. Tyrosinase interacts with AP-3 through a dileucine-sorting signal [41]. Moreover, a dileucine signal is needed for the interaction between AP-3 and the lysosomal protein LIMP-II [39]. For other lysosomal proteins collectively referred to as Lamps, AP-3 deficiency results in their mislocalization, but further characterization suggest that AP-2, but not the other AP complexes, is required for the delivery of these proteins to the lysosomes [42]. This

exemplifies how different adaptor complexes can selectively control the delivery of proteins to the same organelle, and how the sorting signal is important for cargo selection. Coat assembly requires the interaction with scaffolding proteins such as clathrin. Along this line, AP-3 was shown to interact with clathrin in mammals [43]. Important for both cargo selection and coat assembly is the association of AP-3 to membranes by small GTPases of the ADP-Ribosylation factor (ARF) family [44,45].

Experiments done in flies, have uncovered a potential role of AP-3 in the sorting of the white protein [46]. The white protein, encoded by the *white* gene, is an ABC transporter important for the transport of pigment precursors into the LROs called pigment granules. Misorting of white and other unknown proteins could be in part responsible for the abnormal biogenesis of pigment granules in the eyes of AP-3 mutant flies. Previous evidence from this laboratory, have shown that *Drosophila* serves as a model to help elucidate the mechanism underlying the protein network implicated in the LRO biogenesis by genetic approaches [27,47]. The AP-3 hypomorphic known as g^2, provides a sensitized genetic background that could be use as a tool to identify additional proteins involved in pigment granule biogenesis in a mechanism that could be dependent or independent of the function of AP-3.

Chapter 3 of this dissertation discusses the findings of a screening done in *Drosophila melanogaster* for the identification of genetic modifiers of the function of AP-3 in eye pigmentation.

Rabex-5

Rabaptin-5-associated exchange factor for Rab5 (Rabex-5) is one of the Guanine nucleotide exchange factors (GEF) of Rab5. Rab5 is a small GTPase that has been shown to be the master regulator of early endosomal biogenesis [48]. All Rabs act as molecular switches, by alternating from an inactive, to an active state. The active form is achieved through the action of GEF proteins, which catalyses the exchange of GDP by GTP. Activated Rabs can exert their function by the recruitment of effectors molecules important for many steps of protein trafficking [5].

The specific role of Rabex-5 in endosomes is starting to be deciphered. For instance, it has been described that after Rabex-5 activates Rab5, GTP-bound-Rab5 gets stabilized by a complex formed between Rabex-5 and Rabaptin-5 [49]. It has been shown that Rabex-5 is capable of binding ubiquitin, and that this modification is important for its recruitment to endosomes [50]. Rabex-5 mutant mice (*Rabgef*$^{-/-}$) have been generated. Besides a decreased in pups viability, *Rabgef*$^{-/-}$ adult mice developed a severe skin inflammation and increased number of mast cells [51]. Experiments done in *Rabgef*$^{-/-}$ mast cells showed enhanced levels of degranulation, normally observed during the activation of mast cells. Therefore, Rabex-5 was proposed as a negative regulator of Ras signaling, which is the pathway involved in the activation of these cells [51]. Additional involvement of Rabex-5 in the Ras signaling pathway has been proposed [52,53].

Many questions regarding the functional significance of Rabex-5 remain to be answered. If Rabex-5 is involved in Ras signaling pathway, how come mutant mice displayed only a phenotype in mast cells. A potential compensatory mechanism by other Rab5 GEF could explain the *Rabgef*$^{-/-}$ phenotype. For instance, Rin1, another GEF for Rab5 and also a downstream

effector of Ras [54] could be having functional redundancy with Rabex-5. Another question is whether Rabex-5 has tissue-specific roles provided by its domain architecture.

Chapter 4 focuses on the characterization of a null mutant in *Drosophila* Rabex-5 and provides new insights into the physiological function of Rabex-5.

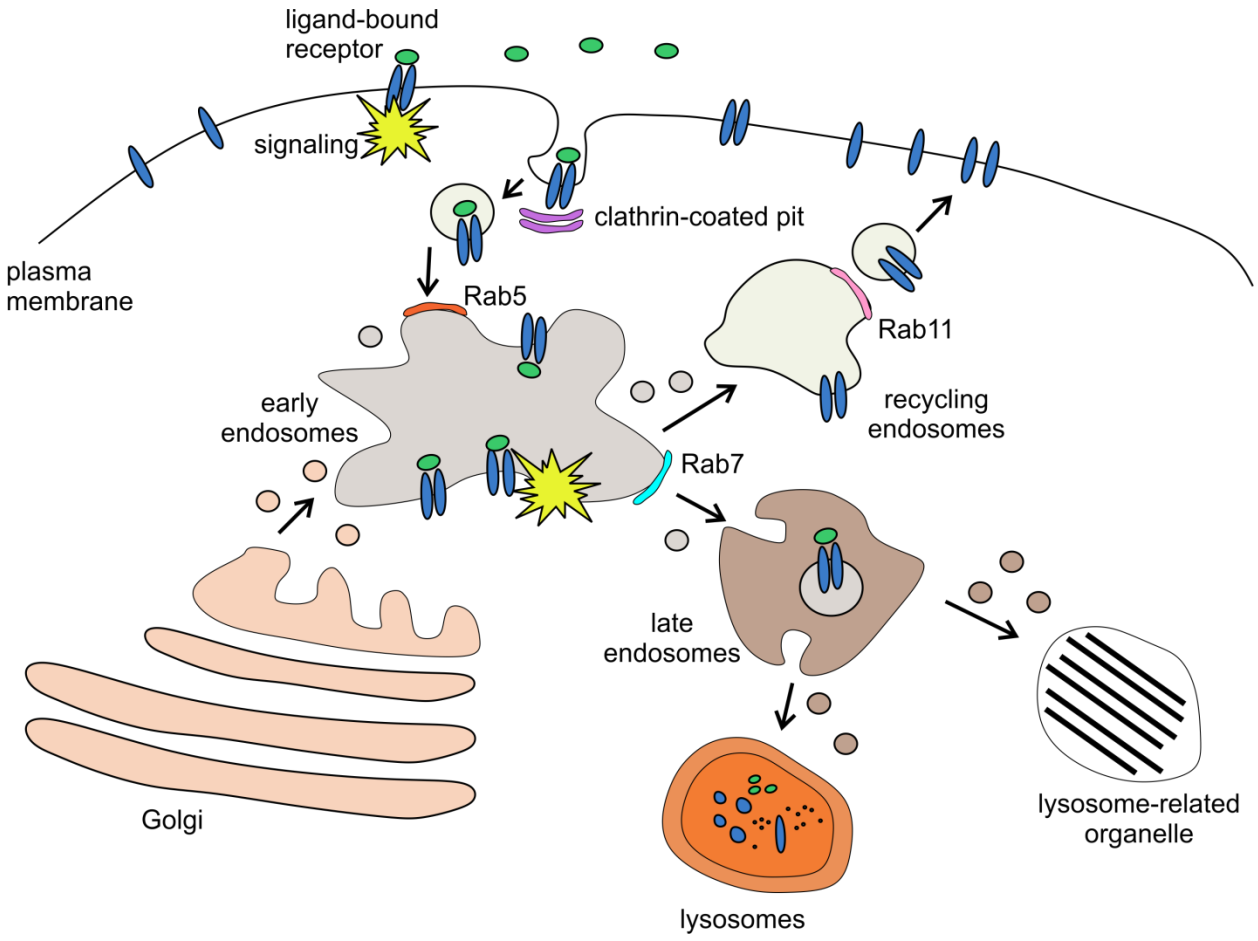

Figure 1.1. Scheme representing clathrin-mediated endocytosis of ligand-bound receptors and protein trafficking across the endosomal-lysosomal system. Clathrin-mediated endocytosis of a ligand-bound receptor involves the invagination of the plasma membrane and the formation of a clathrin-coated pit. This vesicle, containing the ligand-bound receptor as cargo, is docked and fused to the early endosome, sent to the late endosome and the lysosome for degradation. If the receptor is needed again, from the early endosome it is recycled back to the plasma membrane. Signaling can also occur at the endosome. In specialized cells, additional cargo is transported to other compartments such as lysosome-related organelles. Rab GTPases coordinate trafficking events at different compartments. Rab5 and Rab7 are involved in the protein trafficking at the early and late endosome, respectively (shown in red and cyan). Rab11 is involved in trafficking at the recycling endosomes (shown in pink).

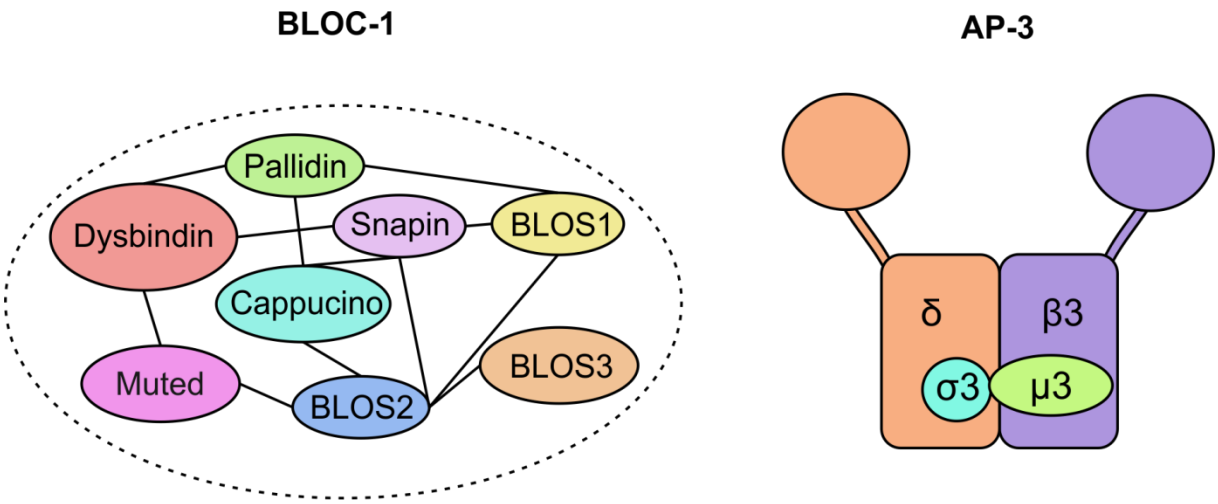

Figure 1.2. Schematic representations of the subunit composition of BLOC-1 and AP-3. BLOC-1 is composed of eight subunits, and shown as black lines are the inter-subunit interactions based on experimental evidence. AP-3 is composed of two large subunits (δ and β3); a medium (μ3) subunit; and a smaller (σ3) subunit.

Table 1.1. Genes encoding BLOC-1 and AP-3 subunits, the resulting HPS type and murine strains when mutated, and its *Drosophila* orthologs.

Protein Complex	Subunit	Human gene(s)	HPS type	Murine Strain	*Drosophila* ortholog
AP-3*	β3A	*AP3B1*	HPS-2	Pearl	*ruby (rb)*
	δ	*AP3D1*	--	Mocha	*garnet (g)*
	μ3A	*AP3M1*	--	--	*carmine (cm)*
	σ3A/ σ3B	*AP3S1/AP3S2*	--	--	*orange (or)*
BLOC-1	Dysbindin	*DTNBP1*	HPS-7	Sandy	*dysbindin*
	Pallidin	*BLOC1S6*	HPS-9	Pallid	*pallidin*
	Muted	*BLOC1S5*	--	Muted	*muted*
	Cappuccino	*BLOC1S4*	--	Cappuccino	*blos4*
	Snapin	*SNAPIN*	--	--	*snapin*
	BLOS1	*BLOC1S1*	--	--	*blos1*
	BLOS2	*BLOC1S2*	--	--	*blos2*
	BLOS3	*BLOC1S3*	HPS-8	Reduced pigmentation	*blos3*

*Ubiquitous form. In brain the β3A and μ3A subunits can be replaced with β3B and μ3B, respectively.

REFERENCES

1. Scita G, Di Fiore PP (2010) The endocytic matrix. Nature 463: 464-473.

2. Raposo G, Marks MS (2007) Melanosomes--dark organelles enlighten endosomal membrane transport. Nat Rev Mol Cell Biol 8: 786-797.

3. Jahn R, Scheller RH (2006) SNAREs--engines for membrane fusion. Nat Rev Mol Cell Biol 7: 631-643.

4. Raposo G, Marks MS, Cutler DF (2007) Lysosome-related organelles: driving post-Golgi compartments into specialisation. Curr Opin Cell Biol 19: 394-401.

5. Stenmark H (2009) Rab GTPases as coordinators of vesicle traffic. Nat Rev Mol Cell Biol 10: 513-525.

6. Miaczynska M, Pelkmans L, Zerial M (2004) Not just a sink: endosomes in control of signal transduction. Curr Opin Cell Biol 16: 400-406.

7. von Zastrow M, Sorkin A (2007) Signaling on the endocytic pathway. Curr Opin Cell Biol 19: 436-445.

8. Sorkin A, von Zastrow M (2009) Endocytosis and signalling: intertwining molecular networks. Nat Rev Mol Cell Biol 10: 609-622.

9. Lanzetti L, Di Fiore PP (2008) Endocytosis and cancer: an 'insider' network with dangerous liaisons. Traffic 9: 2011-2021.

10. Stein MP, Dong J, Wandinger-Ness A (2003) Rab proteins and endocytic trafficking: potential targets for therapeutic intervention. Adv Drug Deliv Rev 55: 1421-1437.

11. Hariharan IK, Bilder D (2006) Regulation of imaginal disc growth by tumor-suppressor genes in Drosophila. Annu Rev Genet 40: 335-361.

12. Futerman AH, van Meer G (2004) The cell biology of lysosomal storage disorders. Nat Rev Mol Cell Biol 5: 554-565.

13. Huizing M, Helip-Wooley A, Westbroek W, Gunay-Aygun M, Gahl WA (2008) Disorders of lysosome-related organelle biogenesis: clinical and molecular genetics. Annu Rev Genomics Hum Genet 9: 359-386.

14. Cutler DF (2002) Introduction: lysosome-related organelles. Semin Cell Dev Biol 13: 261-262.

15. Hermann GJ, Schroeder LK, Hieb CA, Kershner AM, Rabbitts BM, et al. (2005) Genetic analysis of lysosomal trafficking in Caenorhabditis elegans. Mol Biol Cell 16: 3273-3288.

16. Lloyd V, Ramaswami M, Kramer H (1998) Not just pretty eyes: Drosophila eye-colour mutations and lysosomal delivery. Trends Cell Biol 8: 257-259.

17. Di Pietro SM, Dell'Angelica EC (2005) The cell biology of Hermansky-Pudlak syndrome: recent advances. Traffic 6: 525-533.

18. Huizing M, Boissy RE, Gahl WA (2002) Hermansky-Pudlak syndrome: vesicle formation from yeast to man. Pigment Cell Res 15: 405-419.

19. Wei ML (2006) Hermansky-Pudlak syndrome: a disease of protein trafficking and organelle function. Pigment Cell Res 19: 19-42.

20. Cullinane AR, Curry JA, Carmona-Rivera C, Summers CG, Ciccone C, et al. (2011) A BLOC-1 mutation screen reveals that PLDN is mutated in Hermansky-Pudlak Syndrome type 9. Am J Hum Genet 88: 778-787.

21. Falcon-Perez JM, Dell'Angelica EC (2002) The pallidin (Pldn) gene and the role of SNARE proteins in melanosome biogenesis. Pigment Cell Res 15: 82-86.

22. Dell'Angelica EC (2004) The building BLOC(k)s of lysosomes and related organelles. Curr Opin Cell Biol 16: 458-464.

23. Gautam R, Novak EK, Tan J, Wakamatsu K, Ito S, et al. (2006) Interaction of Hermansky-Pudlak Syndrome genes in the regulation of lysosome-related organelles. Traffic 7: 779-792.

24. Di Pietro SM, Falcon-Perez JM, Tenza D, Setty SR, Marks MS, et al. (2006) BLOC-1 interacts with BLOC-2 and the AP-3 complex to facilitate protein trafficking on endosomes. Mol Biol Cell 17: 4027-4038.

25. Setty SR, Tenza D, Truschel ST, Chou E, Sviderskaya EV, et al. (2007) BLOC-1 is required for cargo-specific sorting from vacuolar early endosomes toward lysosome-related organelles. Mol Biol Cell 18: 768-780.

26. Hoyle DJ, Rodriguez-Fernandez IA, Dell'angelica EC (2011) Functional interactions between OCA2 and the protein complexes BLOC-1, BLOC-2, and AP-3 inferred from epistatic analyses of mouse coat pigmentation. Pigment Cell Melanoma Res 24: 275-281.

27. Cheli VT, Daniels RW, Godoy R, Hoyle DJ, Kandachar V, et al. (2010) Genetic modifiers of abnormal organelle biogenesis in a Drosophila model of BLOC-1 deficiency. Hum Mol Genet 19: 861-878.

28. Ghiani CA, Dell'Angelica EC (2011) Dysbindin-containing complexes and their proposed functions in brain: from zero to (too) many in a decade. ASN Neuro 3.

29. Ghiani CA, Starcevic M, Rodriguez-Fernandez IA, Nazarian R, Cheli VT, et al. (2009) The dysbindin-containing complex (BLOC-1) in brain: developmental regulation, interaction with SNARE proteins and role in neurite outgrowth. Mol Psychiatry 15: 115, 204-115.

30. Li W, Feng Y, Hao C, Guo X, Cui Y, et al. (2007) The BLOC interactomes form a network in endosomal transport. J Genet Genomics 34: 669-682.

31. Robinson MS, Bonifacino JS (2001) Adaptor-related proteins. Curr Opin Cell Biol 13: 444-453.

32. Starcevic M, Nazarian R, Dell'Angelica EC (2002) The molecular machinery for the biogenesis of lysosome-related organelles: lessons from Hermansky-Pudlak syndrome. Semin Cell Dev Biol 13: 271-278.

33. Dell'Angelica EC, Shotelersuk V, Aguilar RC, Gahl WA, Bonifacino JS (1999) Altered trafficking of lysosomal proteins in Hermansky-Pudlak syndrome due to mutations in the beta 3A subunit of the AP-3 adaptor. Mol Cell 3: 11-21.

34. Kantheti P, Qiao X, Diaz ME, Peden AA, Meyer GE, et al. (1998) Mutation in AP-3 delta in the mocha mouse links endosomal transport to storage deficiency in platelets, melanosomes, and synaptic vesicles. Neuron 21: 111-122.

35. Feng L, Seymour AB, Jiang S, To A, Peden AA, et al. (1999) The beta3A subunit gene (Ap3b1) of the AP-3 adaptor complex is altered in the mouse hypopigmentation mutant pearl, a model for Hermansky-Pudlak syndrome and night blindness. Hum Mol Genet 8: 323-330.

36. Ooi CE, Moreira JE, Dell'Angelica EC, Poy G, Wassarman DA, et al. (1997) Altered expression of a novel adaptin leads to defective pigment granule biogenesis in the Drosophila eye color mutant garnet. EMBO J 16: 4508-4518.

37. Mullins C, Hartnell LM, Bonifacino JS (2000) Distinct requirements for the AP-3 adaptor complex in pigment granule and synaptic vesicle biogenesis in Drosophila melanogaster. Mol Gen Genet 263: 1003-1014.

38. Mullins C, Hartnell LM, Wassarman DA, Bonifacino JS (1999) Defective expression of the mu3 subunit of the AP-3 adaptor complex in the Drosophila pigmentation mutant carmine. Mol Gen Genet 262: 401-412.

39. Bonifacino JS, Traub LM (2003) Signals for sorting of transmembrane proteins to endosomes and lysosomes. Annu Rev Biochem 72: 395-447.

40. Theos AC, Tenza D, Martina JA, Hurbain I, Peden AA, et al. (2005) Functions of adaptor protein (AP)-3 and AP-1 in tyrosinase sorting from endosomes to melanosomes. Mol Biol Cell 16: 5356-5372.

41. Honing S, Sandoval IV, von Figura K (1998) A di-leucine-based motif in the cytoplasmic tail of LIMP-II and tyrosinase mediates selective binding of AP-3. EMBO J 17: 1304-1314.

42. Janvier K, Bonifacino JS (2005) Role of the endocytic machinery in the sorting of lysosome-associated membrane proteins. Mol Biol Cell 16: 4231-4242.

43. Dell'Angelica EC, Klumperman J, Stoorvogel W, Bonifacino JS (1998) Association of the AP-3 adaptor complex with clathrin. Science 280: 431-434.

44. Ooi CE, Dell'Angelica EC, Bonifacino JS (1998) ADP-Ribosylation factor 1 (ARF1) regulates recruitment of the AP-3 adaptor complex to membranes. J Cell Biol 142: 391-402.

45. Austin C, Boehm M, Tooze SA (2002) Site-specific cross-linking reveals a differential direct interaction of class 1, 2, and 3 ADP-ribosylation factors with adaptor protein complexes 1 and 3. Biochemistry 41: 4669-4677.

46. Lloyd VK, Sinclair DA, Alperyn M, Grigliatti TA (2002) Enhancer of garnet/deltaAP-3 is a cryptic allele of the white gene and identifies the intracellular transport system for the white protein. Genome 45: 296-312.

47. Falcon-Perez JM, Romero-Calderon R, Brooks ES, Krantz DE, Dell'Angelica EC (2007) The Drosophila pigmentation gene pink (p) encodes a homologue of human Hermansky-Pudlak syndrome 5 (HPS5). Traffic 8: 154-168.

48. Zeigerer A, Gilleron J, Bogorad RL, Marsico G, Nonaka H, et al. (2012) Rab5 is necessary for the biogenesis of the endolysosomal system in vivo. Nature 485: 465-470.

49. Lippe R, Miaczynska M, Rybin V, Runge A, Zerial M (2001) Functional synergy between Rab5 effector Rabaptin-5 and exchange factor Rabex-5 when physically associated in a complex. Mol Biol Cell 12: 2219-2228.

50. Mattera R, Tsai YC, Weissman AM, Bonifacino JS (2006) The Rab5 guanine nucleotide exchange factor Rabex-5 binds ubiquitin (Ub) and functions as a Ub ligase through an atypical Ub-interacting motif and a zinc finger domain. J Biol Chem 281: 6874-6883.

51. Tam SY, Tsai M, Snouwaert JN, Kalesnikoff J, Scherrer D, et al. (2004) RabGEF1 is a negative regulator of mast cell activation and skin inflammation. Nat Immunol 5: 844-852.

52. Yan H, Jahanshahi M, Horvath EA, Liu HY, Pfleger CM (2010) Rabex-5 ubiquitin ligase activity restricts Ras signaling to establish pathway homeostasis in Drosophila. Curr Biol 20: 1378-1382.

53. Xu L, Lubkov V, Taylor LJ, Bar-Sagi D (2010) Feedback regulation of Ras signaling by Rabex-5-mediated ubiquitination. Curr Biol 20: 1372-1377.

54. Bliss JM, Venkatesh B, Colicelli J (2006) The RIN family of Ras effectors. Methods Enzymol 407: 335-344.

CHAPTER 2

A DATA-MINING APPROACH TO RANK CANDIDATE PROTEIN-BINDING PARTNERS – THE CASE OF BIOGENESIS OF LYSOSOME-RELATED ORGANELLES COMPLEX-1 (BLOC-1)

Rodriguez-Fernandez IA, Dell'Angelica EC (2009) A data-mining approach to rank candidate protein-binding partners-The case of biogenesis of lysosome-related organelles complex-1 (BLOC-1). *J Inherit Metab Dis* 32: 190-203.

J Inherit Metab Dis (2009) 32:190–203
DOI 10.1007/s10545-008-1014-7

SSIEM SYMPOSIUM 2008

A data-mining approach to rank candidate protein-binding partners—The case of biogenesis of lysosome-related organelles complex-1 (BLOC-1)

I. A. Rodriguez-Fernandez · E. C. Dell'Angelica

Received: 21 July 2008 / Submitted in revised form: 19 September 2008 / Accepted: 23 September 2008 /
Published online: 12 December 2008

Summary The study of protein–protein interactions is a powerful approach to uncovering the molecular function of gene products associated with human disease. Protein–protein interaction data are accumulating at an unprecedented pace owing to interactomics projects, although it has been recognized that a significant fraction of these data likely represents false positives. During our studies of biogenesis of lysosome-related organelles complex-1 (BLOC-1), a protein complex involved in protein trafficking and containing the products of genes mutated in Hermansky–Pudlak syndrome, we faced the problem of having too many candidate binding partners to pursue experimentally. In this work, we have explored ways of efficiently gathering high-quality information about candidate binding partners and presenting the information in a visually friendly manner. We applied the approach to rank 70 candidate binding partners of human BLOC-1 and 102 candidates of its counterpart from *Drosophila melanogaster*. The top candidate for human BLOC-1 was the small GTPase encoded by the *RAB11A* gene, which is a paralogue of the Rab38 and Rab32 proteins in mammals and the *lightoid* gene product in flies. Interestingly, genetic analyses in *D. melanogaster* uncovered a synthetic sick/lethal interaction between *Rab11* and *lightoid*. The data-mining approach described herein can be customized to study candidate binding partners for other proteins or possibly candidates derived from other types of 'omics' data.

Communicating editor: Markus Grompe

Competing interests: None declared

References to electronic databases: Hermansky–Pudlak syndrome: OMIM #203300; Dystrobrevin-binding protein 1 (*DTNBP1*): OMIM #607145. Biogenesis of lysosome-related organelles complex 1 subunit 3 (*BLOC1S3*): OMIM #609762. Alliance for Cell Signaling: http://www.afcs.org. Drosophila Interactions Database: http://www.droidb.org. Entrez Gene (NCBI): http://www.ncbi.nlm.nih.gov/sites/entrez?db=gene. Saccharomyces Genome Database: http://www.yeastgenome.org/. Human Protein Reference Database (HPRD): http://www.hprd.org/. BLAST (NCBI): http://blast.ncbi.nlm.nih.gov/Blast.cgi. Network Protein Sequence Analysis Tools server: http://npsa-pbil.ibcp.fr/cgi-bin/npsa_automat.pl?page=/NPSA/npsa_server.html.

Presented at the Annual Symposium of the SSIEM, Lisbon, Portugal, 2–5 September 2008

Electronic supplementary material The online version of this article (doi:10.1007/s10545-008-1014-7) contains supplementary material, which is available to authorized users.

I. A. Rodriguez-Fernandez · E. C. Dell'Angelica
Department of Human Genetics,
David Geffen School of Medicine, University of California,
Los Angeles, California, USA

E. C. Dell'Angelica (✉)
Department of Human Genetics,
David Geffen School of Medicine at UCLA,
Gonda Center, Room 6357B,
Los Angeles, CA 90095, USA
e-mail: edellangelica@mednet.ucla.edu

Abbreviations

AP-3	adaptor protein-3
BLOC	biogenesis of lysosome-related organelles complex
BLOS	BLOC subunit
HPRD	Human Protein Reference Database
HPS	Hermansky–Pudlak syndrome

NCBI National Center for Biotechnology Information
Y2H yeast two hybrid

Introduction

The postgenomic era is witnessing a blossoming of so-called systems-biology 'omics' approaches to understand the function of genes through studies on their products (transcripts and/or proteins) on an unprecedentedly large scale. Among them are the 'interactomics' approaches aimed at elucidating the network of protein–protein interactions that occur *in vivo* (Gandhi et al 2006; von Mering et al 2002). Considering the extensive success in understanding the molecular function of proteins through the study of individual protein–protein interactions, the expectation for the impact of the field in interactomics to biology—and eventually to medicine—is very high.

However, at least two main drawbacks have been recognized. First, intrinsic limitations of each interactomics approach can result in large numbers of false-negative and false-positive results. While the problem of false negatives tends to be minimized because negative results are typically not reported, one must consider that not all positive interactions being reported will turn out to be 'real' (i.e. to occur *in vivo* and be of biological significance). In the case of the yeast two-hybrid (Y2H) system, which so far has been the method most extensively used to study the interactomes of organisms other than yeast, false-positive rates of 50% or higher have been estimated (Deane et al 2002). Consequently, follow-up experimentation is always required to validate interactions of interest. The second drawback, which is common to other systems-biology approaches, is the potential of 'data overload' caused by an unprecedented wealth of experimental observations. This has led to a proliferation of successful bioinformatics strategies to filter, organize and extract useful information from the experimental data (Camargo et al 2007; Gandhi et al 2006; Giot et al 2003; Rual et al 2005; Stelzl et al 2005; von Mering et al 2002).

We have recently faced a combination of the two problems mentioned above, i.e. having to pursue experimentally too many candidate binding partners resulting from Y2H projects, during our studies on biogenesis of lysosome-related organelles complex-1 (BLOC-1). BLOC-1 is a stable protein complex that in mammals comprises eight known subunits: pallidin, muted, cappuccino, dysbindin, snapin, BLOC subunit 1 (BLOS1), BLOS2 and BLOS3 (Fig. 1A; for a recent review see Raposo and Marks 2007). Mutations in the *DTNBP1* gene encoding dysbindin and the *BLOC1S3* gene encoding BLOS3 cause Hermansky–Pudlak

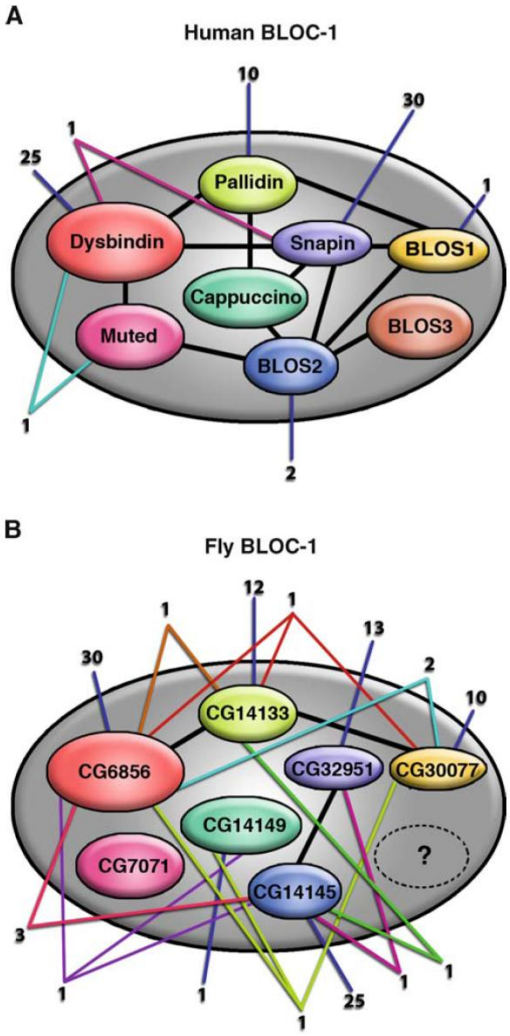

Fig. 1 Schematic representations of the subunit composition of BLOC-1 from humans (**A**) and the corresponding orthologues encoded by the genome of *Drosophila melanogaster* (**B**). Thick black lines denote published experimental evidence for binary inter-subunit interactions. Numbers connected by blue lines represent unique binding partners described for individual BLOC-1 subunits, and numbers connected by lines of other colour denote candidate binding partners shared by two or more subunits

syndrome (HPS) type 7 (HPS-7) and HPS-8, respectively (Li et al 2003; Morgan et al 2006). All types of HPS, including the two associated with BLOC-1 deficiency, follow an autosomal-recessive mode of inheritance and are characterized by partial loss of pigmentation in hair, skin and eyes (i.e. oculocutaneous albinism) and prolonged bleeding times due to platelet storage pool deficiency (reviewed by Wei 2006). Both clinical manifestations arise from defects in the biogenesis of so-called 'lysosome-related' organelles, namely melanosomes and platelet dense granules (Raposo and Marks 2007). The other known types of HPS are associated with deficiencies in another three protein complexes: HPS-3, -5 and -6 are due to mutations in the *HPS3*, *HPS5* and *HPS6* genes encoding subunits of BLOC-2; HPS-1 and -4 diseases arise from mutations in the *HPS1* and *HPS4* genes encoding subunits of BLOC-3; and HPS-2 is due to mutations in the *AP3B1* gene encoding a subunit of adaptor protein-3 (AP-3) (Di Pietro and Dell'Angelica 2005; Wei 2006). While the molecular role of AP-3 as a sorting-signal-decoding device mediating intracellular protein trafficking between endosomes and lysosomes (or between endosomes and lysosome-related organelles) is well established, the molecular functions of the BLOCs remain poorly understood (Di Pietro and Dell'Angelica 2005; Raposo and Marks 2007). Nevertheless, BLOC-1 was localized in melanocytes to early-endosome-associated tubules and found to facilitate the trafficking of tyrosinase-related protein 1 and the Menkes disease protein, ATP7A, to maturing melanosomes (Di Pietro et al 2006; Setty et al 2007, 2008).

As part of our efforts aimed at elucidating the molecular mechanism of BLOC-1 function, we have focused our attention on direct protein–protein interactions reported in the literature, either as the focus of individual studies (reviewed by Li et al 2007; see also Bao et al 2008; Felten et al 2007; Granata et al 2008; Mistry et al 2007; Nian et al 2007; Sun et al 2008; Suzuki et al 2007) or as part of large sets of interactomics data (Camargo et al 2007; Rual et al 2005; Stelzl et al 2005). In all of these cases, the initial—or only—experimental evidence was obtained by Y2H analysis. In the case of human BLOC-1, the number of candidate binding partners for one or more of its subunits added up to 70 (Fig. 1A). The existence of a BLOC-1 counterpart in the fruit fly, *Drosophila melanogaster*, was predicted by the presence in its genome of recognizable orthologues for seven of the eight subunits of the mammalian complex (Falcón-Pérez et al 2007); for the products of these seven fly genes the total number of candidate binding partners derived from large-scale Y2H analyses (Formstecher et al 2005; Giot et al 2003) was 102 (Fig. 1B). No homologues of BLOC-1 subunits have been found in the genome of the yeast *Saccharomyces cerevisiae*.

The above numbers of candidate binding partners for human and *Drosophila* BLOC-1 would exceed our ability to pursue them experimentally, especially if one considers that multiple approaches would be required to test whether each putative interaction might occur *in vivo* and be relevant to the function of BLOC-1 in intracellular protein trafficking. Various methods have been described to assess the reliability of interactions within large sets of Y2H data (Deane et al 2002; Goldberg and Roth 2003), or to attempt to reduce the very high false-positive rates (~90%) of *in silico* predictions of protein–protein interactions (Mahdavi and Lin 2007; Scott and Barton 2007). These methods were designed to assess simultaneously thousands of putative interactions; hence they rely on either global properties of the dataset (e.g. small-world network properties) or scoring criteria that tend to be simplistic as they are restricted to information that can be gathered automatically (e.g. co-occurrence of keywords in GeneOntology descriptions, existence of paralogues reported to interact with each other).

In this work, we explored ways to efficiently gather high-quality information about the candidate binding partners of BLOC-1 subunits from humans and flies, and to rank the candidates and present the information in a visually friendly manner. For the top candidate resulting from this analysis, the endosomal Ras-related GTPase Rab11, follow-up experimental work uncovered an unexpected genetic interaction with the product of the fly gene *lightoid*, which is the orthologue of the *Ruby* gene defective in a rat model of HPS (Oiso et al 2004) and encodes a Rab protein implicated in the biogenesis of lysosome-related organelles (Ma et al 2004; Wasmeier et al 2006). The possibility of applying a similar data-mining approach to analysis of other subsets of 'omics' data is discussed.

Methods

Literature and database searches

Literature searches for candidate binding partners of human BLOC-1 were performed by using all alternative names of each BLOC-1 subunit as keywords in PubMed (http://www.pubmed.gov) and subsequently browsing the abstracts of all resulting papers. In addition, the supplementary materials of four papers reporting large-scale human protein–protein interaction studies (Camargo et al 2007; Ewing et al 2007;

Rual et al 2005; Stelzl et al 2005) and a publicly available database of Y2H data generated by the Alliance for Cell Signaling (http://www.afcs.org) were searched using the subunit names as keywords. Candidate binding partners for BLOC-1 subunits from *D. melanogaster* were identified by searching the Drosophila Interactions Database (http://www.droidb.org) using the names of subunit-encoding genes (Fig. 1B). Information about official gene symbol, chromosome number, protein name and reported or proposed function was gathered from the Entrez Gene database at the National Center for Biotechnology Information (NCBI) (http://www.ncbi.nlm.nih.gov/sites/entrez?db=gene). Patterns of gene expression were inferred from the analysis of Expression Sequence Tag counts available through the NCBI UniGene database (http://ncbi.nlm.nih.gov/UniGene/). Information about reported or proposed functions for S. cerevisiae orthologues was obtained from the Saccharomyces Genome Database (http://www.yeastgenome.org/). When available, information about the presence in human proteins of regions with predicted propensity to adopt coiled-coil folds or transmembrane domains was gathered from the Human Protein Reference Database (HPRD) (http://www.hprd.org/) (Mishra et al 2006).

Protein sequence analyses

Sequence analyses of candidate binding partners were carried out using the reference amino acid sequences downloaded from the NCBI Entrez Gene database; if more than one isoform were predicted (owing to alternative splicing of the encoding gene), the longest protein sequence was used. Homology searchers for readily recognizable orthologues in *D. melanogaster* and *S. cerevisiae* (for human proteins) or in *H. sapiens* and *S. cerevisiae* (for fly proteins) from the non-redundant protein sequence database were carried out using the Gapped-BLASTP algorithm (Altschul et al 1997) with default parameters as available at the NCBI website (http://blast.ncbi.nlm.nih.gov/Blast.cgi). Information about predicted functional domains was obtained from the conserved-domain search tool available at NCBI as part of the BLASTP server. In the cases of *Drosophila* proteins, or of human proteins where no predictions of coiled-coil or transmembrane regions were available at the HPRD, predictions of such regions were carried out at the Network Protein Sequence Analysis Tools server (http://npsa-pbil.ibcp.fr/cgi-bin/npsa_automat.pl?page=/NPSA/npsa_server.html) using default parameters (Combet et al 2000).

Candidate ranking

The information gathered about candidate binding partners of BLOC-1 subunits was organized in a table using Microsoft Excel 2004 for Mac Version 11.2, where each row represented a candidate binding partner and the columns corresponded to various scoring criteria. A colour-code was adopted whereby green, yellow and red at each column position represented 'encouraging', 'less encouraging' or 'discouraging' information about the candidate, respectively. White was used to denote lack of information or information that was too general to be considered either encouraging or discouraging. Further details about the colour-based scoring system are available in Supplementary Table 1. In order to rank the candidates, the colour code was converted into numerical values using a custom-made Macro tool (available upon request), and the sum of all derived values was calculated for each row and used to sort the rows (in descending order) using the Data AutoFilter tool of Excel.

Genetic experiments in flies

Flies were reared at 25°C in a designated room with automatic 12 h light/12 h dark cycles, using standard food and following conventional fly husbandry procedures (Greenspan 1997). The following *D. melanogaster* lines were obtained from the Bloomington *Drosophila* Stock Center at Indiana University (Bloomington, IN, USA): $y^2wy^2g^2$ (stock 192), ltd^1 (stock 338) and y^1w^*; $P\{w^{+mC}=lacW\}Rab11^{j2D1}/TM3$, Sb^1 (stock 12148). Wild-type Canton-S flies and lines carrying the modified chromosome *FM7* as well as the chromosome balancers *CyO* and *TM3*, Sb^1 were kind gifts from David E. Krantz (University of California, Los Angeles, CA, USA). The g^2 line was derived from $y^2wy^2g^2$ by multiple outcrosses into Canton-S and was kindly provided by Anne F. Simon (University of California, Los Angeles, CA, USA). For some experiments, the ltd^1 line was partially 'cantonized' by three outcrosses into the genetic background of Canton-S.

Results

Ranking of candidate binding partners of human BLOC-1 subunits

Literature and databases searches for candidate binding partners of BLOC-1 resulted in a total of 68 gene

products reported to interact with individual subunits, and two gene products reported to interact with dysbindin and another subunit (Fig. 1A). Twenty-seven of these candidates resulted from small-scale Y2H screenings (reviewed by Li et al 2007; see also Bao et al 2008; Felten et al 2007; Granata et al 2008; Mistry et al 2007; Nian et al 2007; Sun et al 2008; Suzuki et al 2007), while the rest of them were found as part of large-scale Y2H projects (Camargo et al 2007; Rual et al 2005; Stelzl et al 2005; no candidates were found in a large-scale mass spectrometry study reported by Ewing et al 2007). In order to select the most promising candidates for experimental analyses, we sought to rank them according to a number of specific criteria that would be relevant to the likelihood that a given candidate would interact with BLOC-1 *in vivo* and participate in its role in intracellular protein trafficking between endosomes, lysosomes and related organelles. Because none of these criteria would constitute an absolute requirement for a candidate to be considered further, we reasoned that the combination of all criteria (i.e. the sum of all scores) would represent our best estimate of how promising each candidate would be. To allow for rapid visual analysis, for each criterion we used green and red colour to represent 'encouraging' or 'discouraging' information, respectively; yellow was used to represent information that was not as encouraging as that labelled with green, and white was used to represent lack of information or information that was too vague to be considered either encouraging or discouraging (see Supplementary Table 1 for details about the colour code for each criterion).

Ten different criteria were applied to prioritize candidate binding partners of human BLOC-1 subunits (Fig. 2). The first three corresponded to experimental evidence found in the original article describing an interaction between a BLOC-1 subunit and a given candidate gene. The criteria were based on three commonly used types of protein–protein interaction assays: Y2H data, affinity-pulldown assay, and co-immunoprecipitation. The Y2H data were considered encouraging (i.e. green colour) if resulting from a small-scale screening (assuming that the authors had a valid reason to select a given interaction partner out of several prey constructs that might have led to expression of reporter genes) or if deemed to be of high confidence by a large-scale Y2H project. The affinity-pulldown data were considered most encouraging if a recombinant form of the binding partner was able to pull-down the native BLOC-1, not just an isolated subunit in recombinant form or overexpressed in cells by transfection. Likewise, the co-immunoprecipitation data were considered most encouraging if involving native BLOC-1 as opposed to a transiently overexpressed subunit. Such stringency level for these two criteria, i.e. considering most encouraging only those positive pulldown and co-immunoprecipitation results involving the entire BLOC-1 complex, stemmed from our own study (Nazarian et al 2006) on the previously reported interaction of the dysbindin subunit of BLOC-1 with α- and β-dystrobrevins (Benson et al 2001). In that study, we had found that dysbindin can interact with the dystrobrevins when isolated from the complex (i.e. in the context of the Y2H or in recombinant form) but not in the context of native BLOC-1, likely because the region of dysbindin that can bind dystrobrevins *in vitro* is engaged in multiple inter-subunit interactions within BLOC-1 and not available for dystrobrevin binding *in vivo* (Nazarian et al 2006). Although immunofluorescence co-localization is another criterion often used to validate protein–protein interactions, inspection of the relevant literature led us to exclude it from our analyses. This is because BLOC-1 subunits have been reported to 'co-localize' with various binding partners at dissimilar locations such as the plasma membrane (Benson et al 2001, 2004), cytoplasm (Fukui et al 2005), both plasma membrane and cytoplasm (Mistry et al 2007; Yuan et al 2006), the perinuclear region (Rüder et al 2005), the Golgi complex (Wolff et al 2006) and even inside nuclei (Felten et al 2007; Nian et al 2007).

The information for scoring criteria 4–10 was obtained from databases and, upon initial training, could be gathered at a rate of ~6 min per candidate. Criteria 4 and 5 corresponded to the prediction of coiled-coil-forming and transmembrane regions, respectively, and high-quality information was found readily available at HPRD for most human proteins. Coiled-coil-forming regions are involved in protein–protein interactions but are also notorious for their tendency to give false-positive results in the Y2H system. Because all BLOC-1 subunits except for BLOS3 (for which no candidate binding partner has been described) contain coiled-coil-forming domains, we decided that not finding these regions in the candidate binding partners would be encouraging and finding them would be discouraging. Similarly, for transmembrane regions we decided to consider their presence discouraging, in part because of concerns about false positives in the Y2H and the expectation that, by analogy to well-known membrane trafficking pathways, most components of the pathway in which BLOC-1 functions will turn out to be peripheral membrane proteins. Criterion 6 was based on information about structural or functional domains

predicted for the candidate binding partners. Here, conserved functional domains specifically related to protein/membrane trafficking, also known as vesicle-mediated trafficking, were considered most encouraging. Criterion 7 was based on mRNA expression patterns as inferred from 'virtual dot blots' available at the UniGene database. Because all BLOC-1 subunits are expressed ubiquitously (reviewed by Di Pietro and Dell'Angelica 2005; Wei 2006) and evidence for a role of BLOC-1 in protein trafficking within non-specialized cells has been obtained (Di Pietro et al 2006; Salazar et al 2006), detection of the candidate's transcript in a wide variety of tissues and cell types was considered most encouraging. Criteria 8 and 9 were based on the ability to detect homologues of the candidate binding partner in *D. melanogaster* and *S. cerevisiae*, respectively. Because BLOC-1 subunit orthologues can be found in the former but not in the latter, we scored as most encouraging detecting a homologue of the human candidate binding partner in *D. melanogaster* (with E-value $<10^{-4}$) and not finding it in *S. cerevisiae*. For the sake of time, the search for homologues was carried out in a single BLASTP round using the non-redundant protein sequence database, and subsequently using an in-built tool to restrict the viewing of results to proteins from the only two species of interest. If a homologue was found in *S. cerevisiae* through the BLASTP search, information about its potential function was gathered from the *Saccharomyces* Genome Database, and if it was related to protein trafficking the result was considered less encouraging (yellow) than not finding such a homologue (green) but more than finding a homologue with an unrelated function (red).

The final criterion was based on the functions reported or proposed for the candidates. We first performed a pilot analysis focusing on over a dozen

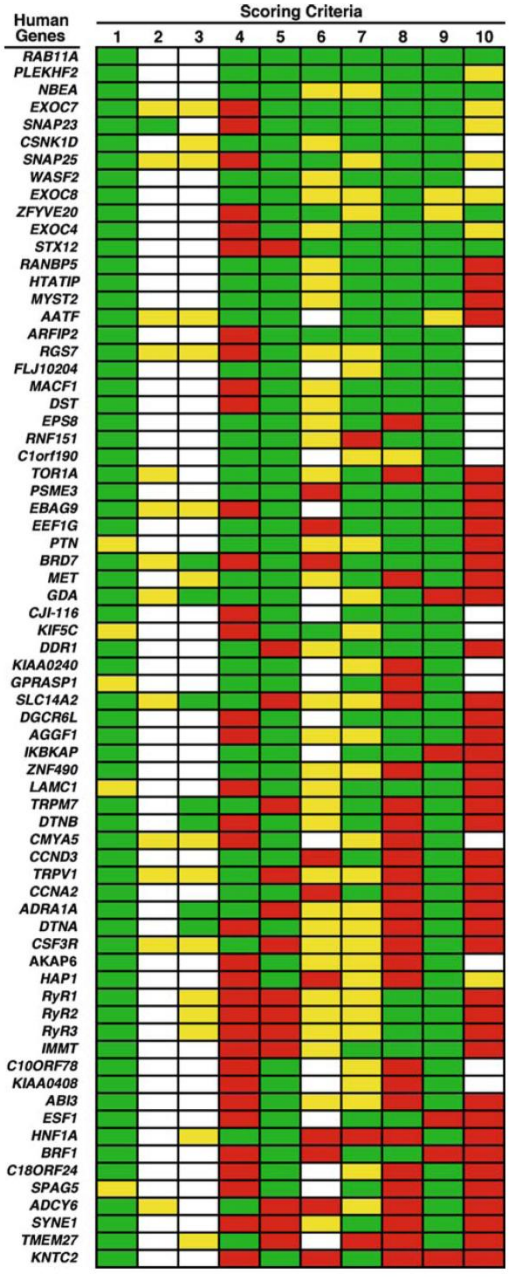

Fig. 2 Ranking of candidate binding partners for human BLOC-1 subunits. Candidates are listed using the official names of the encoding human genes, with the top position in the list representing the first place in the ranking. Scoring criteria: 1, confidence level on the Y2H interaction (*green* is for high confidence in a large-scale Y2H project or isolated from an small-scale Y2H screen); 2, interaction detected by affinity pulldown (*green* is for a positive result obtained using native BLOC-1); 3, interaction detected by co-immunoprecipitation (*green* is for a positive result obtained using native BLOC-1); 4, predicted regions with propensity to fold into coiled-coils (*green* is for their absence from candidate); 5, predicted transmembrane regions (*green* is for their absence from candidate); 6, predicted functional domains (*green* is for the prediction of at least one domain previously implicated in protein/membrane trafficking); 7, expression pattern (*green* is for ubiquitous expression); 8, homology to fruit fly proteins (*green* is for the presence of a recognizable orthologue encoded by the genome of *D. melanogaster*); 9, homology to yeast proteins (*green* is for failure to detect a clearly recognizable homologue encoded by the genome of *S. cerevisiae*); 10, proposed biological function (*green* is for a role in protein/membrane trafficking on endosomes or lysosomes)

candidates, for which the original literature was scanned and read either completely or, in cases with too many original research articles, through a selection of recent reviews. The collected information was then used as a reference to assess the potential quality of functional information readily available in various databases. Although our analysis was neither quantitative nor extensive enough to provide a definitive comparison of the quality of different databases, in our opinion it was the combination of the Summary sections in the NCBI Entrez Gene database and the GeneOntology terms (also available from the same database) that more efficiently captured the information on what is known or predicted about the function of most human proteins analysed. We considered most encouraging those descriptions about a function in protein/membrane trafficking (or vesicle-meditated protein transport) with reference to endosomes or lysosomes, less encouraging similar descriptions without specific references to endosomes or lysosomes, and discouraging those descriptions about unrelated functions such as transcription or translation.

In order to rank the candidates, the colour code was converted into numerical values using a rather simple rule: green=+2, yellow=+1, white=0 and red=−1. The only exception was the criterion 10, for which the above values were doubled (green=+4, yellow=+2, white=0, red=−2) to give extra weight to the information gathered about the candidate's function. As mentioned above, two of the candidates (CK1δ and β-dystrobrevin) had been reported to interact with more than one BLOC-1 subunit (Benson et al 2001; Li et al 2003; Wolff et al 2006; Yin et al 2006). Although we first considered the possibility of giving extra weight to candidates interacting with multiple BLOC-1 subunits, we also gave consideration to a counterargument whereby these multiple interactions could reflect a tendency of 'sticky' proteins to give multiple false positives. Hence, we adopted the conservative approach of giving to the candidate only the best of the two scores obtained when analysed with each interacting BLOC-1 subunit separately. The resulting ranking is shown in Fig. 2, and additional information is provided in Supplementary Table 2. At the top of the ranking is the product of the *RAB11A* gene, which is a small GTPase of the Rab family of Ras-related proteins. In particular, the *RAB11A* gene product, Rab11, is associated with recycling of endosomes and has been shown to play key roles in protein and membrane trafficking events during development (Alone et al 2005; Giansanti et al 2007; Pelissier et al 2003; Prekeris et al 2000; Riggs et al 2003; Ullrich et al 1996). Rab11 is also a paralogue of Rab38 and Rab32, which are two highly related Rab family members with restricted expression and roles in the biogenesis of melanosomes (Wasmeier et al 2006). At second and third places are the proteins phafin 2 and neurobeachin, respectively. Fourth in the ranking is the product of the *EXO70* gene, which is a subunit of the exocyst complex implicated in the 'tethering' of exocytic vesicles at specific sites of the plasma membrane (reviewed by Munson and Novick 2006). Interestingly, another two subunits of the exocyst, encoded by the *EXOC8* and *EXOC4* genes, had also been reported to interact with BLOC-1 subunits in large-scale Y2H projects and herein ranked at the 9th and 11th places, respectively (Fig. 2 and Supplementary Table 2).

Ranking of candidate binding partners of subunits of *Drosophila* BLOC-1

We next sought to apply our ranking approach to candidate binding partners from a different species: the fruit fly *D. melanogaster*. Here, all interactions but two were derived from a large-scale Y2H study reported by Giot and colleagues (2003), which also observed three of the several inter-subunit interactions observed for human BLOC-1 (Starcevic and Dell'Angelica 2004) (Fig. 1A, B, *black lines*). Ninety-one gene products were reported to interact with a single BLOC-1 subunit, while 11 gene products were found to interact with two or three subunits (Fig. 1B). Although few of these interactions were deemed to be of high confidence according to an automatic scoring system (Giot et al 2003), careful examination of small subsets of interactions derived from large Y2H projects has revealed that even those interactions deemed to be of 'low confidence' in individual datasets might turn out to be real and should not be dismissed (Gandhi et al 2006). Consequently, all candidates were included in our analysis.

We used similar scoring criteria to those described above for the human candidate binding proteins, except for the following differences. First, since the only experimental evidence for interaction of the *Drosophila* proteins was derived from Y2H analysis, the criteria based on affinity-pulldown and co-immunoprecipitation assays were irrelevant and were not used. Second, given that reliable predictions of coiled-coil-forming and transmembrane domains were not readily available for *Drosophila* proteins (as they were in HPRD for human proteins), we ran such predictions using the Network Protein Sequence Analysis Tools server. Third, no criterion based on patterns of mRNA expression was used because the available data on the

expression of BLOC-1 subunits in *D. melanogaster* were sparse and not very consistent. Fourth, by analogy with the criterion that finding *Drosophila* homologues of human candidate binding proteins would be encouraging, we considered encouraging finding a human homologue of a fly candidate binding partner through a simple BLASTP search (with E-value $<10^{-4}$). Finally, given that the information gathered about the function of fly proteins was more limited than that of human proteins, instead of doubling the numerical weight of this criterion we added one more based on the function reported or proposed for the human homologue, if any, and then applied the same simple conversion rule (green = +2, yellow = +1, white = 0 and red = −1) to all criteria.

The resulting ranking of candidate binding partners of *Drosophila* BLOC-1 subunits is shown in Fig. 3, and further details are listed in Supplementary Table 3. There were virtually no common binding partners for human and fly BLOC-1, which is not entirely surprising given the well-documented lack of overlap between interactomic data obtained for different species—or even for the same species—by different projects (reviewed by Gandhi et al 2006). However, ranked at the 7th place was the product of the *CG2095* gene (Fig. 3), which is a subunit of the exocyst complex from flies and the orthologue of the human *EXOC4* gene product that was ranked 11th among the human candidates (Fig. 2).

Genetic interactions in flies

We next attempted to pursue experimentally the top candidate binding partner of human BLOC-1, the Rab11 GTPase. Preliminary affinity-pulldown assays,

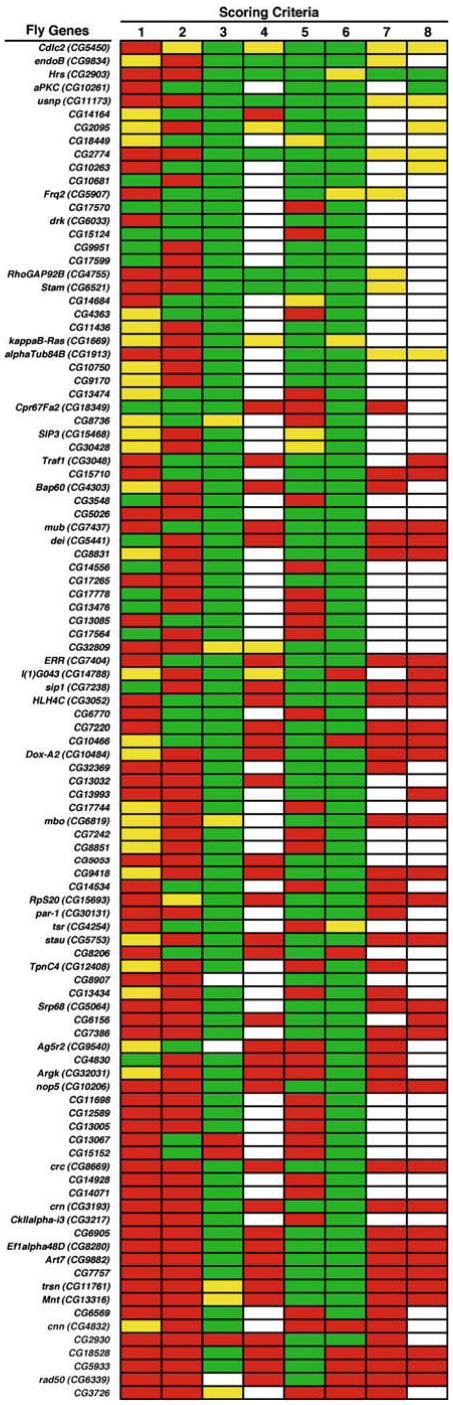

Fig. 3 Ranking of candidate binding partners for subunits of BLOC-1 from flies. Candidates are listed using the official names of the encoding genes from *D. melanogaster* (alternative names in parentheses), with the top position in the list representing the first place in the ranking. Scoring criteria: 1, confidence level on the Y2H interaction (*green* is for high confidence); 2, predicted regions with propensity to fold into coiled-coils (*green* is for their absence from candidate); 3, predicted transmembrane regions (*green* is for their absence from candidate); 4, predicted functional domains (*green* is for the prediction of at least one domain previously implicated in protein/membrane trafficking); 5, homology to human proteins (*green* is for the presence of a recognizable orthologue encoded by the human genome); 6, homology to yeast proteins (*green* is for failure to detect a clearly recognizable homologue encoded by the genome of *S. cerevisiae*); 7, proposed biological function of the fly protein (*green* is for a role in protein/membrane trafficking on endosomes or lysosomes); 8, proposed biological function of the human orthologue, if any (*green* is for a role in protein/membrane trafficking on endosomes or lysosomes)

using recombinant Rab11 expressed in bacteria and native BLOC-1 from bovine brain cytosol, have so far yielded no significant interaction (I. A. Rodriguez-Fernandez and E. C. Dell'Angelica, unpublished results). However, additional experiments will be required to rule out the possibility that our negative results may have been a consequence of the experimental conditions used; for example, the interaction of small GTPases such as Rab11 with other proteins is known to depend strictly on their binding to GDP or GTP (Jagoe et al 2006; Prekeris et al 2000) and differences in the protein-binding abilities of soluble and membrane-associated BLOC-1 have been documented (Di Pietro et al 2006). In an alternative approach, we sought for evidence of genetic interaction between a mutant allele of *Rab11* in flies and mutations in components of the molecular machinery that is conserved between humans and flies and required for the biogenesis of lysosome-related organelles in both species. Unfortunately, direct genetic interaction between Rab11 and BLOC-1 could not be tested in flies, because so far no mutant lines deficient in *Drosophila* BLOC-1 have been reported in the literature or made available at public repositories. Consequently, we focused on genes like those encoding subunits of the AP-3 complex, which are required for the biogenesis of melanosomes and platelet-dense granules in humans as well as for the biogenesis of eye pigment granules in flies. Actually, the association of AP-3 subunit mutations with HPS in humans (Dell'Angelica et al 1999) was demonstrated only after the role of *Drosophila* AP-3 in eye pigment granule biogenesis was discovered (Ooi et al 1997; Simpson et al 1997). Other reasons for focusing on AP-3 were the reported physical and functional interactions between this complex and BLOC-1 in mammals (Di Pietro et al 2006; Salazar et al

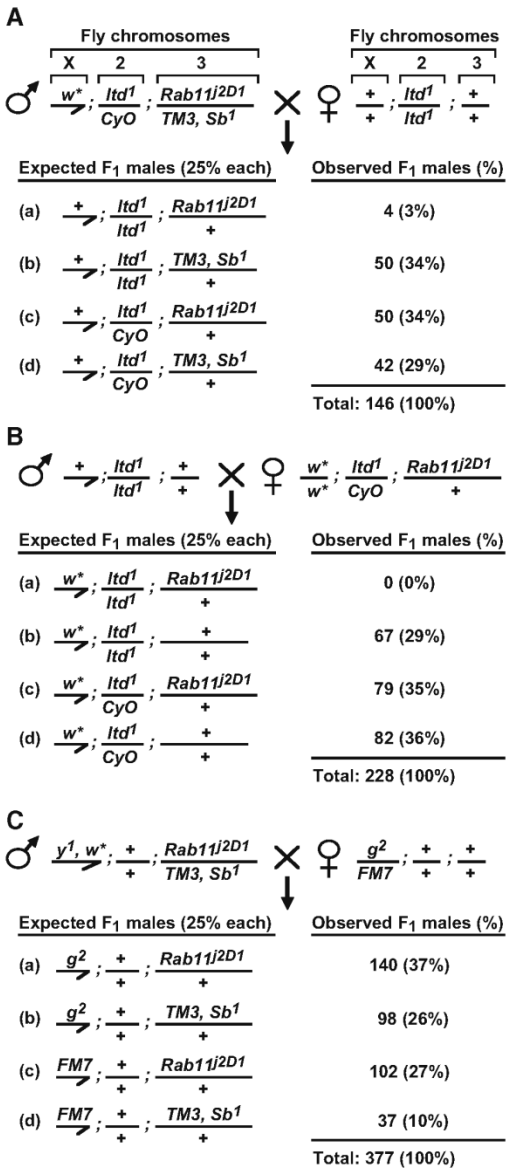

Fig. 4 Synthetic sick/lethal interaction between mutant alleles of the fly genes *Rab11* and *lightoid* encoding related Rab GTPases. (**A**) Male flies carrying a null-mutant allele of the *white* gene (*w**) on chromosome X, a copy of a null-mutant allele of the *lightoid* gene (ltd^1) over a second-chromosome balancer (*CyO*, which induces a 'curly-wing' phenotype) and a copy of a mutant allele of *Rab11* ($Rab11^{j2D1}$) over a third-chromosome balancer (*TM3,* Sb^1, which induces a 'short-and-thick-hair' phenotype) were crossed with virgin females homozygous for the ltd^1 mutation. (**B**) Male flies homozygous for the ltd^1 mutation were crossed with virgin females homozygous for the *w** mutation on chromosome X and carrying a copy of ltd^1 over the second-chromosome balancer *CyO* and a single copy of the $Rab11^{j2D1}$ allele on the third chromosome. (**C**) Male flies carrying mutations in the *yellow* (y^1) and *white* (*w**) genes on chromosome X and heterozygous for the $Rab11^{j2D1}$ allele over the third-chromosome balancer (*TM3,* Sb^1) were crossed with virgin females heterozygous for a mutant allele of the *garnet* gene (g^2) over a modified X-chromosome, *FM7* (which in males leads to abnormally small eyes). Shown in all panels (**A**–**C**) are the four possible genotypes expected for the males in the progeny at a theoretical frequency of 25% each, as well as the absolute numbers (and percentages) of adult male flies observed within 24 h after eclosion. Note in (**A**) and (**B**) the significantly low numbers of male flies that survived to adulthood when homozygous for ltd^1 and carrying a single copy of the $Rab11^{j2D1}$ allele

2006). Another relevant example involves two Rab proteins, Rab38 and Rab32, which are required for proper biogenesis of melanosomes in mammals (Wasmeier et al 2006); mutations in the Rab38-encoding gene were documented for rat models of HPS (Oiso et al 2004), and mutations in the only *Drosophila* orthologue of Rab38 and Rab32, *lightoid*, were shown to cause defects in the biogenesis of fly eye pigment granules (Ma et al 2004). Because *Rab11* is a paralogue of *lightoid*, the possibility of partial functional overlap between them deserved consideration. Consequently, we performed fly genetic analyses to test whether the $Rab11^{j2D1}$ mutant allele, which causes lethality in homozygous form owing to essential roles of Rab11 in cytokinesis and tissue development (Alone et al 2005; Giansanti et al 2007; Pelissier et al 2003; Riggs et al 2003), could enhance the eye pigmentation defects of flies deficient in AP-3 (i.e. homozygous for the g^2 mutant allele) or in the Rab38/Rab32 orthologue (i.e. homozygous for the ltd^1 mutant allele). The eye pigmentation of flies homozygous for g^2 and heterozygous for $Rab11^{j2D1}$ was indistinguishable from that of homozygous g^2 flies (data not shown). Unexpectedly, almost no fly homozygous for ltd^1 and carrying a single copy of the $Rab11^{j2D1}$ allele survived to young adulthood. Thus, upon a fly crossing designed to yield about 25% of male flies homozygous for ltd^1 and heterozygous for $Rab11^{j2D1}$, only four male flies with this genotype out of more than a hundred (3%) were recovered within 24 h after eclosion (Fig. 4A). Similar results were obtained using a different mutant allele of *Rab11*, $Rab11^{93Bi}$ (data not shown). As an attempt to rule out effects caused by other loci, we outcrossed the ltd^1 allele into the genetic background of Canton-S and performed a new set of crosses searching for flies homozygous for ltd^1 and heterozygous for $Rab11^{j2D1}$; this time, however, the number of males with this genotype was zero (Fig. 4B). On the other hand, male flies homozygous for g^2 and heterozygous for $Rab11^{j2D1}$ were viable; actually, they were observed in excess of the theoretical 25% frequency owing to detrimental effects of *FM7* and *TM3* chromosomes on viability (Fig. 4C). Taken together, these results demonstrated a synthetic sick/lethal interaction between *Rab11* and *lightoid*, likely due to partially overlapping functions of the encoded Rab proteins.

Discussion

The goal of this work was to find ways of obtaining high-quality information to prioritize candidate binding partners in cases where the number of reported interactions exceeds the capacity of individual laboratories to perform all of the necessary validation experiments. Such is the situation that we have faced through our studies of BLOC-1, for which 70 candidate binding partners have been found in humans and 102 in flies—mostly by large-scale Y2H projects. Bearing in mind that a large proportion of Y2H data represents false positives (Deane et al 2002; Gandhi et al 2006; von Mering et al 2002), the assumption that all interactions reported for BLOC-1 may be 'real' appears unwarranted; rather, many of them are probably not worth pursuing experimentally. We suspect that researchers working on other proteins of medical relevance may be facing a similar dilemma. For example, over 280 candidate binding partners have been described for DISC1, the product of a gene that is truncated upon a chromosomal translocation strongly associated with psychiatric disease and for which the molecular function remains poorly understood (Camargo et al 2007).

Various methods have been described for the global assessment of large sets of interactomics data (Camargo et al 2007; Deane et al 2002; Giot et al 2003; Goldberg and Roth 2003; Mahdavi and Lin 2007; Rual et al 2005; Scott and Barton 2007; Stelzl et al 2005). Some approaches to assess the reliability of Y2H data rely on the existence of paralogues shown to interact with each other (Deane et al 2002); although successful for many proteins, in the case of BLOC-1 only two of its subunits display homology to other human sequences, and for them virtually no interaction data are available (data not shown). Other approaches give weight to finding the corresponding interaction between the orthologues from another species; again such an idea has been successful for several proteins (e.g. Gandhi et al 2006), yet it cannot be applied to binding partners of BLOC-1 because the only protein shared by the lists of human and fly candidate binding partners (the Sec8 protein encoded by human *EXOC4* and *Drosophila CG2095*) was reported to interact with dysbindin in humans and BLOS2 in flies (Supplementary Tables 2 and 3). Our approach is unique in that it 'customizes' the scoring criteria according to prior knowledge by the researcher about characteristics of the candidates that the researcher would find encouraging to pursue with experimental work. We believe that a customized approach can be very powerful when focusing on candidate binding partners of well-characterized proteins or of proteins with unique properties (e.g. tissue-specific expression, well-established localization to a specific cellular compartment). On the other hand, we recognize that the choice of criteria is intrinsically arbitrary, which could adversely affect the usefulness

of the ranking. For example, some researchers might disagree with our choice to consider encouraging the absence of predicted coiled-coil-forming and transmembrane domains in the candidate's primary structure. Nevertheless, it is worth emphasizing that no single criterion is sufficient to completely exclude a candidate from further consideration. For example, 6 of the top 12 human candidates do contain coiled-coil-forming regions, compared with a total of 35 out of 70 candidates in the entire list, and the human candidate ranked 12th does contain a transmembrane domain. Finally, despite our best efforts, some of the information gathered about the candidates may be inaccurate. For example, practical reasons led us to restrict our search for experimental evidence to only the first article reporting the interaction, although for a few candidate binding partners (e.g. SNAP25; Ilardi et al 1999) subsequent work has brought the original findings into question (Vites et al 2004). In addition, some of the candidates for which failure to detect a yeast homologue in a BLASTP search was considered encouraging do contain orthologues in yeast (e.g. the exocyst subunits encoded by *EXOC7* and *EXOC4*; Munson and Novick 2006) that probably would have been detected by more sensitive but time-consuming algorithms such as PSI-BLAST. These limitations notwithstanding, we find the data-mining approach, and the idea of summarizing the information using a colour code, potentially very useful. For example: we have previously invested significant amounts of resources and time to pursue experimentally the reported interactions between the dysbindin subunit of BLOC-1 and the dystrobrevins (Benson et al 2001), with negative results (Nazarian et al 2006); in retrospect, the current ranking of the two dystrobrevins (encoded by the *DTNB* and *DTNA* genes) to the 45th and 51st places would have discouraged us from pursuing these interactions in particular.

At the top of the ranking of human candidates was the product of the *RAB11A* gene. Rab11 is a small GTPase associated with a subset of endosomes known as recycling endosomes, which accumulate at a perinuclear region of the cell and play important roles in the sorting of proteins for recycling to the plasma membrane as well as in asymmetric distribution of signalling molecules during mitosis (Emery et al 2005; Prekeris et al 2000; Ullrich et al 1996). Moreover, Rab11 is required for normal cytokinesis, and for development of various tissues in flies (Alone et al 2005; Giansanti et al 2007; Pelissier et al 2003; Riggs et al 2003). Consistent with these important functions, homozygous mutations in the only *Rab11* gene in flies cause lethality as embryos or early larvae (Alone et al 2005). This is in contrast with homozygous null mutations in *lightoid*, the only fly orthologue of both Rab32 and Rab38, which result in viable flies that display specific defects in the biogenesis of a lysosome-related organelle: the fly eye pigment granule (Ma et al 2004). Likewise, mutations in the Rab38-encoding gene in mice and rats result in viable animals with defective biogenesis of melanosomes, and the rat mutant is considered an animal model of HPS (Loftus et al 2002; Oiso et al 2004). At first sight, one might conclude that Rab32/Rab38/*lightoid*, and not Rab11, would be the key Rab protein for lysosome-related organelles and with which BLOC-1 might interact. However, genetic analyses in flies have suggested that *lightoid* is unlikely to be the only Rab involved in this process. Thus, the pigmentation phenotype of homozygous null ltd^{1} is not as severe as those of other eye colour mutants, and enhancement of the phenotype was observed for double mutants simultaneously deficient in *lightoid* and AP-3 (Ma et al 2004) or in *lightoid* and BLOC-2 (Falcón-Pérez et al 2007). These considerations led us to evaluate the possibility that Rab11, which is a paralogue of Rab32/Rab38/*lightoid*, could have some degree of functional overlap with the latter. Our results did provide evidence for functional overlap, but in an unexpected manner: while ltd^{1} homozygous flies and $Rab11^{j2D1}$ heterozygous flies were viable as adults and fertile, flies that were both ltd^{1} homozygous and $Rab11^{j2D1}$ heterozygous barely survived to young adulthood. This synthetic sick/lethal effect leads us to speculate that these two related Rab proteins may indeed have overlapping functions, for instance by interacting with common effector proteins, although such overlap would extend to some of the essential functions of Rab11. Further work will be required to understand the molecular basis for this intriguing genetic interaction, and the possible involvement of BLOC-1 in this process.

Other candidate binding partners that ranked close to the top should also deserve future experimentation. Second in the list of the human candidates is phafin 2, a novel protein predicted to associate with early endosomes owing to the presence of a FYVE domain. At third place is neurobeachin, a member of a family of large proteins that also includes Lyst, which is mutated in Chediak–Higashi syndrome and—like BLOC-1—is required for normal biogenesis of lysosome-related organelles (Shiflett et al 2002). At the 4th, 9th and 11th places rank three of the eight subunits of the exocyst complex, and the orthologue of one of them ranks 7th among the candidate binding partners of *Drosophila* BLOC-1 subunits. Interestingly, solid evidence indicates that both mammalian and

Drosophila exocyst components interact with Rab11 (Beronja et al 2005; Zhang et al 2004). Finally, ranking at the top of the candidate binding partners of *Drosophila* BLOC-1 are a subunit of the microtubule-associated motor, dynein, a member of the endophilin family of membrane-curvature-sensing proteins, and the Hrs subunit of the endosome-associated protein complex, ESCRT-0, which also contains the Stam subunit ranked in 19th place.

It is likely that approaches similar to that described here could be useful to researchers who face other situations with an exceedingly high number of candidate genes or proteins. For example, a single Y2H screening typically results in a large number of 'colonies' representing a number of candidate binding partners. Other lists of candidates may arise from other types of 'omics' approaches, e.g. genes whose transcripts are found upregulated under certain experimental conditions, or proteins identified by mass spectrometric analysis of a partially purified sample. In all of these situations, the researcher may need to rank the candidates to select those more 'encouraging' for experimental analysis. We believe that our 'customized' criteria approach with visually friendly presentation could be helpful also in those situations.

Acknowledgements We thank David E. Krantz and Anne F. Simon for reagents, and Julián A. Martínez-Agosto and Verónica T. Cheli for critical reading of the manuscript. This work was supported in part by grant HL068117 from the National Institutes of Health. I. A. Rodriguez-Fernandez was supported by National Institutes of Health training grant T32 HG002536.

References

Alone DP, Tiwari AK, Mandal L, Li M, Mechler BM, Roy JK (2005) *Rab11* is required during *Drosophila* eye development. *Int J Dev Biol* **49**: 873–879. doi:10.1387/ijdb.051986da.

Altschul SF, Madden TL, Schäffer AA, et al (1997) Gapped and PSI-BLAST: a new generation of protein database search programs. *Nucleic Acids Res* **25**: 3389–3402. doi:10.1093/nar/25.17.3389.

Bao Y, Lopez JA, James DE, Hunziker W (2008) Snapin interacts with the Exo70 subunit of the exocyst and modulates GLUT4 trafficking. *J Biol Chem* **283**: 324–331. doi:10.1074/jbc.M706873200.

Benson MA, Newey SE, Martin-Rendon E, Hawkes R, Blake DJ (2001) Dysbindin, a novel coiled-coil-containing protein that interacts with the dystrobrevins in muscle and brain. *J Biol Chem* **276**: 24232–24241. doi:10.1074/jbc.M010418200.

Benson MA, Tinsley CL, Blake DJ (2004) Myospryn is a novel binding partner for dysbindin in muscle. *J Biol Chem* **279**: 10450–10458. doi:10.1074/jbc.M312664200.

Beronja S, Laprise P, Papoulas O, Pellikka M, Sisson J, Tepass U (2005) Essential function of *Drosophila* Sec6 in apical exocytosis of epithelial photoreceptor cells. *J Cell Biol* **169**: 635–646. doi:10.1083/jcb.200410081.

Camargo LM, Collura V, Rain JC, et al (2007) Disrupted in Schizophrenia 1 interactome: evidence for the close connectivity of risk genes and a potential synaptic basis for schizophrenia. *Mol Psychiatry* **12**: 74–86. doi:10.1038/sj.mp.4001880.

Combet C, Blanchet C, Geourjon C, Deléage G (2000) NPS@: Network Protein Sequence Analysis. *Trends Biochem Sci* **25**: 147–150. doi:10.1016/S0968-0004(99)01540-6.

Deane CM, Salwinski L, Xenarios I, Eisenberg D (2002) Protein interactions. Two methods for assessment of the reliability of high throughput observations. *Mol Cell Proteomics* **1**: 349–356. doi:10.1074/mcp.M100037-MCP200.

Dell'Angelica EC, Shotelersuk V, Aguilar RC, Gahl WA, Bonifacino JS (1999) Altered trafficking of lysosomal proteins in Hermansky–Pudlak syndrome due to mutations in the β3A subunit of the AP-3 adaptor. *Mol Cell* **3**: 11–21. doi:10.1016/S1097-2765(00)80170-7.

Di Pietro SM, Dell'Angelica EC (2005) The cell biology of Hermansky–Pudlak syndrome: recent advances. *Traffic* **6**: 525–533. doi:10.1111/j.1600-0854.2005.00299.x.

Di Pietro SM, Falcón-Pérez JM, Tenza D, et al (2006) BLOC-1 interacts with BLOC-2 and the AP-3 complex to facilitate protein trafficking on endosomes. *Mol Biol Cell* **17**: 4027–4038. doi:10.1091/mbc.E06-05-0379.

Emery G, Hutterer A, Berdnik D, et al (2005) Asymmetric Rab11 endosomes regulate delta recycling and specify cell fate in the *Drosophila* nervous system. *Cell* **122**: 763–773. doi:10.1016/j.cell.2005.08.017.

Ewing RM, Chu P, Elisma F, et al (2007) Large-scale mapping of human protein–protein interactions by mass spectrometry. *Mol Syst Biol* **3**: 89. doi:10.1038/msb4100134.

Falcón-Pérez JM, Romero-Calderón R, Brooks ES, Krantz DE, Dell'Angelica EC (2007) The *Drosophila* pigmentation gene *pink* (*p*) encodes a homologue of human Hermansky–Pudlak syndrome 5 (HPS5). *Traffic* **8**: 154–168. doi:10.1111/j.1600-0854.2006.00514.x.

Felten A, Leister P, Burgdorf S, Uhlmann L, Scheidtmann KH (2007) Characterization of rat BLOS2/Ceap, a putative yeast She3 homolog, as interaction partner of apoptosis antagonizing transcription factor/Che-1. *Biol Chem* **388**: 569–582. doi:10.1515/BC.2007.073.

Formstecher E, Aresta S, Collura V, et al (2005) Protein interaction mapping: A *Drosophila* case study. *Genome Res* **15**: 376–384. doi:10.1101/gr.2659105.

Fukui K, Yang Q, Cao Y, et al (2005) The HNF-1 target collectrin controls insulin exocytosis by SNARE complex formation. *Cell Metab* **2**: 373–384. doi:10.1016/j.cmet.2005.11.003.

Gandhi TKB, Zhong J, Mathivanan S, et al (2006) Analysis of the human protein interactome and comparison with yeast, worm and fly interaction datasets. *Nat Genet* **38**: 285–293. doi:10.1038/ng1747.

Giansanti MG, Belloni G, Gatti M (2007) Rab11 is required for membrane trafficking and actomyosin ring constriction in meiotic cytokinesis of *Drosophila* males. *Mol Biol Cell* **18**: 5034–5047. doi:10.1091/mbc.E07-05-0415.

Giot L, Bader JS, Brouwer C, et al (2003) A protein interaction map of *Drosophila melanogaster*. *Science* **302**: 1727–1736. doi:10.1126/science.1090289.

Goldberg DS, Roth FP (2003) Assessing experimentally derived interactions in a small world. *Proc Natl Acad Sci USA* **100**: 4372–4376. doi:10.1073/pnas.0735871100.

Granata A, Watson R, Collinson LM, Schiavo G, Warner TT (2008) The dystonia-associated protein torsinA modulates synaptic vesicle recycling. *J Biol Chem* **283**: 7568–7579. doi:10.1074/jbc.M704097200.

Greenspan RJ (1997) *Fly Pushing: The Theory and Practice of Drosophila Genetics*. New York: Cold Spring Harbor Laboratory Press.

Ilardi JM, Mochida S, Sheng ZH (1999) Snapin: a SNARE-associated protein implicated in synaptic vesicle transmission. *Nat Neurosci* **2**: 119–124. doi:10.1038/5673.

Jagoe WN, Lindsay AJ, Read RJ, McCoy AJ, McCaffrey MW, Khan AR (2006) Crystal structure of rab11 in complex with rab11 family interacting protein 2. *Structure* **14**: 1273–1283. doi:10.1016/j.str.2006.06.010.

Li W, Zhang Q, Oiso N, et al (2003) Hermansky-Pudlak syndrome type 7 (HPS-7) results from mutant dysbindin, a member of the biogenesis of lysosome-related organelles complex 1 (BLOC-1). *Nat Genet* **35**: 84–89. doi:10.1038/ng1229.

Li W, Feng Y, Hao C, Guo X, Cui Y, He M, He X (2007) The BLOC interactomes form a network in endosomal transport. *J Genet Genomics* **34**: 669–682. doi:10.1016/S1673-8527(07)60076-9.

Loftus SK, Larson DM, Baxter LL, et al (2002) Mutation of melanosome protein RAB38 in chocolate mice. *Proc Natl Acad Sci USA* **99**: 4471–4476. doi:10.1073/pnas.072087599.

Ma J, Plesken H, Treisman JE, Edelman-Novemsky I, Ren M (2004) *Lightoid* and *Claret*: a rab GTPase and its putative guanine nucleotide exchange factor in biogenesis of *Drosophila* eye pigment granules. *Proc Natl Acad Sci USA* **101**: 11652–11657. doi:10.1073/pnas.0401926101.

Mahdavi MA, Lin Y-H (2007) False positive reduction in protein-protein interaction predictions using gene ontology annotations. *BMC Bioinformatics* **8**: 262. doi:10.1186/1471-2105-8-262.

Morgan NV, Pasha S, Johnson CA, et al (2006) A germline mutation in *BLOC1S3/Reduced Pigmentation* causes a novel variant of Hermansky–Pudlak syndrome (HPS8). *Am J Hum Genet* **78**: 160–166. doi:10.1086/499338.

Mishra GR, Suresh M, Kumaran K, et al (2006) Human Protein Reference Database—2006 update. *Nucleic Acids Res* **34**(Database Issue): D411–414. doi:10.1093/nar/gkj141.

Mistry AC, Mallick R, Frohlich O, et al (2007) The UT-A1 urea transporter interacts with snapin, a SNARE-associated protein. *J Biol Chem* **282**: 30097–30106. doi:10.1074/jbc.M705866200.

Munson M, Novick P (2006) The exocyst defrocked, a framework of rods revealed. *Nat Struc Mol Biol* **13**: 577–581. doi:10.1038/nsmb1097.

Nazarian R, Starcevic M, Spencer MJ, Dell'Angelica EC (2006) Reinvestigation of the dysbindin subunit of BLOC-1 (biogenesis of lysosome-related organelles complex-1) as a dystrobrevin-binding protein. *Biochem J* **395**: 587–598. doi:10.1042/BJ20051965.

Nian H, Fan C, Liao S, et al (2007) RNF151, a testis-specific RING finger protein, interacts with dysbindin. *Arch Biochem Biophys* **465**: 157–163. doi:10.1016/j.abb.2007.05.013.

Oiso N, Riddle SR, Serikawa T, Kuramoto T, Spritz RA (2004) The rat Ruby (*R*) locus is *Rab38*: identical mutations in Fawn-hooded and Tester–Moriyama rats derived from an ancestral Long Evans rat sub-strain. *Mamm Genome* **15**: 307–314. doi:10.1007/s00335-004-2337-9.

Ooi CE, Moreira JE, Dell'Angelica EC, Poy G, Wassarman DA, Bonifacino JS (1997) Altered expression of a novel adaptin leads to defective pigment granule biogenesis in the *Drosophila* eye color mutant *garnet*. *EMBO J* **16**: 4508–4518. doi:10.1093/emboj/16.15.4508.

Pelissier A, Chauvin JP, Lecuit T (2003) Trafficking through Rab11 endosomes is required for cellularization during *Drosophila* embryogenesis. *Curr Biol* **13**: 1848–1857. doi:10.1016/j.cub.2003.10.023.

Prekeris R, Klumperman J, Scheller RH (2000) A Rab11/Rip11 protein complex regulates apical membrane trafficking via recycling endosomes. *Mol Cell* **6**: 1437–1448. doi:10.1016/S1097-2765(00)00140-4.

Raposo G, Marks MS (2007) Melanosomes—dark organelles enlighten endosomal membrane transport. *Nat Rev Mol Cell Biol* **8**: 786–797. doi:10.1038/nrm2258.

Riggs B, Rothwell W, Mische S, et al (2003) Actin cytoskeleton remodeling during early *Drosophila* furrow formation requires recycling endosomal components Nuclear-fallout and Rab11. *J Cell Biol* **163**: 143–154. doi:10.1083/jcb.200305115.

Rual JF, Venkatesan K, Hao T, et al (2005) Towards a proteome-scale map of the human protein-protein interaction network. *Nature* **437**: 1173–1178. doi:10.1038/nature04209.

Rüder C, Reimer T, Delgado-Martinez I, et al (2005) EBAG9 adds a new layer of control on large dense-core vesicle exocytosis via interaction with snapin. *Mol Biol Cell* **16**: 1245–1257. doi:10.1091/mbc.E04-09-0817.

Salazar G, Craige B, Styers ML, et al (2006) BLOC-1 complex deficiency alters the targeting of adaptor protein complex-3 cargoes. *Mol Biol Cell* **17**: 4014–4026. doi:10.1091/mbc.E06-02-0103.

Scott MS, Barton GJ (2007) Probabilistic prediction and ranking of human protein-protein interactions. *BMC Bioinformatics* **8**: 239. doi:10.1186/1471-2105-8-239.

Setty SRG, Tenza D, Truschel ST, et al (2007) BLOC-1 is required for cargo-specific sorting from vacuolar early endosomes toward lysosome-related organelles. *Mol Biol Cell* **18**: 768–780. doi:10.1091/mbc.E06-12-1066.

Setty SRG, Tenza D, Sviderskaya EV, Bennett DC, Raposo G, Marks MS (2008) Cell-specific ATP7A transport sustains copper-dependent tyrosinase activity in melanosomes. *Nature* **454**: 1142–1147. doi:10.1038/nature07163.

Shiflett SL, Kaplan J, Ward DM (2002) Chediak-Higashi syndrome: a rare disorder of lysosomes and lysosome related organelles. *Pigment Cell Res* **15**: 251–257. doi:10.1034/j.1600-0749.2002.02038.x.

Simpson F, Peden AA, Christopoulou L, Robinson MS (1997) Characterisation of the adaptor-related protein complex, AP-3. *J Cell Biol* **137**: 835–845. doi:10.1083/jcb.137.4.835.

Starcevic M, Dell'Angelica EC (2004) Identification of snapin and three novel proteins (BLOS1, BLOS2, and BLOS3/reduced pigmentation) as subunits of biogenesis of lysosome-related organelles complex-1 (BLOC-1). *J Biol Chem* **279**: 28393–28401. doi:10.1074/jbc.M402513200.

Stelzl U, Worm U, Lalowski M, et al (2005) A human protein-protein interaction network: a resource for annotating the proteome. *Cell* **122**: 957–968. doi:10.1016/j.cell.2005.08.029.

Sun J, Nie J, Hao B, et al (2008) Ceap/BLOS2 interacts with BRD7 and selectively inhibits its transcription-suppressing effect on cellular proliferation-associated genes. *Cell Signal* **20**: 1151–1158. doi:10.1016/j.cellsig.2008.02.002.

Suzuki F, Morishima S, Tanaka T, Muramatsu I (2007) Snapin, a new regulator of receptor signaling, augments alpha1A–adrenoceptor–operated calcium influx through TRPC6. *J Biol Chem* **282**: 29563–29573. doi:10.1074/jbc.M702063200.

Ullrich O, Reinsch S, Urbé S, Zerial M, Parton RG (1996) Rab11 regulates recycling through the pericentriolar recycling endosome. *J Cell Biol* **135**: 913–924. doi:10.1083/jcb.135.4.913.

Vites O, Rhee J-S, Schwarz M, Rosenmund C, Jahn R (2004) Reinvestigation of the role of snapin in neurotransmitter release. *J Biol Chem* **279**: 26251–26256. doi:10.1074/jbc.M404079200.

von Mering C, Krause R, Snel B, et al (2002) Comparative assessment of large-scale data sets of protein-protein interactions. *Nature* **417**: 399–403. doi:10.1038/nature750.

Wasmeier C, Romao M, Plowright L, Bennett DC, Raposo G, Seabra MC (2006) Rab38 and Rab32 control early post-Golgi trafficking of melanogenic enzymes. *J Cell Biol* **175**: 271–281. doi:10.1083/jcb.200606050.

Wei ML (2006) Hermansky-Pudlak syndrome: a disease of protein trafficking and organelle function. *Pigment Cell Res* **19**: 19–42. doi:10.1111/j.1600-0749.2005.00289.x.

Wolff S, Stöter M, Giamas G, et al (2006) Casein kinase 1 delta (CK1δ) interacts with the SNARE associated protein snapin. *FEBS Lett* **580**: 6477–6484. doi:10.1016/j.febslet.2006.10.068.

Yin H, Laguna KA, Li G, Kuret J (2006) Dysbindin structural homologue CK1BP is an isoform-selective binding partner of human casein kinase-1. *Biochemistry* **45**: 5297–5308. doi:10.1021/bi052354e.

Yuan X, Shan Y, Zhao Z, Chen J, Cong Y (2006) Interaction between snapin and G-CSF receptor. *Cytokine* **33**: 219–225. doi:10.1016/j.cyto.2006.01.008.

Zhang X-M, Ellis S, Sriratana A, Mitchell CA, Rowe T (2004) Sec15 is an effector for the Rab11 GTPase in mammalian cells. *J Biol Chem* **279**: 43027–43034. doi:10.1074/jbc.M402264200.

A. Scoring criteria for candidate binding partners of human BLOC-1

Criteria & color	Definitions
1	**Yeast-two-hybrid (Y2H) data**
Green	Interaction from a small-scale Y2H screen or with high-confidence score from a large-scale Y2H project
Yellow	Medium-confidence score obtained in a large-scale Y2H project
2	**Affinity-pulldown data**
Green	Recombinant form of binding partner was able to pull-down native BLOC-1
Yellow	Recombinant form of binding partner was able to pull-down recombinant or overexpressed BLOC-1 subunit
White	No information
3	**Coimmunoprecipitation data**
Green	Postive coimmunoprecipitation involving native BLOC-1
Yellow	Coimmunprecipitation involving overexpressed BLOC-1 subunit (epitope-tagged or not)
White	No information
4	**Predicted Coiled-coil domains**
Green	Absence of predicted coiled-coil-forming domains
Red	Presence of predicted coiled-coil-forming domains
5	**Predicted transmembrane regions**
Green	Absence of predicted transmembrane regions
Red	Presence of predicted transmembrane regions
6	**Predicted structural or functional conserved domains**
Green	Conserved domains specifically related to protein/membrane trafficking, such as FYVE, RAB, SNARE, BAR
Yellow	Conserved domains involved in multiple functions besides protein/membrane trafficking
Red	Conserved domains with unrelated function, such as DNA or RNA binding
White	No conserved domains with known function
7	**mRNA expression patterns**
Green	Transcript expressed in a wide variety of tissues and cell types
Yellow	Transcript with restricted expression including brain (due to potential association of BLOC-1 with schizophrenia)
Red	Transcript with restricted expression not including brain tissue
8	**Detection of a *D. melanogaster* homologue**
Green	Positive detection of a homologue in *D. melanogaster* (with E-value $<10^{-4}$)
Yellow	Potential *D. melanogaster* homologue (E-value $>10^{-4}$)
Red	No *D. melanogaster* homologue detected on a BLASTP search
9	**Detection of a *S. cerevisiae* homologue**
Green	No homologue detected in *S. cerevisiae* through BLASTP search
Yellow	Homologue detected in *S.cerevisiae* (E-value $<10^{-4}$) with role in membrane/protein trafficking
Red	Homologue detected in *S.cerevisiae* (E-value $<10^{-4}$) with role unrelated to membrane/protein trafficking
10	**Reported or proposed function**
Green	Role in protein/membrane trafficking (vesicle-mediated transport) on endosomes or lysosomes
Yellow	Role in protein/membrane trafficking but not necessarily on endosomes or lysosomes
Red	Unrelated function such as transcription or translation
White	No information or multiple functions (e.g., cytoskeleton regulation)

B. Scoring criteria for candidate binding partners of fly BLOC-1

Criteria & color	Definitions
1	**Yeast-two-hybrid (Y2H) data**
Green	High-confidence score from a large-scale Y2H project (Confidence score > 0.66 on a 0-1 scale)
Yellow	Medium-confidence score from a large-scale Y2H project (Confidence score 0.33-0.66 on a 0-1 scale)
Red	Low-confidence score from a large-scale Y2H project (Confidence score < 0.33 on a 0-1 scale)
2	**Predicted Coiled-coil domains**
Green	Absence of predicted coiled-coil-forming domains (P-value << 0.5)
Yellow	Prediction for the coiled-coil domain not convincing (P-value ~ 0.5)
Red	Presence of predicted coiled-coil-forming domains (P-value >> 0.5)
3	**Predicted transmembrane regions**
Green	Absence of predicted transmembrane regions
Yellow	Not convincing predicted transmembrane region (15-20 amino acid long)
Red	Presence of predicted transmembrane regions (> 20 amino acid long)
4	**Predicted sructural or functional conserved domains**
	Same as scoring criteria #6 for human BLOC-1 candidate binding partners
5	**Detection of a *H. sapiens* homologue**
Green	Positive detection of a homologue in *H.sapiens* (with E-value $<10^{-4}$)
Yellow	Potential *H.sapiens* homologue (E-value $>10^{-4}$)
Red	No *H.sapiens* homologue detected on a BLASTP search
6	**Detection of a *S. cerevisiae* homologue**
	Same as scoring criteria #9 for human BLOC-1 candidate binding partners
7	**Candidates' reported or proposed function**
	Same as scoring criteria #10 for human BLOC-1 candidate binding partners
8	**Candidates' reported or proposed function for the human homologue**
	Same as scoring criteria #10 for human BLOC-1 candidate binding partners

Rodriguez-Fernandez and Dell'Angelica
Supplementary Table 2

Rank	Human Gene name	Chr.	Protein name (alternative name)	Summary of reported/proposed function[a]	Interacting BLOC-1 subunit	Reference (PMID)[b]
1	*RAB11A*	15	Rab11a	GTPase, Protein/membrane trafficking, endosomes	Dysbindin	17043677
2	*PLEKHF2*	8	Phafin 2	Protein/membrane trafficking	Pallidin	16189514
3	*NBEA*	13	neurobeachin	Protein/membrane trafficking, post-Golgi/endosomes	Dysbindin	17043677
4	*EXOC7*	17	EXO70 (exocyst complex component 7)	Protein/membrane trafficking, exocytosis	Snapin	17947242
5	*SNAP23*	15	SNAP-23	Protein/membrane trafficking, membrane fusion	Snapin	12877659
6	*CSNK1D*	17	casein kinase 1 delta (CK1delta)	Protein kinase, multiple functions	Snapin, Dysbindin	17101137
7	*SNAP25*	20	SNAP-25	Protein/membrane trafficking, synaptic vesicle exocytosis	Snapin	10195194
8	*WASF2*	1	WAS protein family, member 2	Cytoskeleton, actin binding	Dysbindin	AfCS
9	*EXOC8*	1	exocyst complex 84-kDa subunit	Protein/membrane trafficking, exocytosis	Pallidin	16189514
10	*ZFYVE20*	3	rabenosyn-5	Protein/membrane trafficking, endosomes	Dysbindin	17043677
11	*EXOC4*	7	SEC8 protein (exocyts complex component 4)	Protein/membrane trafficking, exocytosis	Dysbindin	17043677
12	*STX12*	1	syntaxin 13 (syntaxin 12, syntaxin 14)	Protein/membrane trafficking, endosomes, fusion	Pallidin	10610180
13	*RANBP5*	13	Ran binding protein (Karyopherin beta 3)	Nucleocytoplasmic transport	Dysbindin	17043677
14	*HTATIP*	11	HIV-1 Tat interacting protein, 60kDa	Chromatin remodeling, transcription, DNA repair	Snapin	16169070
15	*MYST2*	17	MYST histone acetyltransferase 2	Histone acetyltransferase, DNA replication	Snapin	16169070
16	*AATF*	17	apoptosis antagonizing transcription factor	Transcription factor	BLOS2	17552904
17	*ARFIP2*	11	Arfaptin2	Cytoskeleton regulation	Dysbindin	16189514
18	*RGS7*	1	regulator of G-protein signaling 7	Signal transduction	Snapin	12659861
19	*FLJ10204*	8	C8ORF32 (hypothetical protein LOC55093)		Pallidin	16189514
20	*MACF1*	1	microtubule-actin crosslinking factor 1	Cytoskeleton, actin binding	Dysbindin	17043677
21	*DST*	6	Dystonin (MACF2)	Cytoskeleton regulation	Dysbindin	17043677
22	*EPS8*	12	epidermal growth factor receptor substrate 8	Signal transduction	Pallidin	16189514
23	*RNF151*	16	RNF151 (ring finger protein 151)		Dysbindin	17577571
24	*C1orf190*	1	hypothetical protein LOC541468		Pallidin	16189514
25	*TOR1A*	9	torsinA	AAA-type ATPase	Snapin	18167355
26	*PSME3*	17	proteasome 3 (prosome, macropain)	Immunoproteasome regulator	Dysbindin	17043677
27	*EBAG9*	8	RCAS1	Estrogen responsive gene, regulation of transcription	Snapin	15635093
28	*EEF1G*	11	Eukaryotic Elongation factor 1 gamma	Translation	Snapin	16169070
29	*PTN*	7	pleiotrophin	Cytokine, cell proliferation, development	BLOS1	16169070
30	*BRD7*	16	bromodomain containing 7	Histone binding, transcription factor	BLOS2	18329849
31	*MET*	7	receptor tyrosine kinase MET (TRP)	Hepatocyte growth factor receptor	Snapin	15546961
32	*GDA*	9	cypin	Guanine deamination	Snapin	16120643
33	*CII-116*	12	CCDC53 (coiled-coil domain containing 53)		Pallidin	16189514
34	*KIF5C*	2	kinesin family member 5	ATP binding, microtubule motor activity	Snapin	16169070
35	*DDR1*	6	discoidin domain receptor family, member 1	Cell growth, communication and differentiation	Snapin	16169070
36	*KIAA0240*	6	hypotethical protein LOC23506		Dysbindin	17043677
37	*GPRASP1*	X	G protein-coupled receptor sorting 1		Snapin	16169070
38	*SLC14A2*	18	urea transporter, member 2	Renal tubular urea transporter	Snapin	17702749
39	*DGCR6L*	22	DiGeorge syndrome critical region gene 6 like	Cell migration	Dysbindin	16189514
40	*AGGF1*	5	angiogenic factor VG5Q	Cell surface binding and cell adhesion	Pallidin	16189514
41	*IKBKAP*	9	IKAP	Regulator of kinases involved in pro-inflammatory signal	Snapin	16169070
42	*ZNF490*	19	zinc finger protein 490	Transcription factor	Dysbindin	17043677
43	*LAMC1*	1	laminin, gamma 1	Cell adhesion, differentiation, neurite outgrowth	Snapin	16169070
44	*TRPM7*	15	TRPM7	Ion channel, kinase	Snapin	17088214
45	*DTNB*	2	beta-dystrobrevin	Plasma membrane stability, signaling	Dysbindin, Muted	11316798
46	*CMYA5*	5	myospryn/cardiomyopathy associated 5		Dysbindin	14688250
47	*CCND3*	6	cyclin D3	Cell cycle regulation	Dysbindin	16189514
48	*TRPV1*	17	vanilloid receptor-1 (TRPV1)	Receptor for capsaicin, transducer of pain stimulation	Snapin	15066994
49	*CCNA2*	4	cyclinA2	Cell cycle regulation	Dysbindin	17043677
50	*ADRA1A*	8	alpha-1A-adrenergic receptor	G-coupled receptor, regulation of growth and proliferation	Snapin	17684020
51	*DTNA*	18	alpha-dystrobrevin	Plasma membrane stability, signaling	Dysbindin	11316798
52	*CSF3R*	1	colony stimulating factor 3 receptor	Cytokine receptor	Snapin	16595180
53	AKAP6	14	A kinase anchor protein 6 (PRKA)	Binds the regulatory subunit of protein kinase A	Dysbindin	17043677
54	*HAP1*	17	huntingtin-associated protein 1	Protein/membrane trafficking or organelle transport	Snapin	16169070
55	*RyR1*	19	ryanodine receptor type1	Calcium release channel in sarcoplasmic reticulum	Snapin	16723744

56	*RyR2*	1	ryanodine receptor type 2	Calcium channel in cardiac muscle	Snapin	16723744
57	*RyR3*	15	ryanodine receptor type 3	Calcium release channel	Snapin	16723744
58	*IMMT*	2	IMMT (Mitofilin)	Protein binding, mitochondria	Snapin	16169070
59	*C10ORF78*	10	hypothetical protein LOC119392		Dysbindin	17043677
60	*KIAA0408*	6	hypothetical protein LOC9729		Dysbindin	17043677
61	*ABI3*	17	NESH protein	Cell mobility	Dysbindin	16189514
62	*ESF1*	20	ABT1-associated protein	Regulation of transcription	Dysbindin	17043677
63	*HNF1A*	12	HNF1 homeobox A	Transcription factor	Snapin	16330323
64	*BRF1*	14	subunit of RNA polymerase III	Transcription factor	Dysbindin	17043677
65	*C18ORF24*	18	spindle and KT (kinetochore) associated 1	Cell cycle	Pallidin	16189514
66	*SPAG5*	17	sperm associated antigen 5	Mitotic spindle, cell cycle, mitosis	Snapin	16169070
67	*ADCY6*	12	adenylate cyclase 6	cAMP catalysis	Snapin	15319443
68	*SYNE1*	6	nesprin (Synaptic nuclear envelope p1)	Localizes to nuclear membrane, spinocerebellar ataxia	Dysbindin	17043677
69	*TMEM27*	X	collectrin	Amino acid transport	Snapin	16330323
70	*KNTC2*	18	kinetochore associated 2	Cell cycle	Pallidin	16189514

Footnotes:

[a] As reported on either GeneOntology or the Summary section of NCBI Entrez Gene
[b] PMID, PubMed identification number: http://www.ncbi.nlm.nih.gov/sites/entrez?db=pubmed

References:

10195194 Hardi JM, Mochida S, Sheng ZH (1999) Snapin: a SNARE-associated protein implicated in synaptic transmission. *Nat Neurosci* **2**:119-124.
10610180 Huang L, Kuo YM, Gitschier J (1999) The pallid gene encodes a novel, syntaxin 13-interacting protein involved in platelet storage pool deficiency. *Nat Genet* **23**:329-332.
11316798 Benson MA, Newey SE, Martin-Rendon E, Hawkes R, Blake DJ (2001) Dysbindin, a novel coiled-coil-containing protein that interacts with the dystrobrevins in muscle and brain. *J Biol Chem* **276**:24232-24241
12659861 Hunt RA, Edris W, Chanda PK, Nieuwenhuisen B, Young KH (2003) Snapin interacts with the N-terminus of regulator of G protein signaling 7. *Biochem Biophys Res Commun* **303**:594-599
12877659 Buxton P, Zhang XM, Walsh B, Sriratana A, Schenberg I, Manickam E, Rowe T (2003) Identification and characterization of Snapin as a ubiquitously expressed SNARE-binding protein that interacts with SNAP23 in non-neuronal cells. *Biochem J* **375**:433-440.
14688250 Benson MA, Tinsley CL, Blake DJ (2004) Myospryn is a novel binding partner for dysbindin in muscle. *J Biol Chem* **279**:10450-10458.
15066994 Morenilla-Palao C, Planells-Cases R, Garcia-Sanz N, Ferrer-Montiel A (2004) Regulated exocytosis contributes to protein kinase C potentiation of vanilloid receptor activity. *J Biol Chem* **279**:25665-25672.
15319443 Chou JL, Huang CL, Lai HL, et al (2004) Regulation of type VI adenylyl cyclase by Snapin, a SNAP25-binding protein. *J Biol Chem* **279**:46271-46279.
15546961 Schaaf CP, Benzing J, Schmitt T, et al (2005) Novel interaction partners of the TPR/MET tyrosine kinase. *FASEB J* **19**:267-269.
15635093 Rüder C, Reimer T, Delgado-Martinez I, et al (2005) EBAG9 adds a new layer of control on large dense-core vesicle exocytosis via interaction with Snapin. *Mol Biol Cell* **16**:1245-1257.
16120643 Chen M, Lucas KG, Akum BF, et al (2005) A novel role for snapin in dendrite patterning: interaction with cypin. *Mol Biol Cell* **16**:5103-5114.
16169070 Stelzl U, Worm U, Lalowski M, et al (2005) A human protein-protein interaction network: a resource for annotating the proteome. *Cell* **122**:957-68.
16189514 Rual JF, Venkatesan K, Hao T, et al (2005) Towards a proteome-scale map of the human protein-protein interaction network. *Nature* 437: 1173-1178.
16330323 Fukui K, Yang Q, Cao Y, et al (2005) The HNF-1 target collectrin controls insulin exocytosis by SNARE complex formation. *Cell Metab* **2**:373-384.
16595180 Yuan X, Shan Y, Zhao Z, Chen J, Cong Y (2006) Interaction between Snapin and G-CSF receptor. *Cytokine* **33**:219-225.
16723744 Zissimopoulos S, West DJ, Williams AJ, Lai FA (2006) Ryanodine receptor interaction with the SNARE-associated protein snapin. *J Cell Sci* **119**:2386-2397.
17043677 Camargo LM, Collura V, Rain JC, et al (2007) Disrupted in Schizophrenia-1 interactome: evidence for the close connectivity of risk genes and a potential synaptic basis for schizophrenia. *Mol Psychiatry* **12**: 74-86.
17088214 Krapivinsky G, Mochida S, Krapivinsky L, Cibulsky SM, Clapham DE (2006) The TRPM7 ion channel functions in cholinergic synaptic vesicles and affects transmitter release. *Neuron* **52**:395-397.
17101137 Wolff S, Stöter M, Giamas G, et al (2006) Casein kinase 1 delta (CK1delta) interacts with the SNARE associated protein snapin. *FEBS Lett* **580**:6477-84.
17552904 Felten A, Leister P, Burgdorf S, Uhlmann L, Scheidtmann KH (2007) Characterization of rat BLOS2/Ceap, a putative yeast She3 homolog, as interaction partner of apoptosis antagonizing transcription. factor/Che-1. *Biol Chem* **388**:569-582.
17577571 Nian H, Fan C, Liao S, et al (2007) RNF151, a testis-specific RING finger protein, interacts with dysbindin. *Arch Biochem Biophys* **465**:157-163.
17684020 Suzuki F, Morishima S, Tanaka T, Muramatsu I (2007) Snapin, a new regulator of receptor signaling, augments alpha1A-adrenoceptor-operated calcium influx through TRPC6. *J Biol Chem* **282**: 29563-29573.
17702749 Mistry AC, Mallick R, Fröhlich O, et al (2007) The UT-A1 urea transporter interacts with snapin, a SNARE-associated protein. *J Biol Chem* **282**:30097-30106.
17947242 Bao Y, Lopez JA, James DE, Hunziker W (2008) Snapin interacts with the Exo70 subunit of the exocyst and modulates GLUT4 trafficking. *J Biol Chem* **283**:324-331.
18167355 Granata A, Watson R, Collinson LM, Schiavo G, Warner TT (2008) The dystonia-associated protein torsinA modulates synaptic vesicle recycling. *J Biol Chem* **283**:7568-7579.
18329849 Sun J, Nie J, Hao B, et al (2008) Ceap/BLOS2 interacts with BRD7 and selectively inhibits its transcription-suppressing effect on cellular proliferation-associated genes. *Cell Signal* **20**:1151-1158.
AfCS Alliance for Cellular Signaling, http://www.afcs.org/

Rodriguez-Fernandez and Dell'Angelica
Supplementary Table 3

Rank	Fly Gene name	Chr.	Protein name (alternative name)	Summary of reported/proposed function[a]	Interacting BLOC-1 subunit	Human Ortholog
1	*Cdlc2 (CG5450)*	2L	Cytoplasmic dynein light chain 2	ATPase microtubule-based motor activity	BLOS1	*DYNLL1*
2	*endoB (CG9834)*	2R	endophilin B	Membrane organization and biogenesis	BLOS2	*SH3GLB1*
3	*Hrs (CG2903)*	2L	HGF-regulated tyrosine kinase	Protein/membrane trafficking, endosomes, synaptic vesicles	Dysbindin	*HGS*
4	*aPKC (CG10261)*	2R	Atypical protein kinase C	Protein kinase	Dysbindin	*PRKIC*
5	*usnp (CG11173)*	2R	ubisnap, SNAP-29	Protein/membrane trafficking, membrane fusion	BLOS2	*SNAP29*
6	*CG14164*	3L			BLOS2	*LSM12*
7	*CG2095*	3R			BLOS2	*EXOC4*
8	*CG18449*	2R			Pallidin	?
9	*CG2774*	2L		Cell communication, intracellular protein trafficking	Pallidin	*SNX2*
10	*CG10263*	2L		Protein and zinc ion binding	Snapin	*CBLL1*
11	*CG10681*	3L			BLOS1	*C19ORF50*
12	*Frq2 (CG5907)*	X	Frequenin 2	Calcium ion binding, vesicle-mediated transport	BLOS1	*FREQ*
13	*CG17570*	2L			BLOS2	?
14	*drk (CG6033)*	2R	downstream of receptor kinase	Signal transduction, multiple functions	BLOS2	*GRB2*
15	*CG15124*	2R			Cappucino	?
16	*CG9951*	3L			Dysbindin, BLOS2	*CCDC22*
17	*CG17599*	X			Dysbindin	?
18	*RhoGAP92B (CG4755)*	3R	RhoGAP92B	GTPase activator, signal transduction	Dysbindin	*ARHGAP17*
19	*Stam (CG6521)*	2L	Stam (Signal transducing adaptor molecule)	Synaptic vesicle endocytosis, involved in JAK-STAT cascade	Pallidin	*STAM*
20	*CG14684*	3R			BLOS1	?
21	*CG4363*	2R			BLOS1	?
22	*CG11436*	X			BLOS2	*TTC17*
23	*kappaB-Ras (CG1669)*	2R	kappaB-Ras	GTP binding, regulation of NF-kappaB cascade	BLOS2	*NKIRAS1*
24	*alphaTub84B (CG1913)*	3R	alpha-Tubulin at 84B	GTP binding, structural constituent of cytoskeleton	BLOS2	*TUBA1A*
25	*CG10750*	2L			Dysbindin	*CCDC42*
26	*CG9170*	X		Protein binding	Dysbindin	*CEP164*
27	*CG13474*	3L			Pallidin	?
28	*Cpr67Fa2 (CG18349)*	3L	Cuticular protein 67Fa2	Structural constituent of chitin-based cuticle	BLOS2	?
29	*CG8736*	2R			BLOS2	?
30	*SIP3 (CG15468)*	X	Syntaxin Interacting Protein 3		Dysbindin	?
31	*CG30428*	2R			Pallidin, BLOS2	?
32	*Traf1 (CG3048)*	2L	TNF-receptor-associated factor 1	Multiple functions	Pallidin	*TRAF4*
33	*CG15710*	2R		Nucleic acid and zinc ion binding	Snapin	*PRDM4*
34	*Bap60 (CG4303)*	X	Brahma associated protein 60kD	Transcription factor	BLOS2, Snapin	*SMARCD1*
35	*CG3548*	2R			BLOS1	?
36	*CG5026*	3L		Inositol or phosphatidylinositol phosphatase activity	BLOS1	*MTMR9*
37	*mub (CG7437)*	3L	mushroom-body expressed	Regulation of altenative nuclear mRNA splicing	BLOS1	*PCBP3*
38	*dei (CG5441)*	3R	delilah	Transcription factor	BLOS2	*ATOH1*
39	*CG8831*	2R		Nucleocytoplasmic transporter activity	Cappucino, Dysbindin, BLOS1	*NUP54*
40	*CG14556*	3R			Cappucino, Dysbindin, BLOS2	?
41	*CG17265*	2L			Dysbindin, BLOS1	*CCDC85A*
42	*CG17778*	X			Dysbindin, Pallidin	?
43	*CG13476*	3L			Dysbindin, Pallidin, BLOS1	?
44	*CG13085*	2L			Dysbindin	?
45	*CG17564*	2L			Dysbindin	*CLUAP1*
46	*CG32809*	X		Nucleotide binding	Dysbindin	*KIAA1217*
47	*ERR (CG7404)*	3L	estrogen-related receptor	Transcription factor, nuclear receptor activity	Dysbindin	*ESRRB*
48	*l(1)G043 (CG14788)*	X	lethal (1) G0431	GTP binding	Pallidin	*LSG1*
49	*sip1 (CG7238)*	2L	septin interacting protein 1	Nucleic acid binding	Pallidin	*TFIP11*
50	*HLH4C (CG3052)*	X	Helix loop helix protein 4C	Transcription factor	Snapin	*HLH1*
51	*CG6770*	2L		Oxidative stress response	Snapin	?
52	*CG7220*	2R		Ubiquitin-protein ligase activity	Snapin	*UBE2W*
53	*CG10466*	2L		RNA binding	BLOS2	*RBMX2*
54	*Dox-A2 (CG10484)*	2L	Diphenol oxidase A2	Endopeptidase activity, phenol processing	BLOS2	*PSMD3*
55	*CG32369*	3L		ATP-dependent peptidase activity, ion and protein binding	Dysbindin, BLOS2	*LONRF3*
56	*CG13032*	3R			Dysbindin	*CCDC13*
57	*CG13993*	2L			Dysbindin	*PFDN1*

58	*CG17744*	3L			Dysbindin	?
59	*mbo (CG6819)*	3R	mbo, members only	Immunity, nuclear export/import, nucleoporin	Dysbindin	*NUP88*
60	*CG7242*	3R	lethal (3) c00064		Dysbindin	?
61	*CG8851*	2L			Dysbindin	?
62	*CG5053*	3R			Pallidin	*RASSF8*
63	*CG9418*	2R		DNA binding, regulation of transcription	Pallidin	*HMG20A*
64	*CG14534*	2L		Nutrient reservoir activity	Snapin	?
65	*RpS20 (CG15693)*	3R	Ribosomal protein S20	Translation, structural component of ribosome	Snapin	*RPS20*
66	*par-1 (CG30131)*	2R	par-1	Multiple function, humoral response and ovum development	Snapin	*MARK3*
67	*tsr (CG4254)*	2R	Twinstar, ADFcofilin, Cofilin	Actin binding	Snapin	?
68	*stau (CG5753)*	2R	staufen	RNA binding	Snapin	*STAU1*
69	*CG8206*	X			Snapin	*DNLZ*
70	*TpnC4 (CG12408)*	2R	TpnC4	Calcium ion binding, ciliary or flagellar motility	BLOS2	?
71	*CG8907*	3R			BLOS2	*EPS8L2*
72	*CG13434*	2R		Chromosome segregation	Dysbindin	?
73	*Srp68 (CG5064)*	3L	Srp68	RNA binding, SRP dependent, co-translational protein	Dysbindin	*SRP68*
74	*CG6156*	3R			Dysbindin	*MCC*
75	*CG7386*	3L		Metallopeptidase, nucleic acid binding	Dysbindin	*LOC730087*
76	*Ag5r2 (CG9540)*	X	Antigen 5-related 2		Pallidin	?
77	*CG4830*	3R		Long-chain fatty acid transporter, metabolism	Snapin	?
78	*Argk (CG32031)*	3L	Arginine kinase	Arginine kinase	BLOS1	?
79	*nop5 (CG10206)*	2L	nop5	Ribosomal RNA processing	BLOS2	*NOP5/NOP58*
80	*CG11698*	3R			BLOS2	?
81	*CG12589*	3R			BLOS2	?
82	*CG13005*	X			BLOS2	?
83	*CG13067*	3L			BLOS2	?
84	*CG15152*	2L			BLOS2	?
85	*crc (CG8669)*	2L	cryptocephal	Transcription factor	BLOS2	*ATF4*
86	*CG14928*	2L			Dysbindin, BLOS1	?
87	*CG14071*	2L			Dysbindin, BLOS2	?
88	*crn (CG3193)*	X	Crooked neck, yolky	Malpighian tubule morphogenesis, development	Dysbindin	*CRNKL1*
89	*CkIIalpha-i3 (CG3217)*	3L	CKII-alpha subunit interactor-3		Dysbindin	?
90	*CG6905*	3L		DNA binding, RNA slipicing factor, spliceosome	Dysbindin	*CDC5L*
91	*Ef1alpha48D (CG8280)*	2R	Elongation factor 1alpha48D	GTP binding, translation	Pallidin	*EEF1A1*
92	*Art7 (CG9882)*	2R	Arginine methyltransferase 7	Methyltransferase	Pallidin	*PRMT7*
93	*CG7757*	3L		Nuclear mRNA splicing	Snapin	*PRPF3*
94	*trsn (CG11761)*	2R	translin	DNA binding	Dysbindin	*TSN*
95	*Mnt (CG13316)*	X	Mnt	DNA binding, phagocytosis, regulation of transcription	Dysbindin	*MNT*
96	*CG6569*	3R			Dysbindin	?
97	*cnn (CG4832)*	2R	centrosomin	Microtubule binding, nuclear division	BLOS1	?
98	*CG2930*	X		Proton-dependent oligopeptide, transmembrane transporter	Dysbindin	*SLC15A2*
99	*CG16528*	3R		GTP binding, tRNA modification	BLOS2	*GTPBP3*
100	*CG5933*	3R		Methyltransferase	Dysbindin	*METTL3*
101	*rad50 (CG6339)*	2R	rad50	DNA repair, chromosome organization and biogenesis	Dysbindin	*RAD50*
102	*CG3726*	X		Transcription factor	BLOS2	?

Footnotes:

[a] As reported on either GeneOntology or the Summary section of NCBI Entrez Gene

References:

(For *HRS* and *rad50*):
PMID = 15710747 Formstecher E, Aresta S, Collura V, Hamburger A, et al (2005) Protein interaction mapping: a *Drosophila* case study. *Genome Res* **15**:376-384.

(For all other candidates):
PMID = 14605208 Giot L, Bader JS, Brouwer C, et al (2003) A protein interaction map of *Drosophila melanogaster*. *Science* **302**:1727-36.

CHAPTER 3

IDENTIFICATION OF GENETIC MODIFIERS OF *DROSOPHILA* AP-3 USING THE BLOOMINGTON DEFICIENCY KIT

ABSTRACT

AP-3 is a heterotetrameric complex important for endosomal protein trafficking and lysosome-related organelle biogenesis. Defects in human AP-3 result in Hermansky-Pudlak syndrome (HPS) type 2. Mutations in the *garnet* gene encoding one component of *Drosophila* AP-3 cause eye pigmentation defects, due to abnormal biogenesis of LROs known as pigment granules. A large-scale screening to identify genetic modifiers of the function of AP-3 in the fly eye was performed. The hypomorphic g^2 mutant line was crossed to 213 lines carrying deficiencies covering most of chromosomes 2, 3 and 4 to screen for chromosomal regions that in hemizygous form modified g^2 pigmentation. Secondary screening and validation uncovered four distinct deletions in chromosomes 2 and 3, which in heterozygous form partially suppressed the g^2 phenotype by increasing red pigmentation by over 50%. Further experiments suggested that the *Gap69C* and *Atg2* genes within two of these regions are modifiers of AP-3.

INTRODUCTION

Drosophila eye pigmentation results from a combination of red (pteridines/drosopterin) and brown (ommochromes/xanthommatin) pigments resulting in a bright red-eye color. The biosynthetic pathway that produces each pigment color is independent of each other. Multiple enzymes are involved. Mutation of a gene encoding an enzyme involved in the pteridines pathway will result in a fly with "brownish" eye color, because of impaired of red pigmentation. In addition to eye pigmentation, flies display pigmentation in other tissues such as the malpighian tubules and testes [1]. Pigments are stored within pigment granules, which are lysosome-related organelles. The discovery and study of over 80 pigmentation mutants in flies have helped in elucidating the genes involved in the synthesis and storage of pigments [2]. The products of these genes are divided in three main categories depending on their mutant phenotype and biological function: (1) enzymes involved in the biosynthesis of red and brown pigments, (2) ABC transporters, and (3) proteins involved in the biogenesis of pigment granules [2]. Proteins encoded by genes such as *cinnabar*, *purple* and *vermilion*, are enzymes necessary for the formation of red or brown pigments. Mutations in these genes affect only one type of pigment and not the other. In the case of the ABC transporter *white*, mutations in this gene affect both red and brown pigment deposition, resulting in a white-eyed fly. The other two ABC transporters *scarlet* and *brown*, form separate hetero-dimers with *white* resulting in brown and red pigment formation, respectively [3,4]. Mutations in the genes comprising the last group, also known as the granule group (e.g. *garnet*, *pink*, *blos1*, *deep orange*, *lightoid*), affect both types of pigments, arguing against a direct role in pigment synthesis [2]. Nevertheless, for many of these genes their exact function in pigment granule biogenesis and potential role in other pathways remains to be elucidated.

One of the eye-color mutants within the granule group is *garnet*, which encodes the δ subunit of AP-3 [5]. Mutations in AP-3 result in HPS type 2 in humans, and in two strains known as pearl and mocha in mice [6]. Human, mice and flies with mutant AP-3 share the same phenotype of abnormal biogenesis of lysosome-related organelles, i.e. abnormal melanosomes in human and mice, and abnormal pigment granules in flies. Due to the amenability of working with fruit flies and the genetic tools available, *Drosophila* serves as a good model to study genetic modifiers of the phenotype (i.e. eye pigmentation defects) cause by AP-3 deficiency of the *garnet* hypomorphic mutant allele (g^2). The identification of genetic modifiers of AP-3 may help to understand normal eye pigmentation and granule biogenesis.

This chapter presents the results obtained in a large-scale screening for genetic modifiers of AP-3 function using the Classic Bloomington Deficiency kit (Dk) and the new Bloomington Dk. At least four genomic regions that partially suppress the *garnet* red pigmentation defect were identified. *Gap69C* and *Atg2*, genes found within two of these regions were further evaluated and deemed to represent potential genetic modifiers of AP-3.

EXPERIMENTAL PROCEDURES

Fly stocks

Flies were raised using standard husbandry procedures [7] and all crosses were carried at 25˚C. The *garnet* (g^2) and Canton-S fly lines were kindly provided by D.Krantz (UCLA). The *ruby* (rb^1) fly line was obtained from Bloomington Stock Center at Indiana University (Bloomington, IN). Fly lines used in the screening carrying a deletion in either chromosome 2 or 3 are part of the Classic Bloomington Deficiency kit (Dk) (http://flystocks.bio.indiana.edu/Browse/df/dfkit_retired_July2009.htm), and fly lines carrying a deletion in chromosome 4 are part of the new Bloomington Dk (http://flystocks.bio.indiana.edu/Browse/df/dfkit-info.htm).

Quantification of eye pigments

Red (pteridines/drosopterin) and brown (ommochromes/xanthommatin) pigments were extracted from fly heads of adults 3-5 days after eclosion and quantified as previously described [8]. Each experiment had a minimum of two replicates per genotype and all controls were quantified in parallel. Results were expressed as percentage of Canton-S pigment content.

Statistical analyses

Statistical analyses were performed using GraphPad Prism 5.0b (GraphPad Software, San Diego, CA, USA).

RESULTS

Initial and secondary screening identified six deficiencies that in hemizygous form modified the AP-3 mutant eye color

A genetic screening was performed using a combination of two collections of fly lines carrying deletions (i.e. deficiencies) in chromosomes 2, 3 and 4. Since the *garnet* gene is located on chromosome X, fly lines carrying deficiencies in this chromosome were not analyzed. The cytologically-defined deficiencies in chromosomes 2 and 3 used in this screening were part of the Classic Bloomington Dk. On the other hand, the deficiencies in chromosome 4 used in the screening were part of the new Bloomington Dk, which only included molecularly-defined deficiencies. Because the Dk collection provided the minimum number of fly lines with the greatest genome coverage, it served as an excellent tool to screen for genetic modifiers that upon loss of one copy affect the AP-3 mutant phenotype (Table 3.1).

The AP-3 modifier screening was divided in three parts: initial screening, secondary screening, and validation (Figure 3.1). The initial screening consisted in setting-up a parental cross (P_0) between males carrying a deficiency (*Df*) over a balancer chromosome, and *garnet* (g^2) females. The eye color of the progeny (F_1), g^2 carrying one copy of the *Df,* was analyzed under a dissecting microscope and compared to that of control flies, in this case g^2. If the eye color seemed different to that of g^2, the P_0 cross was repeated and subjected to a secondary screening involving quantification of red pigments. Arbitrary thresholds were for further analyzing deficiencies that had enhancer effects on g^2 pigments. A suppressor of g^2 would be selected based on an increase in red pigmentation of at least 50% (1.5-fold), and an enhancer of g^2 red pigmentation would be selected based on a decrease in pigmentation of at least 33%. The

validation was performed using molecularly-defined deficiencies that overlapped the region deleted in the original deficiency. The use of overlapping deficiencies had two important purposes. First, it allowed an independent validation of the modifying effect on garnet; and second, provided a simple way to fine-mapping the critical chromosomal region carrying the gene (or genes) capable of modifying g^2 when in hemizygous form.

Out of 213 lines screened, 20 lines were selected for the secondary screening (Figure 3.2). The red pigmentation of g^2 is ~27% of wild type flies known as Canton-S. I found that 7 lines were significantly different from g^2 ($P < 0.001$), but only 6 of these lines, *Df(3L)eyg[C1]*, *Df(2R)CB21*, *Df(3R)Exel6195*, *Df(3L)ED4978*, *Df(2L)XE-3801* and *Df(3L)BSC23* passed the 1.5-fold threshold (Figure 3.2). AP-3 is a protein complex composed of the δ, σ3, β3 and μ3 subunits; in the fly genome these subunits are encoded by the genes *garnet*, *orange*, *ruby* and *carmine*. I asked whether the suppression effect on red pigmentation of these 6 deficiency lines in g^2, replicated in the *ruby* (rb^1) mutant. As expected, all 6 hits exhibited a partial but statistically significant suppression of the rb^1eye color phenotype ($P < 0.001$) (Figure 3.3). Next, I investigated the effect on Canton-S red pigmentation. I found that two deficiencies, *Df(3L)eyg[C1]* and *Df(2R)CB21* did not modify Canton-S eye color phenotype, while the other deficiencies did (Figure 3.4). Since the genes belonging to the pigment granule group affect both red and brown pigmentation, I asked whether I could detect an effect on g^2 brown pigmentation in the presence of a copy of each of the 6 deficiency hits. Brown pigmentation was also affected in flies carrying a copy of 5 out of the 6 deficiency hits. However, the relative effect sizes were smaller than those observed in red (Figure 3.5).

Validation and fine-mapping identified four genomic regions that modified g^2 eye color

For *Df(3L)eyg[C1]*, four smaller deficiencies that overlap the initial deletion were tested (Figure 3.6A). Two overlapping deficiencies that replicated the suppression effect on g^2 red pigmentation ($P < 0.001$) were identified and the critical region was narrowed-down to 12 genes (Figure 3.6 B). Several of the genes in that region have unknown molecular functions, while two (i.e. *eyg* and *toe*) encode transcription factors involved in eye development [9], and one gne known as *Gap69C* encodes an ARF GTPase-activating protein (GAP). [10].

In the case of *Df(2R)CB21*, there were 6 available deficiencies that covered most of the original deletion, but red pigment quantification results showed that none of these deficiencies were able to validate the initial effect on *garnet* (Figure 3.7A). However, due to incomplete coverage of the overlapping deficiencies, there is a region of 19 genes that could not be tested (Figure 3.7B). Similarly, for *Df(3R)Exel6195* two deficiencies that covered most of the entire region except one gene with unknown molecular function known as *CG31145* were found (Figure 3.8). Because these two deficiencies failed to replicate the suppression effect on *garnet* eye color phenotype, additional experiments are required to test whether the initial observation was due to removing a copy of *CG31145* (Figure 3.8).

For *Df(3L)ED4978*, two overlapping deficiencies that completely covered the initial deletion were found, yet red pigment quantification results failed to replicate the initial suppression effect (Figure 3.9). Analogously, *Df(2L)XE-3801* failed to validate using 3 overlapping deficiencies (Figure 3.10).

The effect observed for *Df(3L)BSC23* was successfully validated using two deficiencies that replicated the partial suppression on g^2 red eye color (Figure 3.11A). Using a total of seven

overlapping deficiencies, the critical region was successfully mapped to one containing 6 genes (Figure 3.11B). Among these genes is *Autophagy-specific gene 2* (*Atg2*), which encodes a protein involved in autophagy [11].

The fact that two deficiency hits, *Df(3L)ED4978* (Figure 3.9) and *Df(2L)XE-3801* (Figure 3.10), carried a *mini-white* marker gene and the effects could not be validated using overlapping deficiencies (without *mini-white*); prompted me to ask whether the *mini-white* gene was responsible for the increase in red pigmentation observed initially, i.e., a false positive. Applying the same reasoning I asked the same question about the deficiency hit, *Df(3R)Exel6195* (Figure 3.8) and those overlapping deficiencies used to narrow-down the critical regions for *Df(3L)eyg[C1]* (Figure 3.6) and *Df(3L)BSC23* (Figure 3.11). To test the effect of the *mini-white* marker in each deficiency, I designed genetic crosses to obtain progeny carrying one copy of the deficiency in a *white* (w^{1118}) background. The w^{1118} gene mutation results in white-eyed flies because the lack of white protein prevents the production of red and brown pigments. Results of red pigment quantifications of these progeny are shown in Figure 3.12. I found that the *mini-white* of the *Df* hit *Df(3L)ED4978* leads to the highest amount of red pigments (Figure 3.12, arrow). For the other deficiencies, I found that their *mini-white* gene activity promoted the production of various amount of red pigments ranging from 0% to 14% of Canton-S. These results suggests that at least for *Df(3L)ED4978* the *mini-white* gene was responsible of the suppression effect observed on g^2 red pigmentation, confirming our concern regarding a false positive.

Gap69C as a potential genetic modifier of AP-3

Gap69C emerged as an interesting candidate gene within the critical region of *Df(3L)eyg[C1]* (Figure 3.6). The product of this gene has homology to the human ADP-ribosylation factor (Arf) GTPase-activating protein (GAP) 1encoded by the *ARFGAP1* gene [10,12]. Therefore, *Gap69C* encodes a putative *Drosophila* Arf GAP. Arf GAPs inactivate Arf proteins by promoting GTP hydrolysis, which in turn regulates Arf function in membrane trafficking and actin remodeling [13]. In the case of Arf GAP 1, it shows higher substrate specificity towards Arf1 [13]. Interestingly, Arf1 was found to regulate the recruitment of AP-3 to membranes and of other adaptor protein complexes [5,14].

For the above reasons, I decided to test whether the partial suppression effect detected for *Df(3L)eyg[C1]* could be due to removing one copy of *Gap69C*. To this end, I took advantage of the existence of a loss-of function allele, $Gap69C^{G3\text{-}85}$ kindly provided by Dr. Vladimir Alatortsev [10]. This fly line was crossed to g^2, generating g^2 mutants with one copy of $Gap69C^{G3\text{-}85}$ and then red pigment content was quantified (Figure 3.13). Removing one copy of *Gap69C* in the g^2 background, significantly ($P < 0.0001$) suppresses g^2 red pigmentation defect. This result suggests that *Gap69C* is a genetic modifier of AP-3.

Atg2 as a potential genetic modifier of AP-3

Among the 6 genes within the narrowed-down region of *Df(3L)BSC23* (Figure 3.11) lies an autophagy gene known as *Atg2*. Autophagy is a process used by cells to supply macromolecules under starvation conditions, to eliminate pathogens and to remove protein aggregates [15]. Several sequential steps are required for this process to occur, including

formation of a phagosome around the organelle or proteins to be eliminated, and fusion of the phagosome with the lysosome for degradation of the contents [15]. In humans, more than 30 proteins have been identified to have a role in autophagy and the overall organization of the pathway just started to be elucidated [16]. In yeast, Atg2 and Atg18 forms a complex that is essential for autophagic activity [11].

Unfortunately, a null allele for *Drosophila Atg2* was unavailable. Instead I used the allele $Atg2^{EP3697}$, which disrupts *Atg2* by the insertion of the P-element EP3697, to test the effect on red pigmentation when *Atg2* is disrupted. I found that the presence of one copy of the $Atg2^{EP3697}$ results in a small but statistically significant suppression of g^2 red pigmentation (Figure 3.14). To exclude that the *mini-white* gene marker was responsible for the suppression effect observed for flies carrying the P-element, flies were crossed the w^{1118} background and red pigmentation of the progeny carrying a copy of the P-element was measured. These results exclude a *mini-white* gene effect on pigmentation (Figure 3.14).

DISCUSSION

Drosophila melanogaster serves as a good genetic tool for the screening of modifiers of AP-3. Using commercially available deficiencies, I screened most of *Drosophila* genome by crossing 213 fly lines to the AP-3 hypomorph mutant g^2. The fact that 20 lines passed the initial screening, but only 6 lines passed the secondary screening threshold indicate that most lines were selected based on an eye color difference to g^2 most likely due to affecting brown eye color. Therefore, this screening excluded those deficiencies that mainly affected brown pigmentation. The screening was done this way for two reasons: first, red pigment quantification is a faster and more robust technique than the one used for brown pigments, and second because this laboratory is interested in identifying possible genes involved in granule biogenesis. As it was discussed in the introductory section, genes within the granule group affect both types of pigments [2].

The deficiencies hits, *Df(3L)eyg[C1]*, *Df(2R)CB21*, *Df(3R)Exel6195*, *Df(3L)ED4978*, *Df(2L)XE-3801* and *Df(3L)BSC23* also suppressed *ruby* red pigmentation indicating that the effect observed replicated in more than one AP-3 mutant fly. Two of these lines, *Df(3L)eyg[C1]* and *Df(2R)CB21* did not modified Canton-S red pigmentation arguing in favor towards an AP-3-specific effect. Out of these two deficiencies only one, *Df(3L)eyg[C1]*, also suppressed g^2 brown pigmentation. The effect of *Df(3L)eyg[C1]* on both pigments of g^2 were not equally strong. But this is also observed for genes involved in pigment granule biogenesis. For instance in g^2, red pigments are ~27% Canton-S and brown pigments are ~60% of Canton-S.

Overlapping deficiencies were used as a validation tool and for fine-mapping the genomic region obtained for the six initial hits. This strategy resulted in two regions of 12 and 6 genes. Lack of available overlapping deficiencies did not allowed me to find the critical region

for *Df(2R)CB21*and *Df(3R)Exel6195*. In the case of *Df(3L)ED4978*, I found that none of the overlapping deficiencies validated the initial observation and this was due to the *mini-white* red pigmentation resulting in a false-positive. For *Df(2L)XE-3801* the failure of validation was not due to the *mini-white* red pigmentation since when this was measured the red pigment content was of 0% of Canton-S. The initial deletion was covered completely and two of the overlapping deficiencies, *Df(2L)BSC291* and *Df(2L)BSC233* even covered additional genomic region flanking the original deletion. One possibility is that the original effect in g^2 is due to a genetic interaction between removing one copy of multiple genes at a time. Owing to the fact that *Df(2L)XE-3801* deletes 77 genes (as of Flybase FB12_04, released July 6th, 2012). This possibility was not tested with the overlapping deficiencies used and will need further investigation.

The *Df(3L)eyg[C1]* region was narrowed-down to one carrying 12 genes. Within this region is *Gap69C*, encoding a putative *Drosophila* Arf GAP. This gene was an intriguing candidate owing to the role of Arf Gaps in membrane trafficking and actin remodeling [13]. Previous evidence indicates that ARF1, the protein inactivated by Arf Gap, is important in the regulation of AP-3 and other adaptor protein complexes [5,14]. Little is known about *Gap69C* function, and loss-of-function mutants have no apparent phenotype suggesting functional redundancy with other Arf Gaps [10]. My results demonstrating that removing one copy of *Gap69C* using the loss-of-function allele $Gap69C^{G3\text{-}85}$ suppressed the g^2 red color phenotype are exciting. This would indicate that the original effect observed in *Df(3L)eyg[C1]* was pinpointed to one gene, therefore *Gap69C* emerges as modifier of AP-3.

Another genetic modifier of AP-3 is *Atg2*, encoding an autophagy gene. This gene was found within the narrowed-down region of *Df(3L)BSC23*. I found that *garnet* flies carrying a

copy of the P-element *EP3697* mimicked the suppression effect of *Df(3L)BSC23* on red pigmentation. I considered the possibility that the effect observed was due to the presence of the *mini-white* gene marker, but this was excluded since the *mini-white* red pigment levels were barely detectable. Autophagy requires multiple steps including the formation of a phagosome or isolation membrane, which have been proposed to fused with endosomes to provide the machinery needed for lysosome fusion [15]. AP-3 is involved in the protein transport from endosomes to lysosomes in fibroblasts, and to lysosome-related organelles in specialized cells [17]. Marino *et al*. found that AP-3 and BLOC-1 levels were reduced in tissue from $Atg4b^{-/-}$ and $Atg5^{-/-}$ knockout mice and in cells treated with an autophagy inhibitor, suggesting that disrupting autophagy affects the stability of these protein complexes [18]. Taking into account these findings and the results presented here, one potential mechanism in the *Drosophila* eye is that when you disrupt AP-3 there is misorting of one or many of the proteins involved in pigmentation, including white [4]. If we take white protein to exemplify this point, AP-3 mutations results in the misorting of white. The misorting of white, results in its abnormal accumulation at a compartment "X." This white accumulation is removed from the cell by autophagy, resulting in a fly eye with pigmentation phenotype observed in g^2 flies. When both AP-3 function and the autophagy pathway are impaired, the accumulation of white protein is not eliminated by autophagy. The misorted white proteins get delivered to the pigment granules by an alternative pathway resulting in the suppression the g^2 pigmentation defect. A potential involvement between AP-3 function with the autophagy pathway deserves attention.

Table 3.1. General information about the Bloomington Deficiency kit (Dk) used and the initial screening hits.

As of July 20, 2009 (a year after this screening was done) this collection is denoted as the Classic Bloomington Dk which consists mostly of cytologically-defined, except for lines in chromosome 4 (^), which are molecularly-defined deletions.

Chromosome arm	Number of euchromatic genes*	Number of bands	Minumum number of bands deleted	% of coverage minimum	Number of stocks available	Number of stocks screened	Initial screening hits
2L	2,765	804	762	94.8	58	57**	7
2R	3,089	1132	1053	93	53	44**	6
3L	2,845	884	817	92.4	56	53	4
3R	3,535	1178	1113	94.5	56	53	3
4	88	N/A^	N/A^	94.3^	7	6	0
Total	12,322	N/A	N/A	N/A	230	213	20

*Number of euchromatic genes in Drosophila genome as of March 26, 2011, Bloomington Stock Center, Indiana University.
**An initial Dk screening on chromosome 2 was done by Veronica T. Cheli, former postdoctoral fellow in this laboratory.
N/A, not applicable

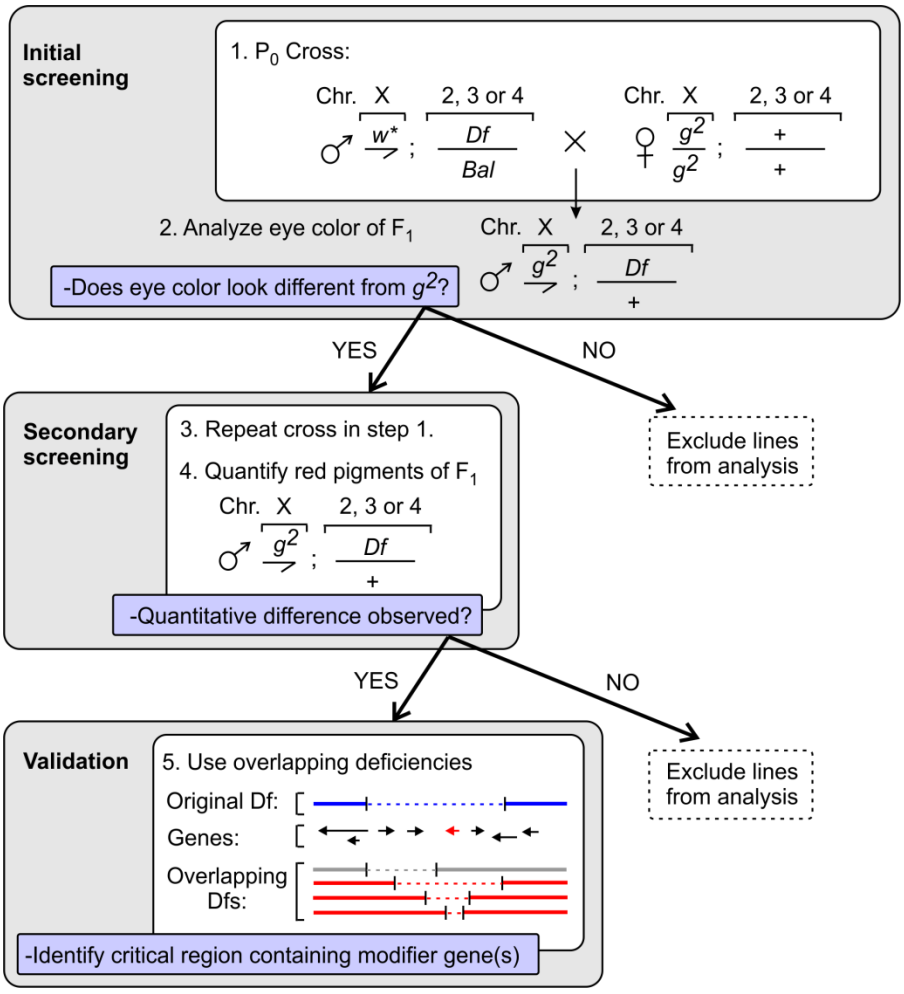

Figure 3.1. Schematic representation of the AP-3 modifier screening using the Dk collection of fly lines. (1) The initial screening consisted in setting-up parental (P_0) crosses between males carrying a deficiency (*Df*) over a balancer (*Bal*) chromosome, and females *garnet* (g^2). A total of 213 lines with *Df's* in chromosome (Chr) 2, 3 or 4 were screened. (2) The eye color of the progeny (F_1) g^2 carrying one copy of the *Df* was analyzed under a dissecting microscope. (4) If the eye color seemed different from that of g^2, the P_0 cross was repeated a subjected to a secondary screening involving quantification of red pigments. (5) Validation was done for those lines with quantitative differences in red color compared to g^2. If in the original deficiency (blue lines) a group of genes (black and red arrows) was deleted and this caused an effect on g^2 red color, then overlapping deficiencies (gray and red lines) were used to identify the gene(s) causing this effect.

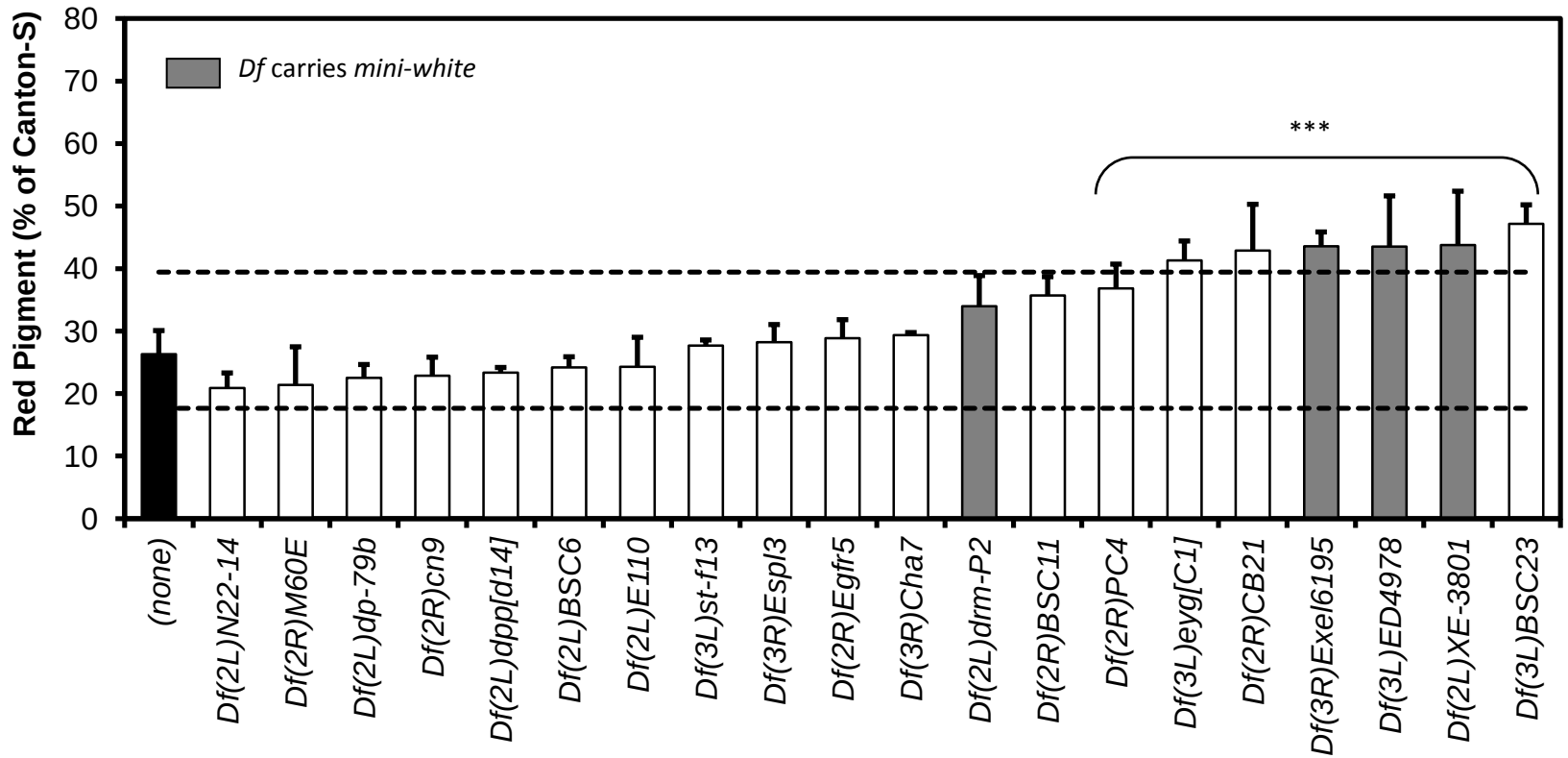

Figure 3.2. Secondary screening using Dk lines selected from the primary screen. Dk screening resulted in 20 lines that when in heterozygous form exhibit a distinct eye color compared to *garnet* (g^2). When the effect in red pigmentation was measured, only 6 lines were suppressing the *garnet* eye color phenotype by at least 50% (upper dashed line). No enhancer below 33% of g^2 red pigment was identified (lower dashed line). Bars represent mean+SD. One-way ANOVA followed by Dunnett's test comparing flies heterozygous for the *Df* to g^2 control: ***$P < 0.001$.

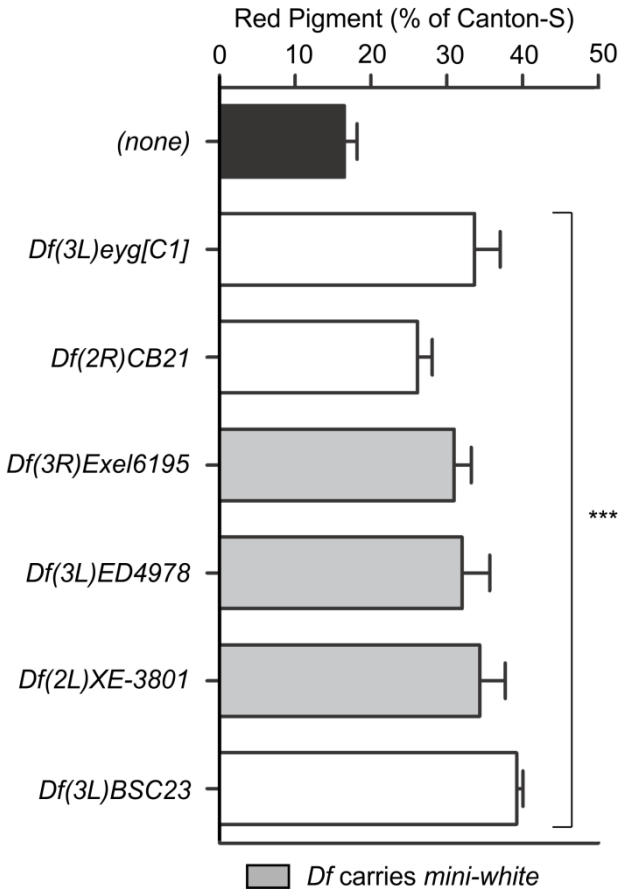

Figure 3.3. Effects of deficiency lines resulting from the secondary screen on *ruby* eye color. The effect in *ruby* (rb^1) red pigmentation was measured for the 6 lines that suppressed *garnet* eye color phenotype and found that they also exhibited a significant suppression in *ruby* eye color phenotype. Bars represent mean+SD. One-way ANOVA followed by Dunnett's test comparing flies heterozygous for the *Df* to rb^1 control: ***$P < 0.001$.

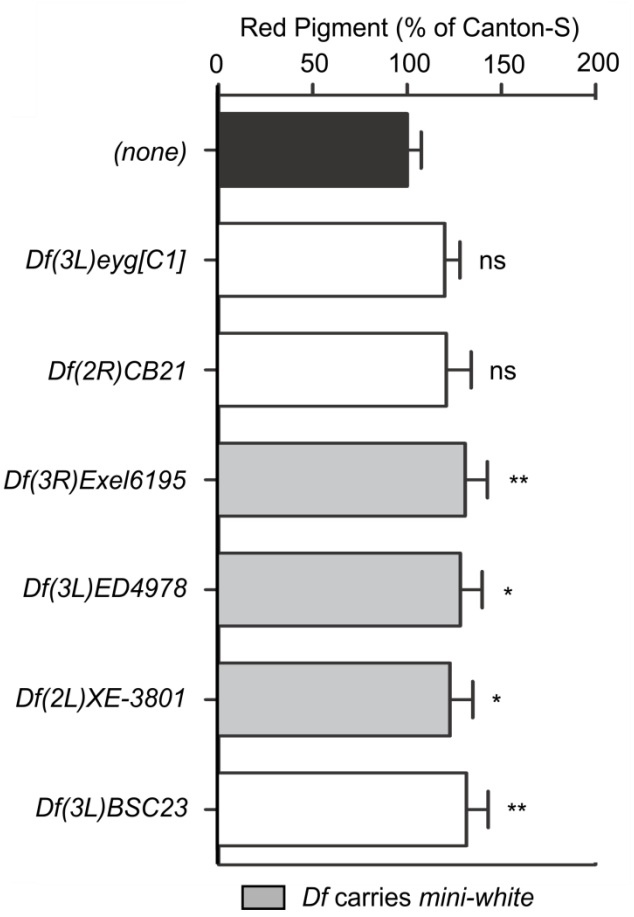

Figure 3.4. Effects of deficiency lines resulting from the secondary screen on wild-type eye color. The effect on wild-type (Canton-S) red pigmentation was measured for the 6 lines that suppressed *garnet* and *ruby* eye color phenotype. Bars represent mean+SD. One-way ANOVA followed by Dunnett's test comparing flies heterozygous for the *Df* to Canton-S control: * $P < 0.05$, ** $P < 0.01$, and *** $P < 0.001$. ns, not significant.

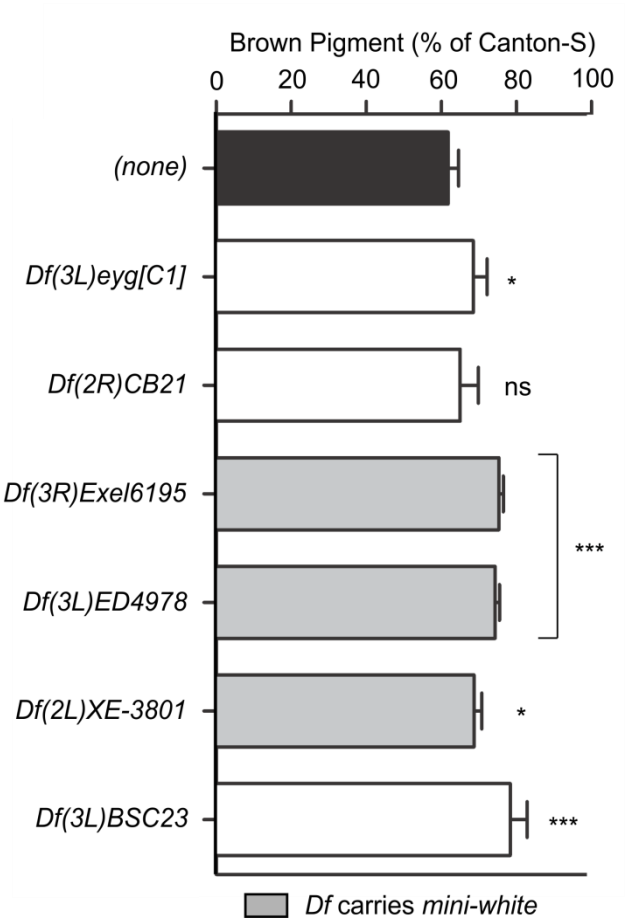

Figure 3.5. Five deficiency lines hits also modified *garnet* brown eye color. The effect in g^2 brown pigmentation was measured for the 6 lines that suppressed *garnet* and *ruby* red eye color phenotype. Bars represent mean+SD. One-way ANOVA followed by Dunnett's test comparing flies heterozygous for the *Df* to g^2 control: * $P < 0.05$, ** $P < 0.01$, and *** $P < 0.001$. ns, not significant.

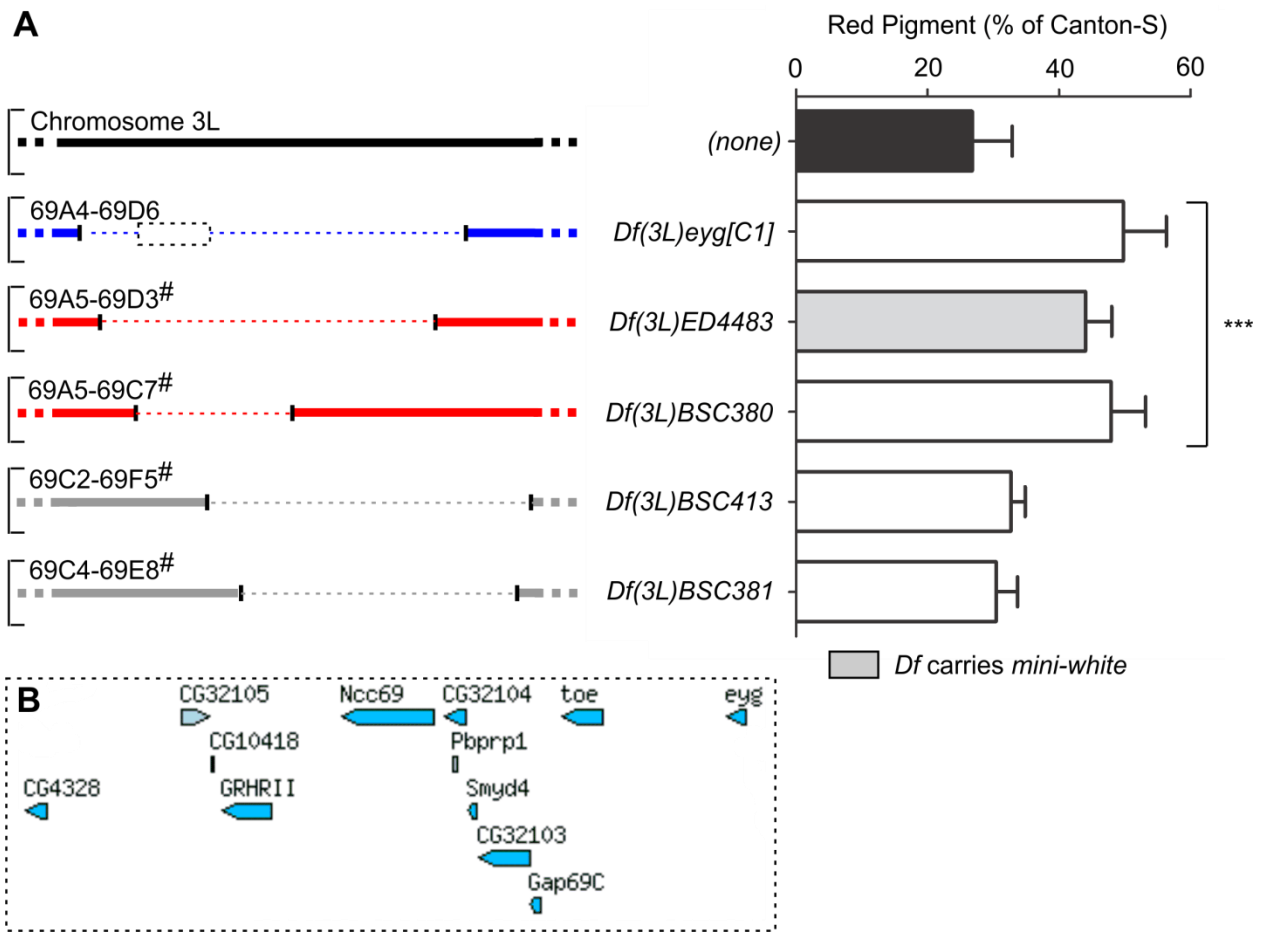

Figure 3.6. Validation and fine-mapping of the critical region mediating the modifier effect first observed for *Df(3L)eyg[C1]*. (A) Scheme representing a normal chromosome 3L (black line), the deficiency *Df(3L)eyg[C1]* obtained in the screening (blue lines), and four overlapping *Dfs* (red and gray lines). Dashed lines represent the deleted segment (cytological location is indicated), and # symbol represents a molecularly defined deletion. Red pigment of *garnet* flies with one copy of the indicated deficiency was quantified. Bars represent Mean+SD. One-way ANOVA followed by Dunnett's test comparing flies heterozygous for the *Df* to g^2 control:***$P < 0.001$. Two *Df* validated the initial observation (red lines) whereas two others did not (gray lines). The critical region was thus narrowed-down to 12-genes (depicted as a dashed box). (B) Scheme adapted from FlyBase (version FB2012_04, released July 6th, 2012) [19] of the 12 genes located at chromosome 3L from ~12.284056Mb to 12.461121Mb.

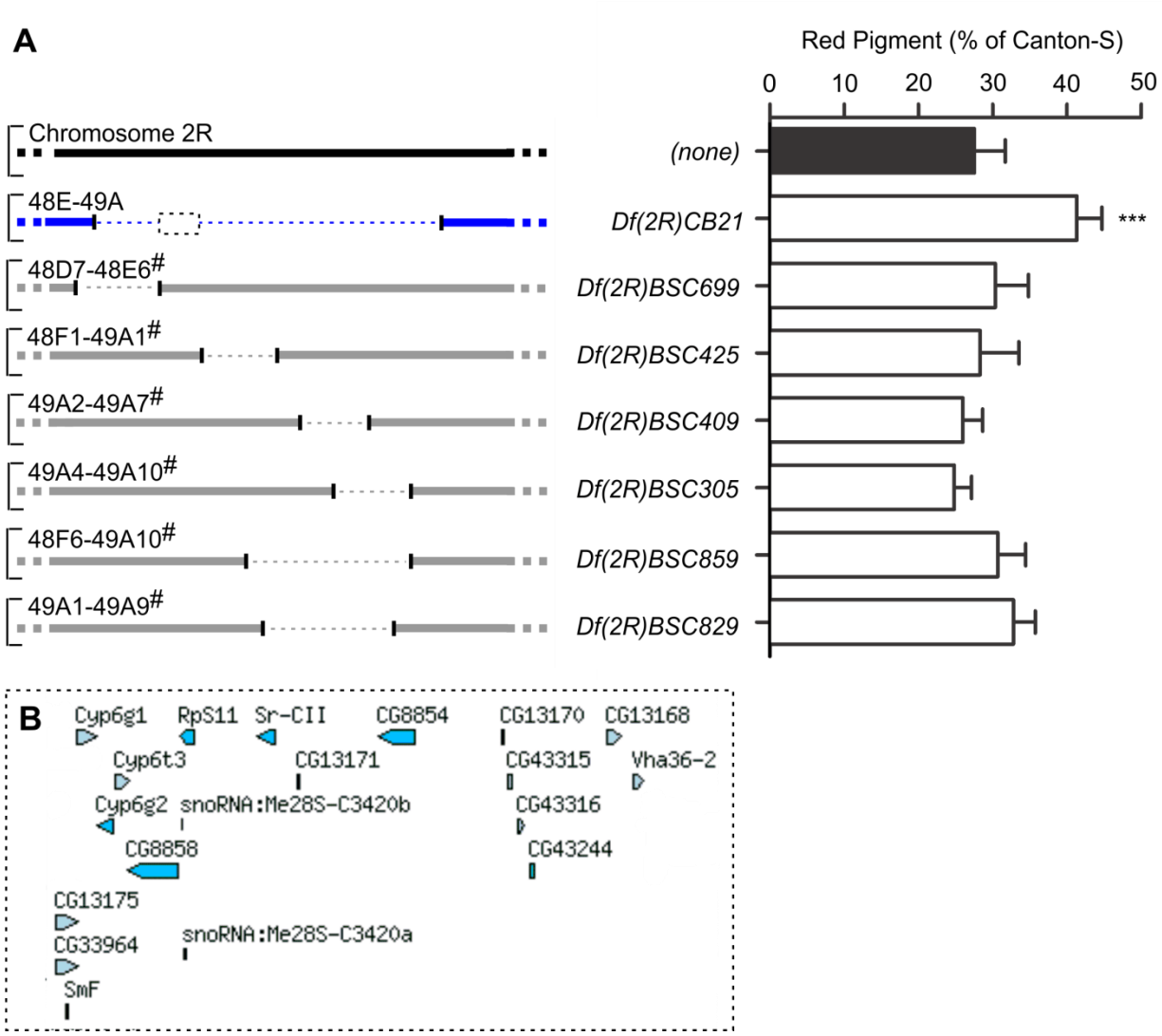

Figure 3.7. Attempts to validate the modifier effect first observed for *Df(2R)CB21*. (A) Scheme representing a normal chromosome 2R (black line), the deficiency *Df(2R)CB21* obtained in the screening (blue lines), and six overlapping *Dfs* (gray lines). Dashed lines represent the deleted segment (cytological location is indicated), and # symbol represents a molecularly defined deletion. Red pigment of *garnet* flies with one copy of the indicated deficiency was quantified. Bars represent Mean+SD. One-way ANOVA followed by Dunnett's test comparing flies heterozygous for the *Df* to g^2 control: ***$P < 0.001$. None of the *Df* validated the initial observation (gray lines). (B) However, a 19-gene region (depicted as a dashed box in A) shown here using an scheme adapted from FlyBase [19], located at chromosome 2R from ~8.070144Mb to 8.146157Mb remains to be tested, because it was not covered by any of the deficiency lines available.

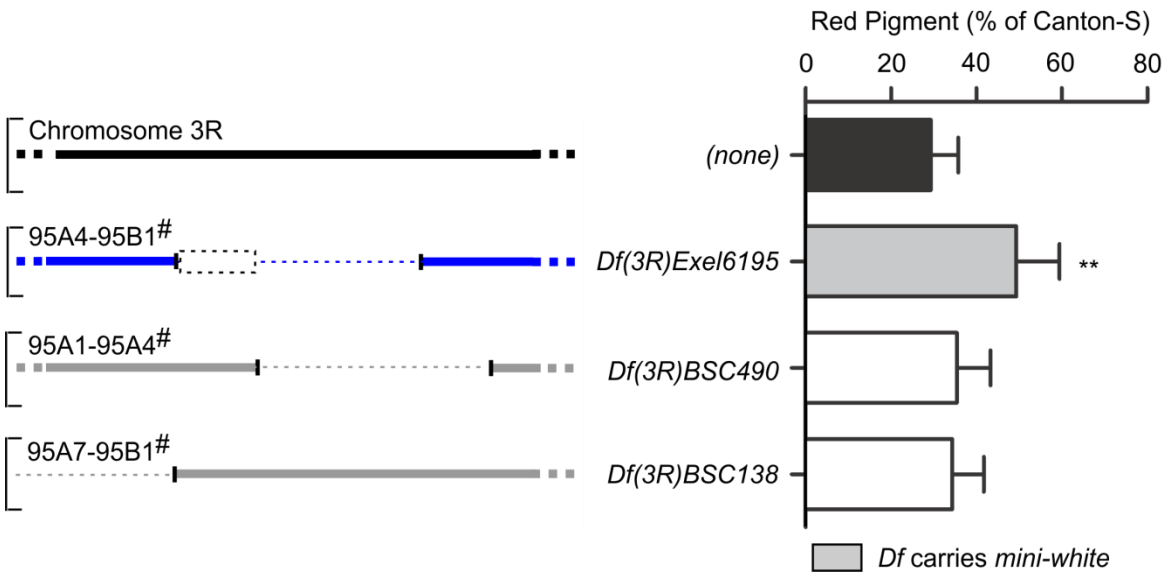

Figure 3.8. Attempts to validate the modifier effect first observed for *Df(3R)Exel6195*. Scheme representing a normal chromosome 3R (black line), the deficiency *Df(3R)Exel6195* obtained in the screening (blue lines), and two overlapping *Dfs* (gray lines). Dashed lines represent the deleted segment (cytological location is indicated), and # symbol represents a molecularly defined deletion. Red pigment of *garnet* flies with one copy of the indicated deficiency was quantified. Bars represent Mean+SD. One-way ANOVA followed by Dunnett's test comparing flies heterozygous for the *Df* to g^2 control: $^{**}P < 0.01$. None of the *Df* validated the initial observation (gray lines). However, a region containing gene *CG31145* (depicted as a dashed box) located at chromosome 3R from 19.431473Mb to 19,495,378Mb remains to be tested.

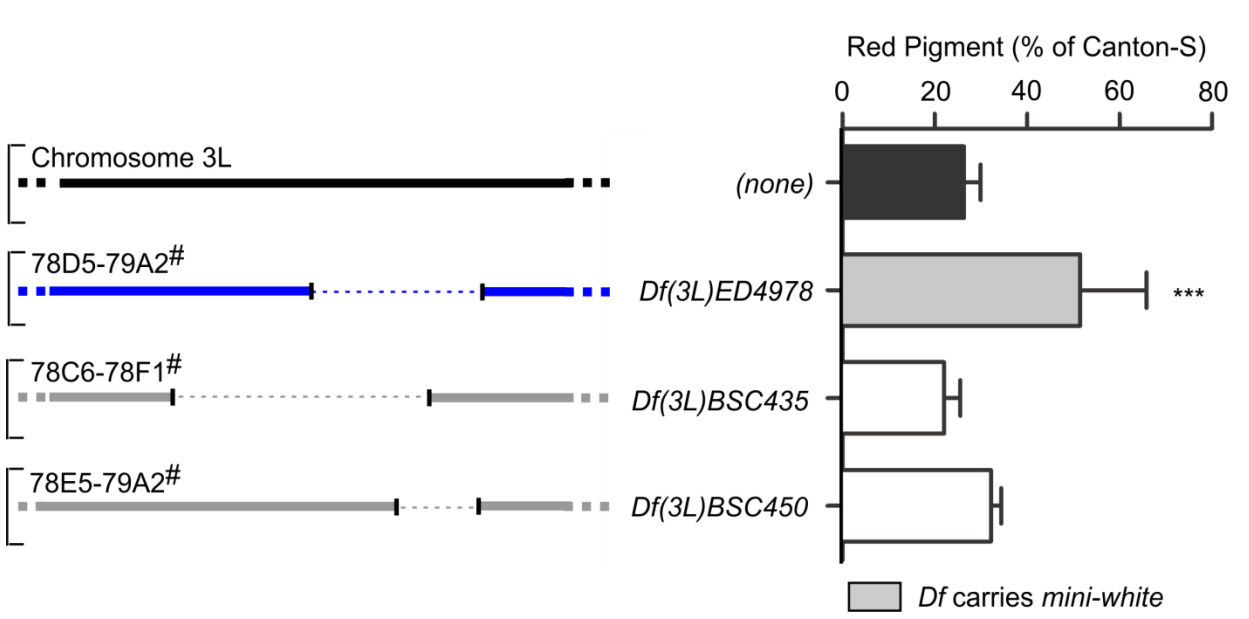

Figure 3.9. Failure to validate the effects observed for *Df(3L)ED4978* . Scheme representing a normal chromosome 3L (black line), the deficiency *Df(3L)ED4978* obtained in the screening (blue lines), and two overlapping *Dfs* (gray lines). Dashed lines represent the deleted segment (cytological location is indicated), and # symbol represents a molecularly defined deletion. Red pigment of *garnet* flies with one copy of the indicated deficiency was quantified. Bars represent Mean+SD. One-way ANOVA followed by Dunnett's test comparing flies heterozygous for the *Df* to g^2 control was used as statistical analysis. ***$P < 0.001$.

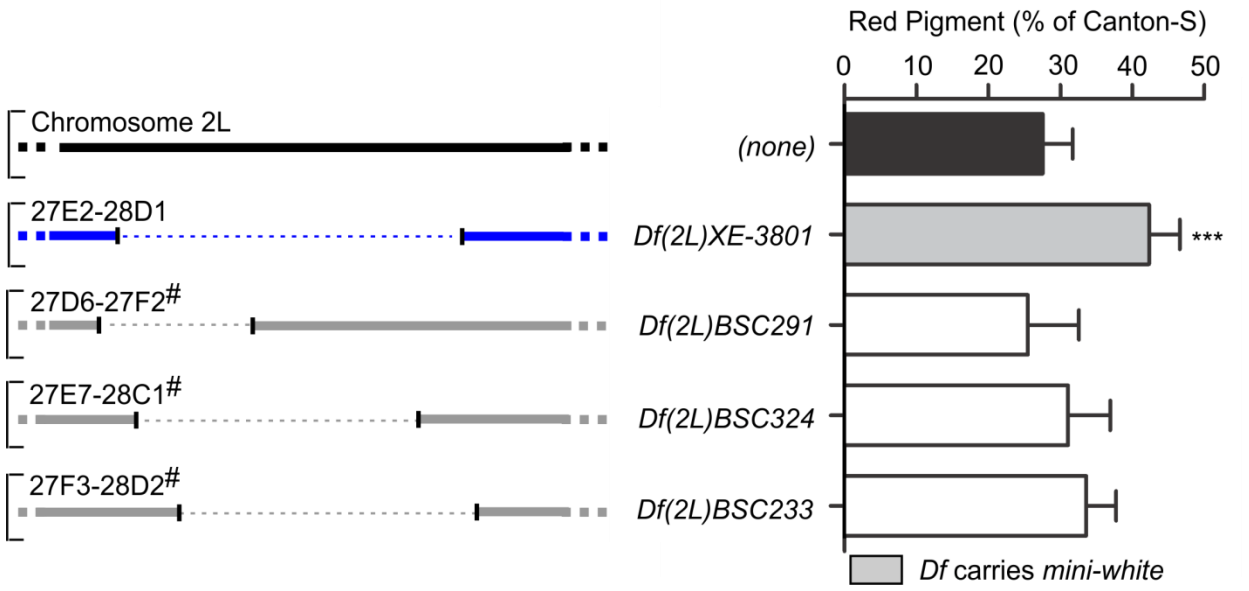

Figure 3.10. Failure to validate the effects observed for *Df(2L)XE-3801*. Scheme representing a normal chromosome 2L (black line), the deficiency *Df(2L)XE-3801* obtained in the screening (blue lines), and three overlapping *Dfs* (gray lines). Dashed lines represent the deleted segment (cytological location is indicated), and # symbol represents a molecularly defined deletion. Red pigment of *garnet* flies with one copy of the indicated deficiency was quantified. Bars represent Mean+SD. One-way ANOVA followed by Dunnett's test comparing flies heterozygous for the *Df* to g^2 control: ***$P < 0.001$.

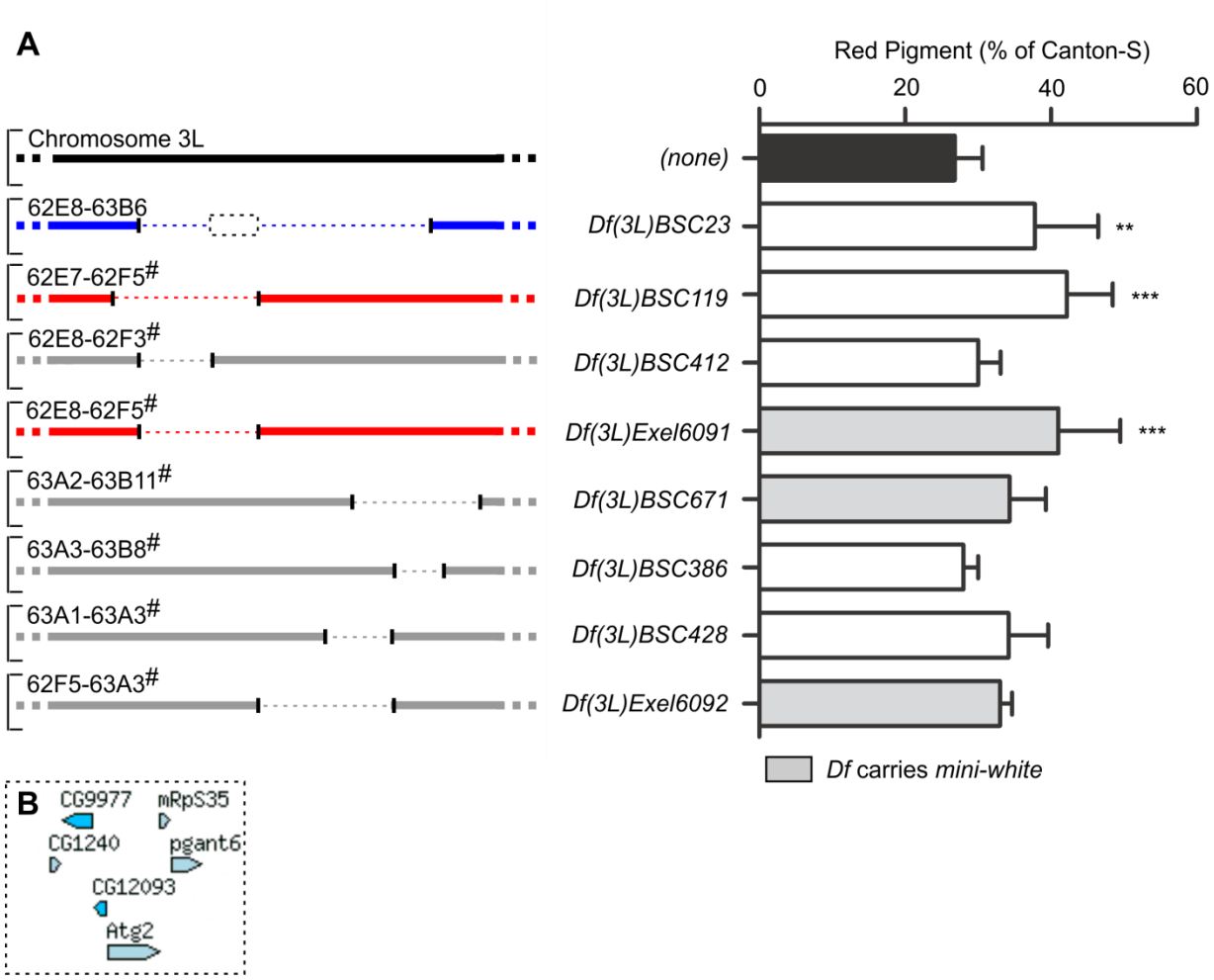

Figure 3.11. Validation and fine-mapping of the critical region mediating the modifier effect first observed for *Df(3L)BSC23*. (A) Scheme representing a normal chromosome 3L (black line), the deficiency *Df(3L)BSC23* obtained in the screening (blue lines), and seven overlapping *Dfs* (red and gray lines). Dashed lines represent the deleted segment (cytological location is indicated), and # symbol represents a molecularly defined deletion. Red pigment of *garnet* flies with one copy of the deficiency indicated was quantified. Bars represent Mean+SD. One-way ANOVA followed by Dunnett's test comparing flies heterozygous for the *Df* to g^2 control: $^{**}P < 0.01$, $^{***}P < 0.001$. Two *Df* validated the initial observation (red lines) whereas four others did not (gray lines). The critical region was narrowed-down to 6 genes (depicted as a dashed box). (B) Flybase.org scheme of the 6 genes located at chromosome 3L from ~2.656263Mb to 2.821245Mb.

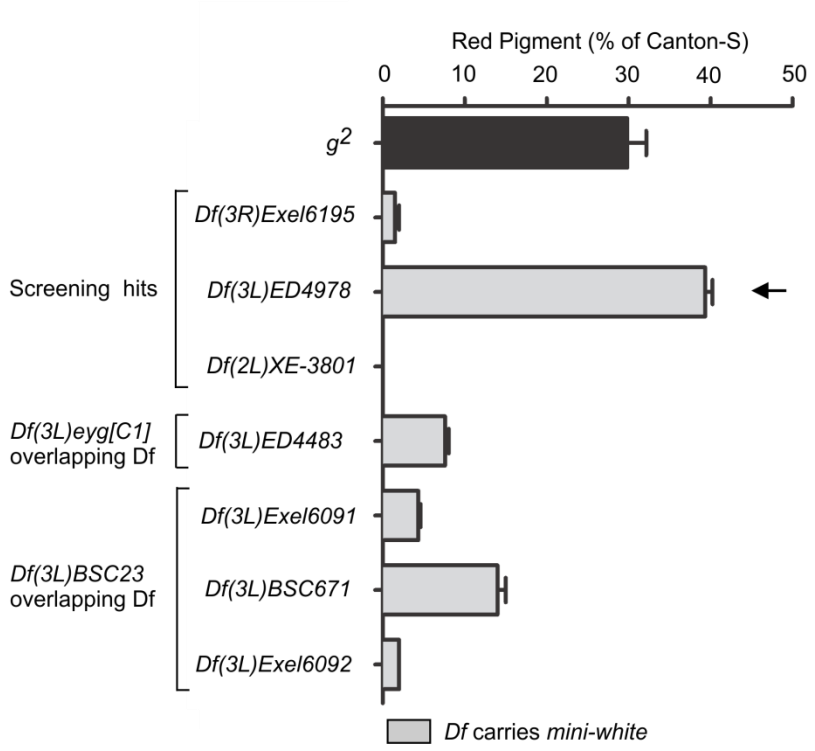

Figure 3.12. Red pigment levels of the *mini-white* gene marker carried by deficiencies was compared to *garnet.* The three screening hits carrying *mini-white Df(3R)Exel6195*, *Df(3L)ED4978*, and *Df(2L)XE-3801*; and four overlapping *Dfs* used to validate hits *Df(3L)eyg[C1]* and *Df(3L)BSC23*; were crossed to *white* flies to obtain white-eyed progeny with one copy of the *Df* carrying *mini-white*. The red eye pigmentation was quantified and compared to that of g^2. Bars represent Mean+SD. Note that the *mini-white* marker of *Df(3L)ED4978* produces ~10% more pigment than g^2 (arrow).

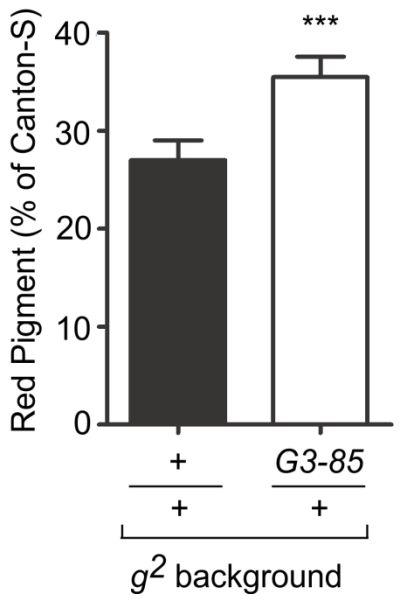

Figure 3.13. Removal of one copy of *Gap69C* partially suppressed *garnet* red color pigmentation. A genetic cross was designed to obtain flies g^2 carrying one copy of a null allele of *Gap69C* ($Gap69C^{G3\text{-}85}$). Red pigmentation was quantified and compared to g^2. Bars represent Mean+SD. Student t-test: ***$P < 0.0001$.

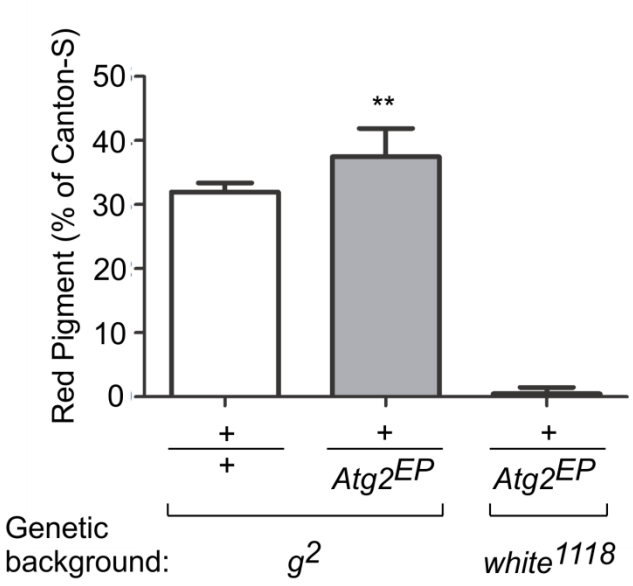

Figure 3.14. Red pigmentation phenotype of *garnet* flies was modified by one copy of the insertion mutant allele *Atg2*^{EP3697}. A genetic cross was generated to obtain g^2 or *white*^{1118} flies with one copy of the *Atg2*^{EP3697} allele (indicated as *Atg2*^{EP}). Red pigmentation was quantified and compared to g^2. Bars represent Mean+SD. Student t-test comparing *garnet* carrying or not one copy *Atg2*^{EP}: ***$P < 0.0001$.

REFERENCES

1. Mackenzie SM, Howells AJ, Cox GB, Ewart GD (2000) Sub-cellular localisation of the white/scarlet ABC transporter to pigment granule membranes within the compound eye of Drosophila melanogaster. Genetica 108: 239-252.

2. Lloyd V, Ramaswami M, Kramer H (1998) Not just pretty eyes: Drosophila eye-colour mutations and lysosomal delivery. Trends Cell Biol 8: 257-259.

3. Ewart GD, Howells AJ (1998) ABC transporters involved in transport of eye pigment precursors in Drosophila melanogaster. Methods Enzymol 292: 213-224.

4. Lloyd VK, Sinclair DA, Alperyn M, Grigliatti TA (2002) Enhancer of garnet/deltaAP-3 is a cryptic allele of the white gene and identifies the intracellular transport system for the white protein. Genome 45: 296-312.

5. Ooi CE, Moreira JE, Dell'Angelica EC, Poy G, Wassarman DA, et al. (1997) Altered expression of a novel adaptin leads to defective pigment granule biogenesis in the Drosophila eye color mutant garnet. EMBO J 16: 4508-4518.

6. Huizing M, Helip-Wooley A, Westbroek W, Gunay-Aygun M, Gahl WA (2008) Disorders of lysosome-related organelle biogenesis: clinical and molecular genetics. Annu Rev Genomics Hum Genet 9: 359-386.

7. Greenspan RJ (1997) Fly pushing: the theory and practice of *Drosophila* genetics. New York: Cold Spring Harbor Laboratory Press.

8. Falcon-Perez JM, Romero-Calderon R, Brooks ES, Krantz DE, Dell'Angelica EC (2007) The Drosophila pigmentation gene pink (p) encodes a homologue of human Hermansky-Pudlak syndrome 5 (HPS5). Traffic 8: 154-168.

9. Yao JG, Weasner BM, Wang LH, Jang CC, Weasner B, et al. (2008) Differential requirements for the Pax6(5a) genes eyegone and twin of eyegone during eye development in Drosophila. Dev Biol 315: 535-551.

10. Frolov MV, Alatortsev VE (2001) Molecular analysis of novel Drosophila gene, Gap69C, encoding a homolog of ADP-ribosylation factor GTPase-activating protein. DNA Cell Biol 20: 107-113.

11. Obara K, Sekito T, Niimi K, Ohsumi Y (2008) The Atg18-Atg2 complex is recruited to autophagic membranes via phosphatidylinositol 3-phosphate and exerts an essential function. J Biol Chem 283: 23972-23980.

12. Bernards A (2003) GAPs galore! A survey of putative Ras superfamily GTPase activating proteins in man and Drosophila. Biochim Biophys Acta 1603: 47-82.

13. Randazzo PA, Hirsch DS (2004) Arf GAPs: multifunctional proteins that regulate membrane traffic and actin remodelling. Cell Signal 16: 401-413.

14. Robinson MS, Bonifacino JS (2001) Adaptor-related proteins. Curr Opin Cell Biol 13: 444-453.

15. Mizushima N (2007) Autophagy: process and function. Genes Dev 21: 2861-2873.

16. Behrends C, Sowa ME, Gygi SP, Harper JW (2010) Network organization of the human autophagy system. Nature 466: 68-76.

17. Theos AC, Tenza D, Martina JA, Hurbain I, Peden AA, et al. (2005) Functions of adaptor protein (AP)-3 and AP-1 in tyrosinase sorting from endosomes to melanosomes. Mol Biol Cell 16: 5356-5372.

18. Marino G, Fernandez AF, Cabrera S, Lundberg YW, Cabanillas R, et al. (2010) Autophagy is essential for mouse sense of balance. J Clin Invest 120: 2331-2344.

19. McQuilton P SPS, Thurmond J and the FlyBase Consortium (2012) FlyBase 101 - the basics of navigating FlyBase. Nucleic Acids Res 40: D706-714.

CHAPTER 4

ROLE OF *DROSOPHILA* RABEX-5 IN TISSUE ORGANIZATION AND THE IMPORTANCE OF ITS RAB5-ACTIVATION FUNCTION

ABSTRACT

Endocytosis regulates many important ligand-induced signaling events that control cell proliferation and tissue growth. Vesicles formed by this process are moved, docked and fused to an acceptor membrane with the aid of multiple proteins. Of particular interest is the family of small GTPases known as Rabs. By acting as molecular switches, Rabs "label" the membranes where effectors and other proteins bind to promote vesicle docking and fusion. Rab5 is crucial in the early endosomal trafficking events. To exert its role, Rab5 needs to be activated by GEFs (Guanine nucleotide exchange factors) such as Rabaptin-5-associated exchange factor for Rab5 (Rabex-5). This chapter describes the generation of a loss-of-function allele of *Drosophila melanogaster Rabex-5* (*Rbx5*^{ex1}). Homozygous mutant flies do not survive to adulthood, have an extended larval period, and eventually die as abnormal prepupae. Growth abnormalities in brain and wing imaginal discs were uncovered. Increased Mmp1 levels were detected in mutant wing imaginal discs as an indication of tissue neoplastic transformation. In the brain, abnormalities in the number of neuroepithelial cells and neuroblasts of the outer optic anlage were found. The mutant phenotype was rescued by ubiquitous expression of wild-type Rabex-5 but not of a catalytically inactive Rabex-5 variant, suggesting that the adult lethality observed is due to impaired Rab5 activation. These results demonstrate that *Drosophila* Rabex-5 is encoded by a neoplastic tumor suppressor gene.

INTRODUCTION

The canonical view of how endocytosis regulates signal transduction is by signal attenuation, involving the internalization and transport of ligand-bound receptors to the lysosome for degradation [1,2]. Recent evidence suggests that, after a ligand-bound receptor has been internalized, signaling may persist within the endosomal compartment in what is termed as the "signaling endosome" [3]. Beyond the idea of the signaling endosome, additional roles of endocytosis and endosomal protein trafficking on signal propagation and amplification have emerged. For instance, the number of receptors found at the plasma membrane, and the transport to specific regions of the cell achieving polarized functions, are controlled by recycling of the receptors to the plasma membrane. Additionally, in the case of epidermal growth factor receptor (EGFR) and transforming growth factor-β (TGF-β) receptor, clathrin-mediated internalization promotes receptor recycling thus signal sustainment, whereas non-clathrin-mediated endocytosis promotes receptor degradation resulting in signal attenuation [1,3]. In other cases, such as in the Notch signaling pathway, endocytosis of Delta, Serrate and LAG-2 is necessary for ligand activation and thus Notch signaling [1,4].

Endosomal protein trafficking is controlled and regulated by the action of Rabs, proteins of a large family of small GTPases [5]. Rabs are reversibly associated to membranes by C-terminal geranylgeranyl groups and localize to distinct membranes. These proteins exert their function by acting as molecular switches, going from an active (GTP-bound) to an inactive (GDP-bound) state. Conversion between states is achieved by a Guanine nucleotide exchange factor (GEF), which catalyses the exchange of GDP by GTP, and by a GTPase-activating protein (GAP), which stimulates GTP hydrolysis. When active, Rabs "label" the membrane where effectors and other proteins get recruited to exert their function in docking and fusing vesicles

[5]. Rabs are highly conserved across species; there are 60 described Rabs in human and 31 in flies [5,6].

Rab5 has been shown to be the master regulator of early endosomal biogenesis [7]. *In vivo* Rab5-knockdown in mouse liver below a critical level resulted in reduction of the number of early endosomes, late endosomes and lysosomes [7]. Additionally, Rab5 mutations were associated to lung and liver cancer [3]. In mammals, there are three isoforms of Rab5 (Rab5A, Rab5B and Rab5C) with at least seven different GEF proteins and over 20 different effectors, some of which are shared among other Rabs [8]. The common structural feature of Rab5 GEFs is the presence of the VPS9 domain, which contains the GEF catalytic core [5,8]. The fruit fly, *Drosophila melanogaster* contains only one Rab5 and four different VPS9-domain-containing proteins [8]. In *Drosophila*, a null mutation in Rab5 results in early larval lethality and tissue-specific null ablation result in tissue overgrowth [9,10].

This laboratory is interested in understanding the physiological role of Rabaptin-5-associated exchange factor for Rab5 (Rabex-5), which is one of the GEF of Rab5 [11]. Preliminary evidence from Marta Starcevic, a former graduate student in the laboratory, suggested a potential physical interaction between BLOC-1 and Rabex-5. Later, Veronica T. Cheli, former postdoctoral fellow, found a potential genetic interaction between the gene encoding the σ3-subunit of AP-3 and *Rabex-5* in flies. The current model of how Rabex-5 functions in endosomal docking/fusion events is defined as follows: (1) Rab5-GDP (inactive state) is delivered to the membrane where Rabex-5 activates Rab5 by facilitating nucleotide exchange to Rab5-GTP, which is stabilized by the Rabex-5/ Rabaptin-5 complex. (2) Activated Rab5 recruits a tethering factor and Rab5 effector, known as EEA1, which mediates vesicle docking by interacting with syntaxin-13. (3) Syntaxin-13 association with other SNARE proteins

results in vesicle fusion [12]. In addition to the VPS9 domain, Rabex-5 has a ZnF domain that displays ubiquitin ligase activity. It has been shown that Rabex-5 binds ubiquitin, and this binding is essential for the recruitment of Rabex-5 to endosomal membranes [13]. In this chapter, results demonstrating that *Rabex-5* is a neoplastic tumor suppressor gene are presented.

EXPERIMENTAL PROCEDURES

Fly stocks

Flies were raised using standard husbandry procedures [14]. Crosses were carried at 25˚C except when stated otherwise. The *Drosophila* lines used in this study are listed in Table 4.1. Two control lines were used based on the genetic background of the experimental lines: *yw* or *Ub-Gal4*.

Mutagenesis by imprecise excision

To generate mutant alleles of the *Rabex-5* gene in *Drosophila*, imprecise excision mutagenesis was done using the fly line EP681. Both P-elements carried in the EP681 fly line (*P{EP}CG9139*^{EP681a} and *P{EP}slmb*^{EP681b}) were excised using the Δ2-3 transposase as previously described [15,16]. All lines were analyzed by PCR followed by agarose gel electrophoresis. Deletion in *Rabex-5* was analyzed by PCR and sequencing. Precise excision of *P{EP}slmb*^{EP681b} was verified by PCR and sequencing of only those lines that had an apparent deletion in *Rabex-5*. Genomic DNA of heterozygous fly lines (excision chromosome over a *TM6* balancer chromosome) was analyzed by PCR using a set of primers in which the forward primer (5'-AGCTGTAAGAGTTGAACGC-3') was unable to hybridize to the expected genomic region in the balancer chromosome likely due to sequence mismatches.

Larvae staging

All larvae staging was done in a set-up designed and established together with Veronica T. Cheli. Experiments were performed using either of two methods: (1) placing the parents in a plastic beaker attached to a food plate (Falcon 60 mm diameter x 15 mm height) or (2) placing the parental cross on a plastic vial glued to a modified petri dish lid and placed on a food plate (Falcon 35 mm diameter x10 mm height). Fly parental crosses (known as P_0) were placed on the set-up used during a period of 48-72 h of acclimatization and then passed to a new food plate. For each new food plate, egg-laying was allowed for 4-6 h before removing the parental flies. Freshly hatched larvae were collected during a window of 2 h and placed on a new food plate ("day 0" time-point) and staged until the desired age. All experiments were staged together to its control and placed in 25˚C temperature-controlled room or incubator.

Immunostaining

Staged larvae were dissected in phosphate-buffered saline (PBS), fixed using 3.7% formaldehyde in PBS for 30 min at room temperature, and then washed three times with PBS. Tissues (e.g. brain, salivary glands and imaginal discs attached to the larva mouth-hooks) were blocked for 1 h at room temperature in 10% Goat Serum (GS) in PBST [PBS with 0.4% Triton X-100 (Sigma-Aldrich, St. Louis, MO, USA)]. Primary antibody was diluted in PBST and incubated with the tissues for 2 h at room temperature or overnight at 4˚C. After four 15 min washes with PBST, tissues were incubated for 2 h at room temperature or overnight at 4˚C with secondary antibodies diluted in 10% GS in PBST. Tissues were washed for 15 min four times with PBST and then washed once with PBS. If DNA staining was used, then after the last PBS wash tissues were

incubated for 10 min in Hoechst 33342 (trihydrochloride, trihydrate; Molecular Probes, Eugene, OR, USA) diluted 1:1000 in PBS and washed with PBS for 15 min before mounting. All tissues were whole-mounted in Vectashield (Vector Laboratories, Burlingame, CA, USA) using two coverslips (0.17-0.25mm thick) covered by a third coverslip on top (as a "bridge") to prevent flattening the three-dimensional structure.

Primary antibodies were used at the following concentrations: mouse anti-Mmp1 1:50 (1:1:1 mixture of 5H7B11, 3B8D12, 3A6B4 antibodies ([17], Developmental Studies Hybridoma Bank, University of Iowa, Iowa City, IA, USA; mouse anti-tubulin 1:20 (Developmental Studies Hybridoma Bank); guinea pig anti-Dpn 1:1000 (kind gift from A. Brand, University of Cambridge, Cambridge, UK) and rat anti-DE-Cadherin 1:200 (DCAD2, Developmental Studies Hybridoma Bank). The following conjugated secondary antibodies were used at a 1:400 dilution: donkey anti-mouse-Cy3; Donkey anti-rat-Alexa488 and rabbit anti-mouse Alexa488 (Molecular Probes). Donkey anti-guinea pig-Cy3 antibody was used in a 1:1000 concentration (Jackson ImmunoResearch Laboratories West Grove, PA, USA).

Fluorescence and confocal microscopy

Immunostained *Drosophila* tissues were visualized using fluorescence microscopy using an Olympus Spinning Disc Confocal Inverted Microscope (IX81), equipped with a CCD camera (Hamamatsu ORCA-ER) and analyzed with the SlideBook^{TM} 4.1 image analysis software (Intelligent Imaging Innovations, San Diego, CA).

Confocal images of whole brain hemispheres and optic lobes were captured using a Zeiss LSM 700 Imager M2 (40x Oil objective with Zoom: 0.5) and analyzed using the ZEN 2009 software (Carl Zeiss Inc.). Z-stacks were taken at 2 µm intervals.

Neuroepithelial cell and neuroblast quantification

Series of confocal Z-stacks images from control and *Rbx5*^{ex1} brain hemispheres were saved using a "blind-code" and given to a experienced observer (unaware of the code); this observer then saved these images using another "blind-code" and gave these new files to a second observer to analyze (also unaware of the code). The analysis was done using ImageJ (National Institutes of Health) and consisted of the following steps: (1) Only one brain hemisphere was counted per brain; (2) from each Z-stack the "best" optical slice was selected, based on the ability of detecting the neuroepithelium (NE) to neuroblast (NB) transition; (3) all quantifications were done on 2 separate slices, the one before and the one after the considered "best" slice; (4) the number of NE and NB (from each side of the optic lobe) were counted using the ImageJ Cell Counter plug-in (National Institute of Health); and (5) NE thickness was measured in these two slices by drawing a straight line from the apical to basal side of the cell using the DE-Cadherin staining as guide using the ImageJ measurement tool. Measurements obtained by these two blind-observers were pooled, averaged per brain, and then de-codified and analyzed. Statistical analyses were done using GraphPad Prism 5.0b (GraphPad Software, San Diego, CA, USA).

Immunoblotting and densitometry analysis

For Mmp1 immunobloting analysis, larvae were dissected on a Sylgard plate on top of ice using the following procedure: one larva at a time was placed in cold PBS, cut at ¾ of its length (from anterior side) and dissected to remove the gut and extra fat. Per genotype, 10 dissected larvae were homogenized in 100 µl of Laemmli sample buffer, and the resulting lysate was incubated at 65˚C and 95˚C for 5 min each and cleared by centrifugation at 13,000 x *g*. Monoclonal antibody against Mmp1 (described above) was used in a 1:100 dilution. Monoclonal Anti β-actin antibody (1:10000, Clone AC-15, Sigma-Aldrich) was used as loading control.

Mmp1 levels normalized to actin levels were analyzed by densitometry analysis using ImageJ. Briefly, three films were scanned, one for actin expression and two for Mmp1 levels (long and short exposures). Each β-Actin and Mmp1 band was measured using the same area in both *yw* and $Rbx5^{ex1}$ samples lanes. Each band was measured a minimum of two times and corrected by its respective averaged background. Mmp1 levels were calculated within an immunoblot-set containing one lane for *yw*, three lanes for $Rbx5^{ex1}$ (5, 10 and 12 days old) larvae extracts, by calculating the ratio of the signal in each lane to the sum of all signals. The same was done to calculate β-Actin signal. In order to normalize Mmp1 signal to actin signal, a ratio of Mmp1 signal to actin signal per sample was calculated. These ratios were analyzed by 1-way ANOVA using GraphPad Prism 5.0b.

Larvae counting and statistical analysis

Larvae were staged as previously explained with the following exceptions: (1) the parental cross was not discarded but was passed to fresh food plates (35 mm diameter x 10 mm height) every 24 h a maximum of eight times and (2) to facilitate this process the lid of a small dish (with a hole made) was glued to a vial, this allowed changing the food plate easily without anesthetizing the P_0 cross. Because we found that larvae expressing Rab5(S43N) were sensitive to food dryness, mostly resulting from under-crowding conditions, large P_0 crosses (e.g. 25 females and 24 males) were set-up in smaller food plates. Crosses were designed to yield larvae with the same *w, ub-Gal4* genetic background and to have 50% or ~67% of the population carrying the *TM6B,* p^{Xp} Tb^{1} balancer chromosome (observed in larvae by a Tubby phenotype). Total number of larvae were counted at day 1 and day 4. The observed/expected ratio was calculated per cross by taking the number of larvae (non-Tubby) at day 4 and dividing it by the total number of larvae at day 1 (Tubby and non-Tubby). Then, that value was multiplied to 2 (if the expected frequency of non-Tubby larvae was 50%) or by 3 (if the expected frequency of non-Tubby larvae was 33%). A minimum of 12 independent plates were generated per cross. Observed/expected ratios were analyzed by a 2-way ANOVA using GraphPad Prism 5.0b.

RESULTS

Generation of a loss-of-function allele for *Rabex-5*

To better understand the physiological function of Rabex-5, a reverse-genetics approach was undertaken. Taken advantage of the availability of the EP^{681} fly line, which carries the EP^{681a} P-element inserted at the 5'-untranslated region (5'-UTR) of *Rbx5*, mutagenesis by imprecise excision was performed. However, this fly line carried a second P-element (EP^{681b}) inserted at the 5'-UTR of the *slmb* gene. Using the Δ2-3 transposase [15,16], both EP^{681a} and EP^{681b} were excised to generate 165 fly lines that showed no activity of *mini-white*, an eye-color marker carried by both P-elements. Initial screening for *Rabex-5* deletions was done by PCR using primers flanking the EP^{681a} insertion site (Figure 4.1A, blue arrows). One hundred and fifty-eight lines homozygous for the excision chromosome displayed no change in *Rbx5* genomic DNA, indicating that the EP^{681a} P-element excised in a precise manner. Only 7 out 165 lines were lethal in homozygous form and kept as heterozygous lines. After PCR and gel electrophoresis analysis, I found that the heterozygous line 37A, herein called $Rbx5^{ex1}$, amplified a smaller genomic region (less than 1.65 kb) than expected (2.164 kb) (Figure 4.1B). This suggested a deletion caused by imprecise excision. Precise excision of the second P-element EP^{681b} was verified by PCR.

Because line $Rbx5^{ex1}$ was lethal in homozygous form, the imprecise excision chromosome was kept over the *TM6B*, p^{Xp} Tb^{1} balancer chromosome (short name: TM6). Contrary to expected for PCR analysis of genomic DNA extracted from heterozygous lines, only one DNA fragment (<1.65 kb) was amplified using the combination of primers R1 and R3 and no wild-type DNA fragment was amplified. I designed a fly cross to obtain offspring carrying this TM6 chromosome over the *Df(3L)ED202* deficiency (a 0.5-Mb deletion that includes the

m*Rbx5* gene) and confirmed that no DNA fragment was amplified from the TM6 chromosome. This unexpected finding allowed me to quickly sequence the *Rbx5* genomic region in the $Rbx5^{ex1}$ chromosome using the line in heterozygous form (i.e. over TM6). DNA sequencing revealed that the $Rbx5^{ex1}$ imprecise excision line carries a 32-bp insertion and a 793-bp deletion that removes 2 exons and a portion of the third, including the start codon. The 32-bp insertion represented a remaining fragment of the P-element. Because $Rbx5^{ex1}$ carries a deletion that removes the start codon, this fly line is considered a loss-of-function mutant of *Rabex-5*.

The $Rbx5^{ex1}$ mutation results in early adult lethality

Viability of homozygous $Rbx5^{ex1}$ flies was determined by quantifying the number of adult flies 24 h after eclosion. Genetic crosses between $Rbx5^{ex1}$ heterozygous flies (one copy $Rbx5^{ex1}$ over TM6) were designed to yield 66.7% heterozygous and 33.3% homozygous $Rbx5^{ex1}$ flies based on prior knowledge of the early lethality of homozygous TM6 flies. To test whether temperature could have an effect on adult viability, experiments were done using 18˚C and 25˚C as rearing temperatures. Crosses reared at 18˚C yield a total of 290 heterozygous flies and no homozygous. Similarly, crosses reared at 25˚C yield a total of 257 heterozygous flies and no homozygous. Therefore, under the conditions tested, $Rbx5^{ex1}$ homozygous flies do not survive to adulthood (Figure 4.2).

To test whether adult lethality was caused by affecting Rabex-5 function or by a second-site mutation, the viability of flies carrying one copy of the $Rbx5^{ex1}$ allele over the deficiency *Df(3L)ED202* (described above) was assayed. In this case, I designed a cross expected to yield 50% flies hemizygous $Rbx5^{ex1}$ carrying one copy of the deficiency (*ex1/Df*), and 50% flies heterozygous over the TM6 balancer (*TM6/Df*) (Figure 4.3). At 25˚C, all adults were *TM6/Df*.

To document the stage at which *Rbx5*^{ex1} mutants were dying, control and mutant flies were examined through development, starting from newly-hatched larvae. Normal development of *Drosophila melanogaster* is a well documented process, and the number of days that it takes an embryo to grow into an adult fly depends on the rearing temperature [14]. Under the experimental conditions used, controls flies reared at 25˚C had a life cycle of about 10 days. After egg-hatching, the larval stage lastsed ~5 days divided into 1st, 2nd and 3rd instar. Then larvae transformed into pupae for ~4 days and after which adult eclosed from the pupal case (Figure 4.4).

Rbx5^{ex1} mutant flies at 3 days old (2nd instar larvae) and 5 days old (late 3rd instar larvae) seemed morphologically normal. (Figure 4.2A-B). At 7 days, control flies entered the pupal stage but *Rbx5*^{ex1} mutants were still in larval stage. Two days later, *Rbx5*^{ex1}mutants displayed a "giant larvae" phenotype (Figure 4.2C). Eventually, 13-day-old *Rbx5*^{ex1}mutants died as abnormal prepupae (Figure 4.2E). The formation of melanotic tumors seen as dark spot under the pupal case was also noticed (Figure 4.2F)

Rbx5^{ex1} adult lethality can be rescued by ubiquitous transgenic expression of *Rabex-5*

To rescue *Rbx5*^{ex1}early adult lethality, Veronica Cheli, a former postdoctoral fellow in the laboratory generated three independent transgenic lines (*UAS-Rbx5* Line1, Line 3 and Line 5) for expression of wild type Rabex-5 using the yeast *GAL4/UAS* system. Briefly, the Upstream Activator Sequence (*UAS*) is an enhancer to which the transcription factor GAL4 binds to activate transcription. The expression of a gene of interest (cloned downstream of *UAS*) can be controlled in a temporal and spatial fashion depending on the expression pattern of *GAL4* [18]. Ubiquitin-Gal4 (*Ub-Gal4*) was used to drive ubiquitous expression of Rabex-5 from *UAS-Rbx5*

lines 1, 3 and 5, in genetic crosses designed to yield 33.3% homozygous *Rbx5*^{ex1} mutant flies (Figure 4.5). Viability of adult flies was quantified within 24 h of eclosion and expressed as an observed/expected ratio of *Rbx5*^{ex1} flies normalized by the total number of progeny. The ubiquitous expression of all three transgenes rescued *Rbx5*^{ex1}adult lethality (Figure 4.5A). No overall morphological defect was observed in rescued adult flies as compared to control (Figure 4.5B). Together with the results shown in Figures 4.2 and 4.3, these results indicate that the lethality observed in *Rbx5*^{ex1} flies is due to the absence of Rabex-5 and not due to a second-site mutation.

Rbx5^{ex1} mutant larvae show tissue abnormalities

When the internal morphology of the *Rbx5*^{ex1} mutant larvae was examined, multiple tissues were found to be affected, including the wing imaginal discs. Wing imaginal discs are epithelial sacs found in larvae that eventually develop into the adult fly wing [19]. From 20-50 cells set aside during embryogenesis, proliferation occurs during larval stages giving rise to 20,000-50,000 cells. This proliferation stops as hormonal changes promote entry into the pupal stage [20]. Wing imaginal discs serve as a good model for studying the mechanisms behind tissue size determination and growth control [19,20,21].

To study the overall morphology of *Rbx5*^{ex1} mutant wing imaginal discs, tissues were dissected from staged larvae at 5, 10 and 12 days after larvae hatching and stained for DNA (Figure 4.6A-D). Five-day-old mutant wing discs were noticeably smaller than age-matched controls (Figure 4.6B). Ten- and 12-day old mutant wing discs showed an increase in tissue size, particularly becoming a "spherical" tissue (instead of a flat tissue like in control larvae) with an apparent loss of the normal organization (Figure 4.6C-D). I next tested the possibility that these

mutant wing discs could be expressing the Matrix Metalloproteinase 1 (Mmp1), which is a known neoplastic transformation marker in flies (Figure 4.6E-H) [17,22]. Based on published Northern Blot analysis, Mmp1 expression is normally restricted to a small band of cells in the wing imaginal discs [17]. The immunostaining did not show detectable levels of Mmp1 protein in controls wing discs (Figure 4.6E). In contrast, mutant wing discs from 5-, 10- and 12-day old larvae displayed high levels of Mmp1 (Figure 4.6F-H). To examine this observation further, I analyzed Mmp1 expression by immunoblot analysis of larval extracts (Figure 4.7). Five-day-old control and 5-, 10- and 12-day-old mutant larval extracts were prepared as explained in the *Experimental Procedures* section; normalization was first done using Coomassie staining and then by β-actin signal. Mmp1 was detected in all samples with the highest levels in the mutant larval extracts (Figure 4.7A). To quantify these effects, three immunoblots were subjected to densitometry analysis. Statistical analysis showed a significant increase in Mmp1 levels for 5-day-old ($P < 0.0001$) and 10-day-old ($P < 0.05$) mutant larval extracts, but not for the 12-day-old time point (Figure 4.7B).

Another tissue considerably affected in the $Rbx5^{ex1}$ mutant larvae was the brain (Figure 4.8). Whole-mount bright-field images of five-day-old mutant larvae revealed a significant smaller brain compared to age-matched controls (Figure 4.8A-B). At later stages (10 and 12 days) mutant brains were larger and, like in the case of the wing imaginal discs, there was a loss of tissue organization (Figure 4.8C, B). At the latest staged examined (12 days) mutant brains were harder to dissect due to their irregular shape (e.g. brain lobes of different sizes, big brain lobes, longer ventral ganglion) and their apparent "fusion" with the imaginal discs surrounding them.

The small size of the *Rbx5*^{ex1} brain hemispheres at 5 days of age suggested a potential developmental delay. One possibility was that at earlier larval stages *Rbx5*^{ex1}mutants had immature but morphologically normal brains; and later in their development the brains became abnormal, particularly the optic lobe. The *Drosophila* optic lobe is the structure of the brain that in the adult fly will integrate the primary visual information coming from the compound eye [23]. The optic lobe is a highly organized and complex structure composed of two distinct epithelial proliferation centers: outer optic anlage (also known as the outer proliferation center) and the inner optic anlage (also known as the inner proliferation center) [24].These centers give rise to distinct neuronal layers known as the medulla, lamina and lobula [23,24]. Of particular interest is the region of neuroepithelial to neuroblast (NE-NB) transition (or NE-NB conversion) which is found within the medial outer optic anlage and is important for the formation of the distal medulla. Briefly, NE-NB transition occurs during the 2nd instar larva stage when symmetrically dividing neuroepithelial cells transition into asymmetrically dividing medulla neuroblasts [23,24]. These neuroblasts will give rise to a self-renewing neuroblast and one ganglion mother cell that divides again into two medulla neurons [25]. Late in larval and early pupal stages, the pools of neuroepithelial cells get depleted as a consequence of the formation of neuroblasts [23].

To examine the optic lobe structure of *Rbx5*^{ex1} mutant, particularly at the NE-NB transition zone, I decided to do an immunostaining of brains at 5, 7, 8 and 9 days of age with anti-DE-cadherin (a marker for neuroepithelial cells) and anti-Dpn (a marker for neuroblasts) [24]. As shown in Figure 9A, G, in a normal 5-day-old (late 3rd instar) brain the NE-NB transition could be clearly identified using these two markers. At 5 days, mutant optic lobes seemed morphologically normal but derived from a younger larva (perhaps at the end of 2nd/early

3rd instar) with a neuroepithelium capable of transitioning into neuroblasts (Figure 9B, H). Nevertheless, the thickness of the neuroepithelium was larger than expected (Figure 9N). At 7 days, mutant optic lobes had grown considerably. Additionally, a great number of neuroblasts were observed without a decrease in the number of neuroepithelial cells, and the neuroepithelium thickness remained abnormally large (Figure 9C, I, O). At 8 days, I observed the same phenotypes seen at 7-day-old (Figure 9D, J, P). Mutant brains at 9 days of age showed the highest variability of phenotypes, including the number of neuroblasts and neuroepithelial cells per brain as well as overall morphology. Figures 9E-R shows examples of two mutant brains. Although the size of both brains was similar, Brain 1 had fewer neuroblasts than Brain 2; both brains had abnormally high number of neuroblasts compared to control. Differences in the number of neuroepithelial cells, neuroblasts and neuroepithelial thickness were quantified (Figure 4.10). Quantitative differences are in agreement with the observations made for the immunstaining experiment. Note that the increased thickness of the neuroepithelium (based on Z-stacks images) suggests that there were multiple layers of NE cells in contrast to a single layer in control brains; therefore, the number of these cells was probably underestimated.

Structure-function analysis of Rabex-5 reveals that its Rab5-activation activity is important for fly viability

An interesting question was regarding which domain or domains in Rabex-5 protein were necessary for rescuing the *Rbx5*^{ex1} adult lethality, and tissue abnormalities observed. To address this question, Veronica Cheli (former postdoctoral fellow in this laboratory) made the following transgenic constructs: (a) Rabex-5 wild type (WT); (b) Rabex-5 ΔZnF, containing a deletion in amino acids 1-47 that includes the Zinc-finger (ZnF) domain, which binds ubiquitin and displays

Ub protein ligase (E3) activity; (c) Rabex-5 EET-VPS9, a truncated protein containing amino acids 81-400 harboring the Early endosomal targeting domain (EET) that includes a helical bundle (HB) and the VPS9 domain that, together with the HB domain, forms the Rab5/Rab21Guanine nucleotide exchange factor (GEF) catalytic core; (d) Rabex-5 ΔCT, a deletion of the C-terminal (CT) region that includes a proline-rich motif (LPxPLxPxV); (f) Rabex-5 Δ[L-CH-CT]), a deletion of the linker (L) region and the C-terminal helical (CH) containing the Rabaptin-5-binding site, and CT; and (g) Rabex-5 (D316A), Rabex-5 with substitution of apartic acid 316 to alanine resulting in a GEF inactive mutant (Figure 4.11, Top). The design of these constructs was mostly based on experiments done using the human counterpart of Rabex-5 by the group of Juan S. Bonifacino and data from Zhu *et al.* [13,26]. Each transgenic construct was inserted at the same chromosomal position 58A using the ΦC31-based integration system [27].

Using the GAL4/UAS system, the ability of these constructs to rescue the homozygous $Rbx5^{ex1}$ adult lethality was tested after driving their expression ubiquitously using *Ub-Gal4* driver. Genetic crosses were designed to yield 33.3% of homozygous $Rbx5^{ex1}$ flies carrying one copy of the transgene and one copy of the driver. Ubiquitous transgenic expression of Rabex-5 WT, ΔZnF and ΔCT constructs rescued adult lethality; while Rabex-5 variants EET-VPS9, Δ[L-CH-CT] and D316A did not rescue (Figure 4.11).

Genetic interactions between $Rbx5^{ex1}$ and Rab5-dominant-negative transgenic expression

The results described above suggested that $Rbx5^{ex1}$ adult fly lethality was likely due to decreased Rab5 function. To further investigate this, it was pertinent to ask whether the

ubiquitous expression of Rab5(S43N)-dominant-negative construct would phenocopy the absence of Rabex-5. Genetic crosses were designed to obtain progeny carrying the ubiquitous driver (*Ub-Gal4*) and one copy of the Rab5(S43N) transgene. Adult flies ubiquitously expressing the Rab5(S43N) transgene were lethal. Staged larvae were dissected; tissues stained for DNA and compared side-by-side to control and $Rbx5^{ex1}$ homozygous mutants (Figure 4.12). Bright field images revealed that a 5-day-old Rab5(S43N) transgenic larva has a slightly smaller brain compared to an age-matched control but bigger in size than an $Rbx5^{ex1}$ brain (Figure 4.12C). Similar to $Rbx5^{ex1}$ mutant brains, 10- and 12-day-old Rab5(S43N)-expressing larvae showed an increased size compared to control (Figure 4.12D-E). Higher magnification of the boxed region in Figures 4.12A-E, shows that the structure of the brain hemispheres in Rab5(S43N)-expressing larvae is similar to $Rbx5^{ex1}$ mutant, particularly when they are 5 days old (Figure 4.12F-J).

Similarly to the experiment showed on Figure 4.6A-D, the overall morphology Rab5(S43N)-expressing larvae wing imaginal discs at 5, 10 and 12 days after larvae hatching was analyzed (Figure 4.13). The wing imaginal discs of 5-day-old Rab5(S43N)-expressing larvae were smaller in size compared to control, but the normal shape was preserved; in contrast to the 5-day-old *Rabex-5* mutant in which the wing disc was small and highly disorganized Figure 4.13A-C). Interestingly, the wing imaginal discs of these transgenic mutants at 10 and 12 days were seemly unaffected (Figure 4.13D-E).

To test for genetic interactions between the $Rbx5^{ex1}$ allele and over expression of Rab5(S43N), six genetic crosses were generated. These crosses produced progeny carrying one copy of the ubiquitous Gal4 driver (*Ub-Gal4*); none, one or two copies of $Rbx5^{ex1}$, and none or one copy of the Rab5(S43N) transgene (Figure 4.14). The total number of larvae at day 1 and 4 was counted, and the results were expressed as observed/expected ratio of the larvae survivors

(with the desired genotype) at day 4 relative to the total counted at day 1. Statistical analysis by two-way ANOVA showed significant differences between the mean larvae counts having the *Rbx5*^{ex1} allele ($F = 35.70$, $P < 0.0001$), Rab5(S43N) expression ($F = 484$, $P < 0.0001$), and the interaction ($F = 3.70$, $P < 0.03$). No significant difference in the ratio was found when comparing larvae with wild type (+/+) alleles to larvae carrying one copy of *Rbx5*^{ex1} (*ex1*/+) (Bonferroni post-test: $P > 0.05$). Similarly, no significant difference was observed for these same genotypes (+/+ vs. *ex1*/+) expressing the Rab5(S43N) transgene (Bonferroni post-test: $P > 0.05$). Interestingly, significant differences were found when comparing larvae with two normal copies (+/+) versus two *Rbx5*^{ex1} copies (*ex1*/*ex1*) in the absence and presence of the Rab5(S43N) a transgene (Bonferroni post-test: $P <0.001$ for both). When comparing *Rbx5*^{ex1} heterozygous versus homozygous mutants with or without Rab5(S43N) expression, statistically significant differences were found (Bonferroni post-test: $P <0.001$ for both). In addition to the noticeable reduced viability of larvae overexpressing Rab5(S43N) construct in a homozygous *Rbx5*^{ex1} background (black arrow in Figure 4.14A), these larvae were particularly small at 5 days old (white arrows in Figure 4.14B). These observations suggest a functional interaction between Rab5(S43N) and Rabex-5.

DISCUSSION

Experiments described in this chapter provide evidence for an important role of Rabex-5 in tissue growth and organization. I found that homozygous loss-of-function mutation in *Rbx5* results in lethality before reaching adulthood. Detailed analysis of the life cycle revealed that *Rbx5*^{ex1}mutants undergo an extended larval period, resulting in a "giant larvae" phenotype, after which they reach an abnormal prepupal stage and die. These phenotypes were rescued by transgenic expression of Rabex-5. Two additional alleles for *Rbx5*, generated in a separate imprecise excision mutagenesis carried out by Kevin D. Blau (a former undergraduate student researcher in this laboratory), displayed identical phenotypes, including abnormal morphology of wing imaginal discs and brain.

At 3rd instar, *Rbx5*^{ex1} larvae exhibited growth abnormalities in tissues such as the wing imaginal discs and brain. At 5 days, mutant wing discs were smaller, and at later days (10 and 12 days) they became abnormally larger, "spherical" and disorganized. Immunostaining of mutant wing imaginal discs demonstrated an increased in the levels of Mmp1, a metalloproteinase which is normally expressed at low levels in wings discs but expressed at high levels in neoplastic tissue [17,22,28]. Mmp1 was detected in larval extracts prepared from control genotype and analyzed by immunoblotting; this was likely because these extracts were prepared from ¾ of the larvae and included not only wing imaginal discs but also other tissues where Mmp1 is normally expressed. Nevertheless, increased Mmp1 levels were detected by immunoblot analysis of extracts prepared from *Rbx5*^{ex1} larvae.

In the last decade, *Drosophila* has emerged as a model for the study of tumor formation due to the discovery of tumor suppressor genes (TSGs) that when mutated, result in excessive

tissue growth [19,20]. Albeit the first TSG was discovered in the late 1960's [29], recent advances in the field have provided evidence for the relevance of studying these genes in understanding the mechanisms behind human cancer [20]. *Drosophila* TSGs are divided into two groups, hyperplastic TSGs and neoplastic TSGs. Mutations in hyperplastic TSGs are characterized by tissue overgrowth with, in the case of imaginal discs, retaining epithelial structure and being capable of differentiation into adult structures. Over a dozen of hyperplastic TSGs have been identified; mutations in these genes affect cell size (e.g. *pten, Tsc1, Tsc2),* increased growth rate combined with defects in apoptosis (e.g. *hippo, Salvador, mats, warts*) and growth-regulation pathways (e.g. *archipielago*) [19]. On the other hand, mutations in neoplastic TSGs are characterized by overgrown tissue with disrupted epithelial structure, inability to differentiate into adult structures, and invasive characteristics (i.e. metastasis) [19,20]. Thus far, seven neoplastic TSGs and at least seven other complementation groups have been identified [19,22]. Three of these genes, *lethal giant larvae* (*lgl*), *discs-large* (*dlg*) and *scribble* (*scrib*) are classified as "junctional scaffolding" neoplastic TSGs given that each gene encodes a protein that forms a complex important for epithelial polarity [19,20]. Four others, *Rab5, avalanche, tsg101*and *vps25* are classified as "endocytic" neoplastic TSG since the products of these genes are involved in the endocytic machinery [19]. Interestingly, zygotic mutants of *lgl, dlg* and *scrib* are able to survive to late 3rd instar larvae, where they develop into "giant larvae." Instead, *Rab5, avalanche, tsg101*and *vps25* homozygotes die before 1st instar larval stage [10,22]. Just recently, several studies have revealed some of the mechanism resulting in tumor growth for some of these mutants (reviewed in [19,20]). Due to the similarities between the known neoplastic TSGs and the *Rabex-5* mutant phenotype described in this chapter, in addition to the known function of its product in endosomal trafficking, *Rabex-5* may be classified as "endocytic" neoplastic TSG.

In 2010, Yan *et al*. proposed that increased body size, extra posterior cross veins in adult wings, and overgrown eyes of Rabex-5 knockdown mutant flies were due to the ubiqutin ligase activity in the ZnF domain and not the GEF activity of the Rabex-5 protein [30]. They suggested a mechanism in which Rabex-5 controlled Ras signaling by direct ubiquitination, resulting in its translocation to endosomal compartments [30]. Simultaneously, Xu *et al*. showed in COS-1 cells that activated Rab5 and Rin1 (another GEF for Rab5) are required for Rabex-5-dependent Ras ubiquitination [31]. They showed that Ras ubiquitination was independent of a functional Rabex-5 GEF domain. Their data suggested a possible model in which Rab5 is activated by RIN1, and GTP-bound Rab5 recruits Rabex-5/Rabaptin-5 complex to endosomal membranes. In the endosome, Rabex-5 ubiquitinates Ras, and this modification retains the Ras pool at this location, culminating in another level of regulation [31]. Evidence from the rescue experiments using Rabex-5 constructs presented in this chapter suggests that at least for adult viability the ZnF domain is dispensable. Moreover, it is shown that Rabex-5 with a catalytically inactive GEF was unable to rescue adult viability. In a separate set of experiments, Veronica T. Cheli showed in this laboratory that brains from transgenic Rabex-5 ΔZnF-expressing larvae have normal morphology compared to the abnormal brain of a Rabex-5 D316A-expressing larvae. This suggests a possible model in which Rabex-5 has tissue-specific functions that could be either dependent on the effectors available in certain types of cells or the activation of specific signaling pathways, or both. For example, in the brain Rabex-5 could have a non-redundant role in Rab5 activation, while in the wing its main role could be the regulation of the Ras-ERK signaling pathway via its ubiquitin ligase function (and the Rab5 activation function could be compensated by other GEFs). In support of this idea, it is shown that Rab5(S43N)-expressing larvae had overgrown brains with normal-shape wing imaginal disc.

Genetic interaction experiments using *Rbx5*^{ex1} mutants and Rab5(S43N)-expressing flies, showed that, while only a fraction of Rab5(S43N)-expressing mutants are able to reach late larval stage; the combination of both the mutation and the dominant-negative approach was more severe, with not only increased larvae lethality but also drastically reduced larval size. This suggests a potential compensatory mechanism in the Rabex-5 mutant, whereby additional GEFs (i.e. VPS9-containing proteins) are capable of activating Rab5 in other tissues including the brain. In addition to Rabex-5, the *Drosophila* genome contains at least three additional genes encoding VPS9-domain containing proteins, *CG1657, sprint* and *CG7158* [8]. Thus far, no mutant fly is available for *CG1657*. Sprint is the fly counterpart of the human proteins RIN1, RIN2, RIN3 and RINL. RIN1 activates Rab5 and interacts with EGFR stimulating its endocytosis [32]. Interestingly, Jekely *et al*. found that sprint loss-of-function mutants are viable and fertile with a phenotype in border cell migration only when EGFR was overexpressed [32]. CG7158-PA is recognized as the counterpart for the human protein Alsin, associated to a neurodegenerative disorder, but so far no mutant fly has been generated [33].

An important role for *Rabex5* in optic lobe development is shown. Optic lobe development has been shown to be affected in others neoplastic TSGs mutants such as *lgl* [20,29]. However, most of the studies focused on the central brain neuroblasts. Lee *et al*. showed that *lgl* and *pins* regulate larval neuroblast self-renewal [34]. In their studies with zygotic mutants, they saw an increased number of neuroblasts in *lgl* mutant and a decrease in *pins* mutants [34]. Alteration in the number of neuroblasts in these mutants was due to altering asymmetric division in central brain neuroblasts [34]. This is different from *Rabex-5* mutant brains because I did not detect any striking difference in central brain neuroblasts (when immunostained using anti-Dpn) but detected a difference in the optic lobe neuroblasts.

The switch from symmetrically dividing neuroepithelial cells to asymmetrically dividing neuroblast is a complex process regulated by several polarity proteins [35], proneural genes [25], and signaling pathways including Notch, JAK/STAT, Fat-Hippo and EGFR/Ras [25,36,37,38,39]. At the moment of writing this chapter, I could not identify in the literature any other mutant affecting symmetric and/or asymmetric division that phenocopied the abnormalities observed in *Rabex-5* mutant optic lobe [34,36,37,38,39,40]. For instance, mutations in *lethal(3) malignant brain tumor* (*L(3)mbt*) result in increased number of Dpn-positive cells in the central brain, similarly to *lgl* mutants, and severe overproliferation of neuroepithelial cells (shown by DE-Cadherin staining) but unaffected localization of polarity determinant in the neuroblasts. All these phenotypes were due to affecting Salvador-Warts-Hippo pathway [40]. These are not necessarily the phenotype observed in $Rbx5^{ex1}$ brains. I found that the optic lobe was the main structure within the brain that continuously growed compared to the central brain. This growth was due to abnormal number of neuroepithelial cells and neuroblasts. I found that neuroepithelium thickness was increased in the mutant at all the stages studied. Based on my observations, a hypothetical model that could explain the brain phenotype is that the neuroepithelial cells and NB are unable to stop dividing, resulting in additional mitose, but because the machinery that promotes the NE-NB transition is presumably unaffected, NB gives rise to progeny eventually becoming neurons. In turn, because the abnormally increased number of cells tries to fit in the same area, the optic lobe enlarges. This model is supported by the observation that, in older mutant brains, the neuroepithelium sometimes fold in unexpected ways and its large size overwhelms the size of the central brain. A modification of this hypothetical model would be that mutant neuroepithelial cells fail to divide normally on the other side of the neuroepithelium, which divides to form lamina progenitors. This would suggest that Rabex-5

function could be involved in the delivery of a signal or signals to stop proliferation in both neuroepithelial cells and neuroblast from the outer optic anlage of the optic lobe and not the central brain.

My observations allow me to speculate against an increase in the growth rate. Younger *Rabex-5* mutants could have a relative normal number of neuroepithelial cells comparable to a younger than 5 days control larva, but because this "normal" number of neuroepithelial cells is trying to fit in a smaller optic lobe area, neuroepithelium thickness is increased. Nevertheless, the number of neuroblasts at this stage is similar to control. Because larval period is extended, this could allow additional mitoses that in a normal fly are avoided due to the entry to the pupal stage. Thus, I propose that it is not that the mutant neuroblasts and neuoepithelial cells divide faster but that they never stop dividing during an extended larval stage.

Recently, *in vivo* experiments done in mouse liver have shown Rab5 to be the main Rab GTPase in endolysosome compartments [7]. Because results shown here demonstrate that the Rabex-5 GEF domain is important for Rab5 function, at least in viability and brain development, it is not outrageous to think that certain signaling pathways may be affected in Rabex-5 mutants. Overall, this chapter shows experiments suggesting a very interesting mechanism in which Rabex-5 is crucial for viability and tissue organization and, because of its distinctive domain architecture, could have tissue-specific functions ranging from a "general" role in the activation of Rab5 at endosomal compartments to the involvement in a very specific signaling pathway controlling proliferation of neuroepithelial cells and neuroblasts of the optic lobe. Future experiments should focus on understanding the contribution of each Rab5 GEF in tissue organization and growth, and whether these roles are dependent on Rab5 function or independent of the VPS9 domain.

Table 4.1. *Drosophila* lines used in Chapter 4 experiments.

Short name	Genotype	Source
yw	*yw*	D.Krantz (UCLA)
EP681	w^{1118}; $P\{EP\}CG9139^{EP681a}$ $P\{EP\}slmb^{EP681b}$	Bloomington #17189*
Δ2-3	y^1 w^*; ry^{506} Sb^1 $P\{\Delta 2\text{-}3\}99B$ / *TM6*	Bloomington #3664*
Df(3L)ED202	w^{1118}; *Df(3L)ED202, P{3'.RS5+3.3'}ED202 /* *TM6C,* cu^1 Sb^1	Bloomington #8051*
Rbx5^{ex1} (TM3)	*yw; Rbx5*^{ex1} */ TM3,* Sb^1	This study
Rbx5^{ex1} (TM6)	*yw; Rbx5*^{ex1} */ TM6B,* p^{Xp} Tb^1	This study
UAS-Rbx5 (Line 1)	*yw; P{Car-y-UAS-Rbx5}1*	V.Cheli (this lab)
UAS-Rbx5 (Line 3)	*yw; P{Car-y-UAS-Rbx5}3*	V.Cheli (this lab)
UAS-Rbx5 (Line 5)	*yw; P{Car-y-UAS-Rbx5}5*	V.Cheli (this lab)
Ub-GAL4	*w,ub-Gal4*	M.Guo (UCLA)
Ub-Gal4; Rbx5^{ex1} */ TM6*	*w,Ub-Gal4; Rbx5*^{ex1} */ TM6B,* p^{Xp} Tb^1	This study
WT	*yw; UAS-Rbx5WT; Rbx5*^{ex1} */ TM6B,* p^{Xp} Tb^1	V.Cheli (this lab)
Δ*ZnF*	*yw; UAS-Rbx5ΔZnF; Rbx5*^{ex1} */ TM6B,* p^{Xp} Tb^1	V.Cheli (this lab)
EET-VPS9	*yw; UAS-Rbx5 EET-VPS9; Rbx5*^{ex1} */ TM6B,* p^{Xp} Tb^1	V.Cheli (this lab)
Δ*CT*	*yw; UAS-Rbx5ΔCT; Rbx5*^{ex1} */ TM6B,* p^{Xp} Tb^1	V.Cheli (this lab)
Δ*[L-CH-CT]*	*yw; UAS-Rbx5Δ[L-CH-CT]; Rbx5*^{ex1} */ TM6B,* p^{Xp} Tb^1	V.Cheli (this lab)
D316A	*yw; UAS-Rbx5D316A ; Rbx5*^{ex1} */ TM6B,* p^{Xp} Tb^1	V.Cheli (this lab)

***** Bloomington # refers to fly lines available from the Bloomington Drosophila Stock Center at Indiana University (Bloomington, IN).

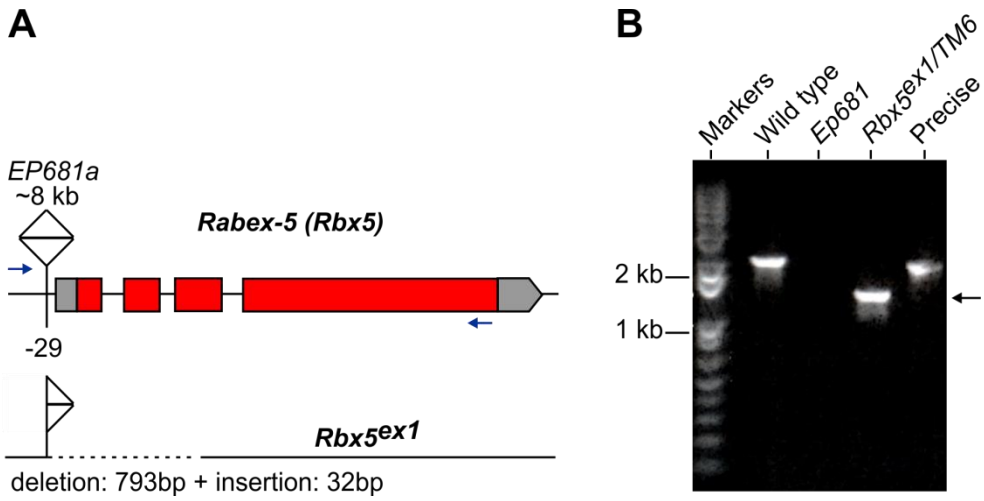

Figure 4.1. Imprecise excision mutagenesis resulted in a null allele for *Rabex-5*. (A) Scheme depicting the structure of the *Rabex-5* (*Rbx5*) gene. Gray boxes represent unstranslated regions (UTRs), red boxes represent the coding sequence and a diamond-shape represent the P-element (*EP681a*) inserted at position -29 from the initiation of transcription site. $Rbx5^{ex1}$ is a mutant allele that contains a 32-bp insertion (half-diamond) and a 793-bp deletion (dashed lines) removing the start codon. (B) Genomic DNA extracted from adult flies of the indicated genotypes, was PCR-amplified using the primers depicted as blue arrows in A. Gel electrophoresis of the PCR products shows the expected size (2,164 bp) for wild type genomic DNA, no band for EP681 line (due to the P-element size of ~8 kb), a smaller band for the heterozygous line $Rbx5^{ex1}$/TM6 indicative of a deletion (black arrow) and 2,164-bp band for a precise excision line.

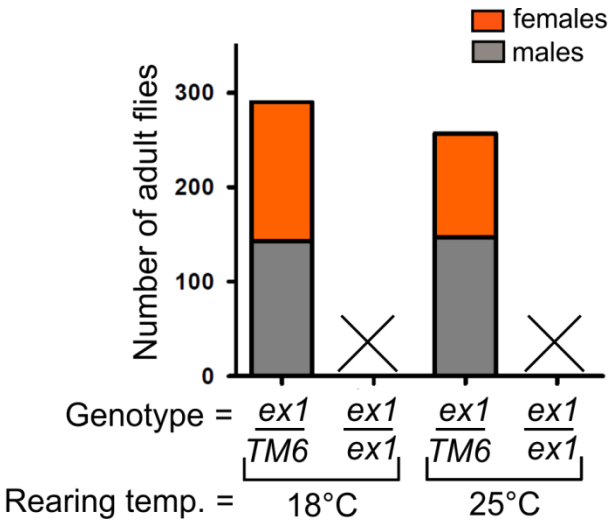

Figure 4.2. *Rbx5*^{ex1} flies do not survive to adulthood. Total number of adult offspring coming from a sibcross between flies carrying Rbx5ex1allele over a TM6 balancer chromosome (TM6) was counted. One third (33.3%) *Rbx5*^{ex1} homozygous flies (*ex1*/*ex1*) was expected but no adult was observed (represented by an X) compared to *Rbx5*^{ex1} heterozygous siblings (*ex1*/*TM6*). Similar results were obtained using different rearing temperatures (18˚C and 25˚C) and between male (gray bars) and female (orange bars) flies.

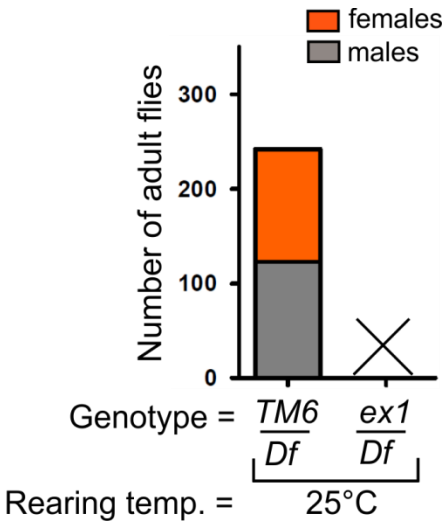

Figure 4.3. Flies heterozygous for *Rbx5*^{ex1} over a large deletion, do not survive to adulthood. Heterozygous flies carrying *Rbx5*^{ex1} allele over a TM6 balancer chromosome (TM6) were crossed to a line carrying the deficiency *Df(3L)ED202* over a balancer chromosome. For those flies carrying the deficiency, I expected to have 50% of each genotype as follows: hemizygous for *Rbx5*^{ex1} carrying one copy of the deficiency (*ex1*/*Df*); and flies with a single copy of the deficiency over a TM6 balancer chromosome (*TM6*/*Df*). No *ex1*/*Df* flies survived to adulthood (represented by an X) compared to *TM6*/*Df* flies. Flies were reared at 25˚C and no difference between male (gray bar) and female (orange bar) counts was observed.

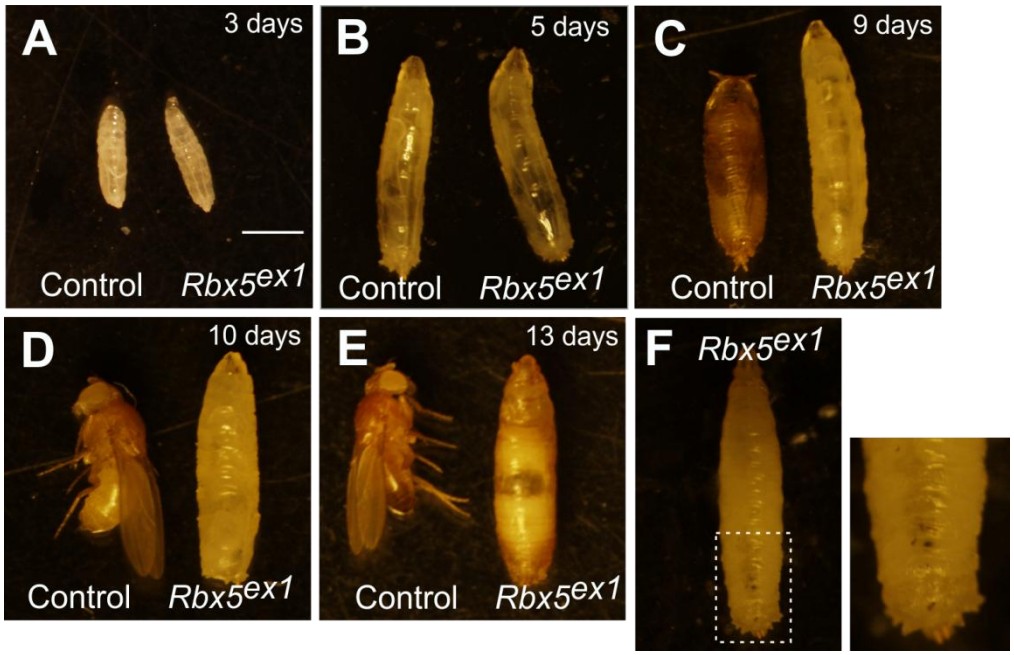

Figure 4.4. *Rbx5*^{ex1} flies die as an abnormal prepupa. (A-E) *Rbx5*^{ex1} larval development was analyzed side-by-side to control to determine at which stage they were dying. (A) 3-day-old *Rbx5*^{ex1} larvae looked very similar to control and (B) the same occurred at 5 days old. (C) At 9 days old, *Rbx5*^{ex1} was at a larval stage whereas control flies entered the pupae stage. (D) Control flies eclosed from the pupal case become an adult fly, but *Rbx5*^{ex1} still remained at a larval stage. (E) *Rbx5*^{ex1} died as abnormal prepupae. (F) Melanotic tumors were observed in many *Rbx5*^{ex1} prepupae. Shown here is an example of melanotic tumors detected as dark spots under the larval cuticle (dashed box is magnified). Scale bar represents 1 mm.

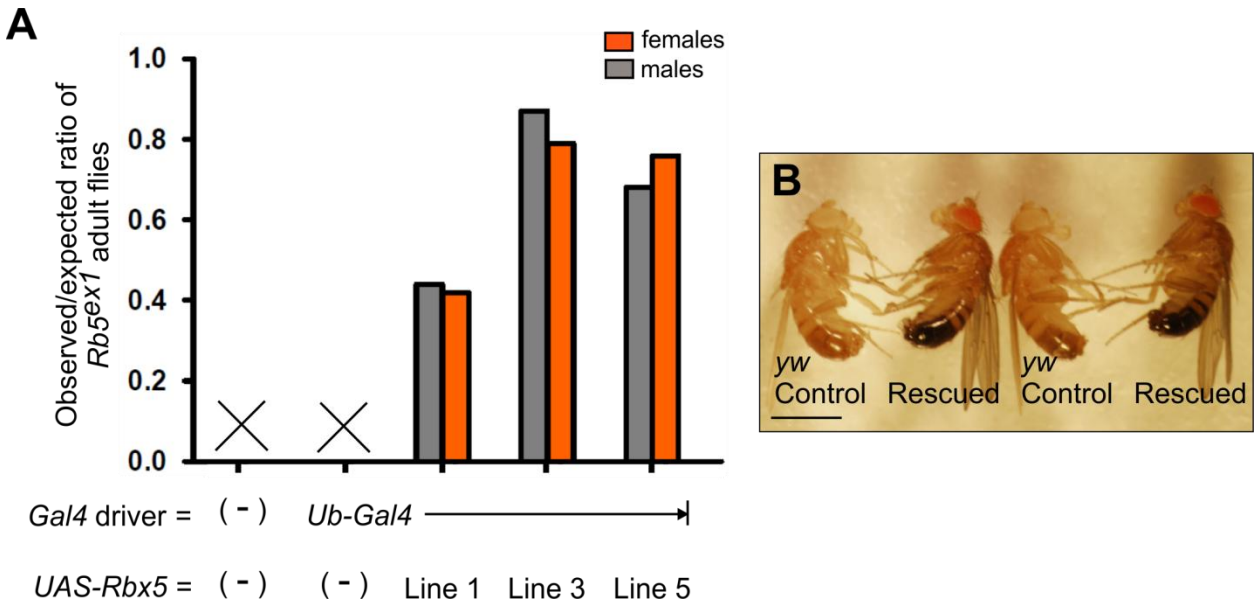

Figure 4.5. Rescue of the lethality of *Rbx5^{ex1}* flies by ubiquitous expression of a Rabex-5 transgene. (A) Ubiquitin-GAL4 (*Ub-GAL4*) was used to drive ubiquitous expression of Rabex-5 from three independent genomic insertions lines (*UAS-Rbx5* Line 1, Line 3 and 5). All crosses were designed to yield 33.3% *Rbx5^{ex1}* homozygous flies. For each genotype, at least 500 adult flies were counted. Counts were normalized to the total number of progeny obtained per parental cross) and are shown as the observed/expected ratio of *Rbx5^{ex1}* adult flies. *Rbx5^{ex1}* flies carrying a copy of *Ub-GAL4* do not survive to adulthood (represented by an X). Ubiquitous expression of the three *UAS-Rbx5* transgenes rescued the lethality. (B) Example of two rescued male flies next to *yellow white* (*yw)* male flies (here used as a control). Except from the difference in genetic backgrounds (yellow and tan body color), these flies seemed apparently healthy with no obvious developmental defect. Scale bar represents 1 mm.

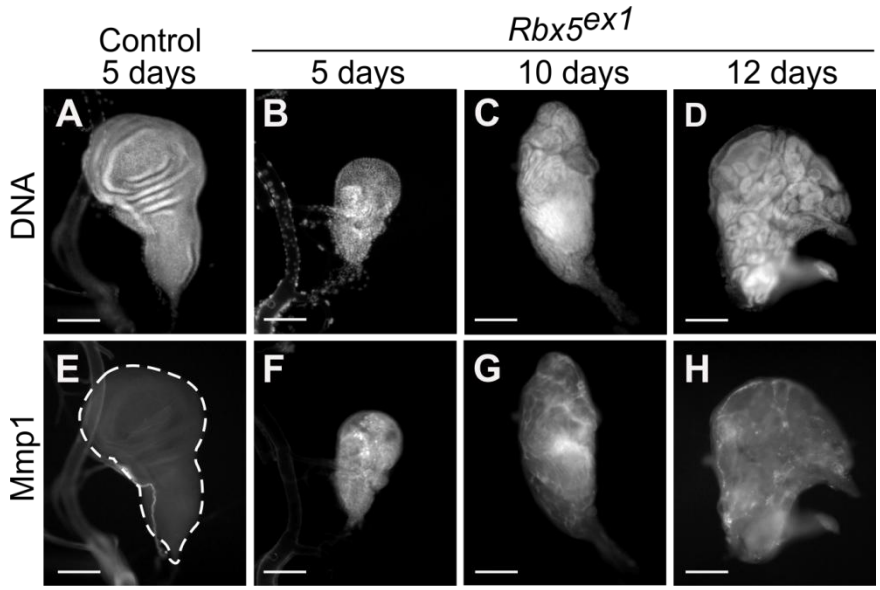

Figure 4.6. *Rbx5*^{ex1} larvae have abnormal wing imaginal discs with detectable levels of a neoplastic transformation marker. (A-H) Mutant and control larvae were dissected at the days indicated, and the wing imaginal discs immunostained for the neoplastic transformation marker, Matrix Metalloproteinase 1 (Mmp1) and DNA (Hoechst). (A) A control wing disc showed the characteristic shape of this tissue. (B) A 5-day-old *Rbx5*^{ex1} wing imaginal disc appeared smaller than the age-matched control in (A). (C-D) Ten- and 12-day-old mutant larvae developed wing discs that increased in size but showed a loss in tissue organization (E) Mmp1 expression was normally low in control wing discs. (F-H) Five-, 10- and 12-day-old *Rabex-5* mutant imaginal discs expressed high levels of Mmp1 as detected by immunostaining. Scale bars represent 100 μm.

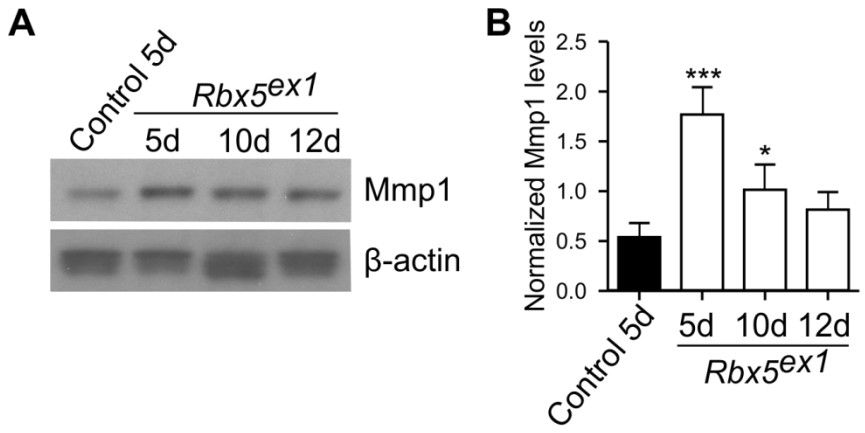

Figure 4.7. Five and ten-day-old *Rbx5*^{ex1} larvae expressed relatively high Mmp1 levels as detected by immunoblot analysis. (A) To assess Mmp1 levels, larval extracts were prepared and analyzed by immunoblot. β-actin was used as loading control. Highest Mmp1-expression was observed for larval extracts prepared from 5-day-old *Rbx5*^{ex1}mutants. (B) Mmp1 and β-actin levels from three immunoblots experiments were analyzed by densitometry. Bars represent Mmp1 levels normalized to β-actin levels. A significant difference in Mmp1 levels was observed for 5- and 10-day-old mutant larvae. One-way ANOVA followed by Dunnett's test comparing mutants to control: $*P < 0.05$ and $***P < 0.001$.

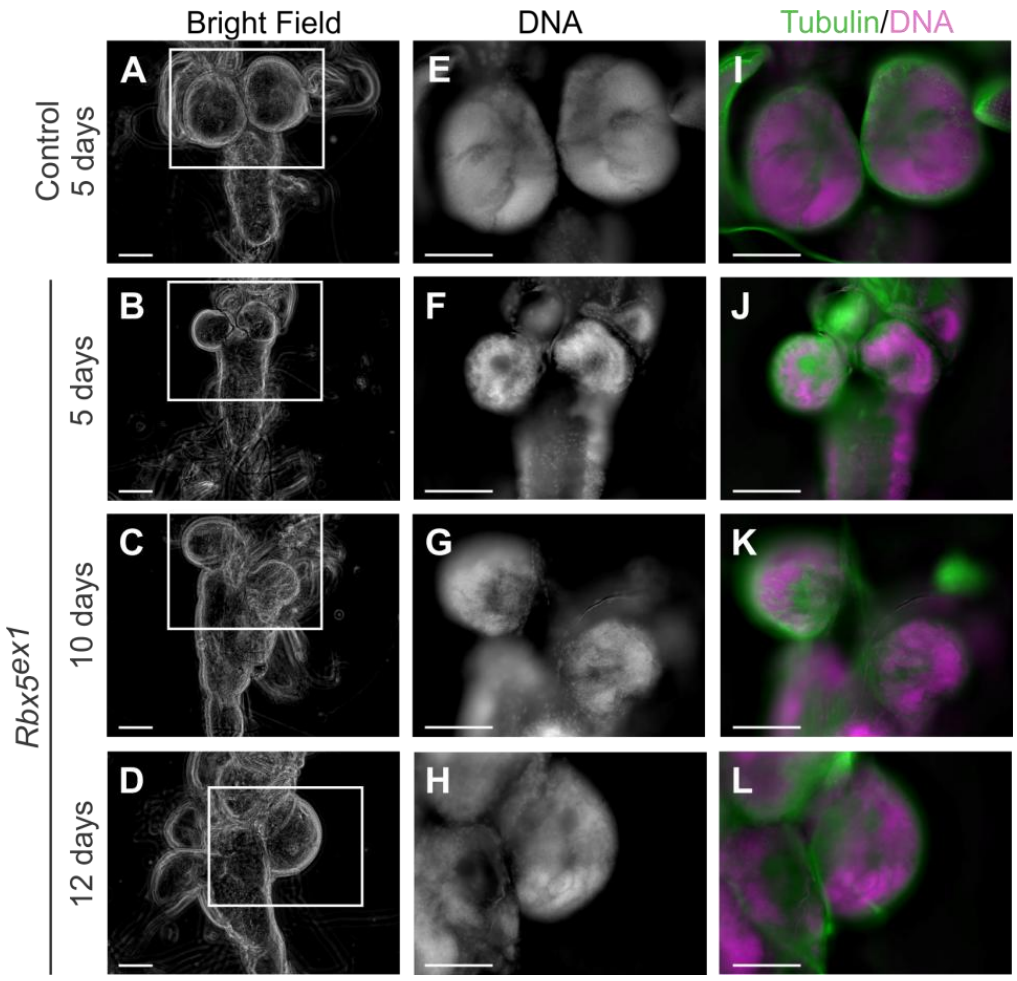

Figure 4.8. *Rbx5*^{ex1} mutant larvae displayed brain abnormalities. (A-L) Staged larvae on the days indicated were dissected, and their brains immunostained with an antibody against tubulin and Hoechst (to visualize DNA). Bright-field and fluorescence images were taken on whole-mount brains. (A) A normal larval brain at 5 days of age was ~500 µm long and the diameter of each brain hemisphere (found within boxed region) was ~200 µm. (B) Mutant brains at 5 days were significantly smaller, particularly the brain hemispheres (found within boxed region) which were <100 µm in diameter. (C and D) At 10 and 12 days, mutant brains reached a similar size to control, but became highly disorganized. (E-L) Higher magnification of boxed region in (A-D) shows the structure of a normal 5-day-old and mutant larval brain hemispheres using DNA staining (E-H) and merged images of tubulin and DNA (I-L). Scale bars represent 100 µm.

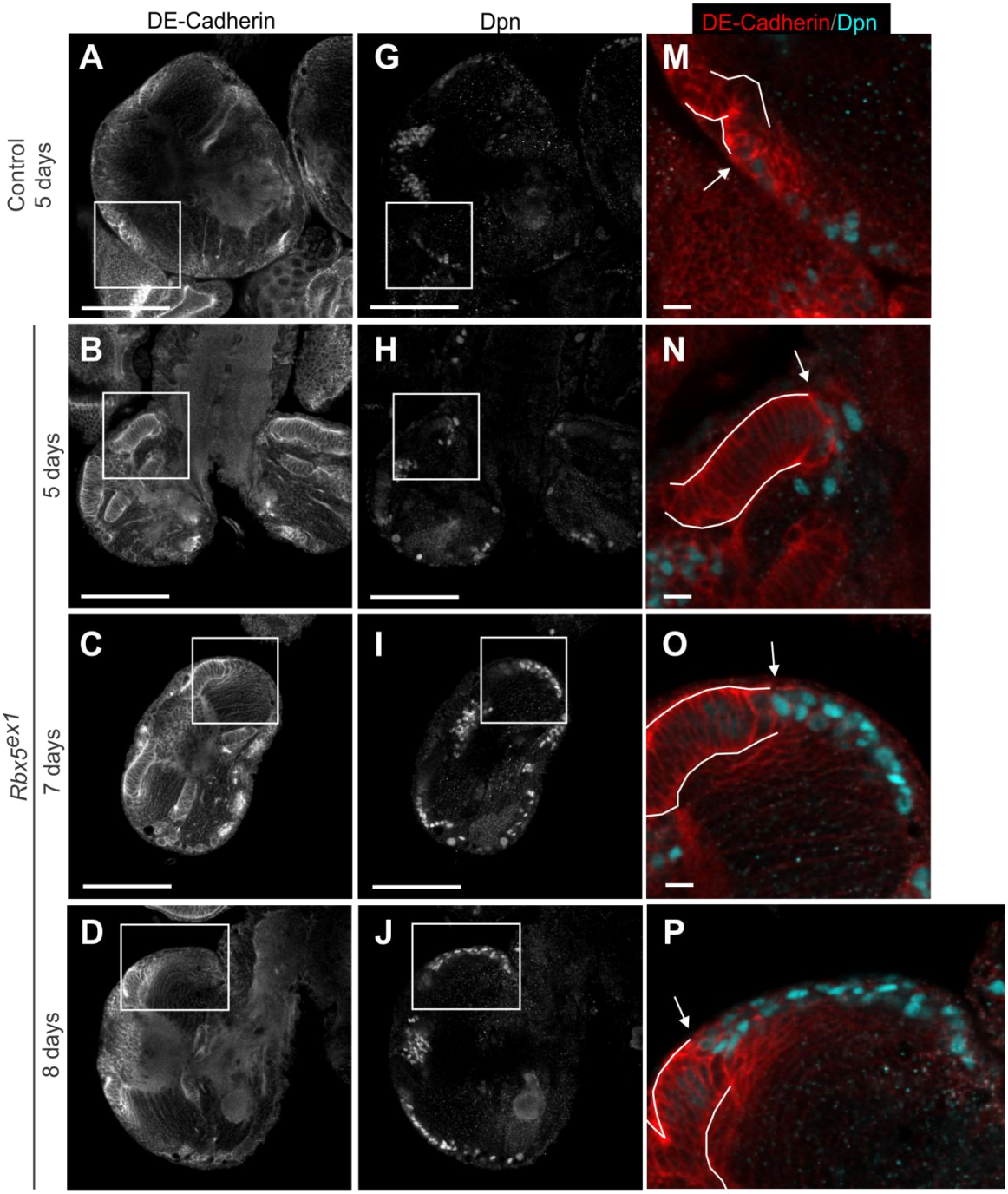

(***Figure 4.9*** *continues on next page)*

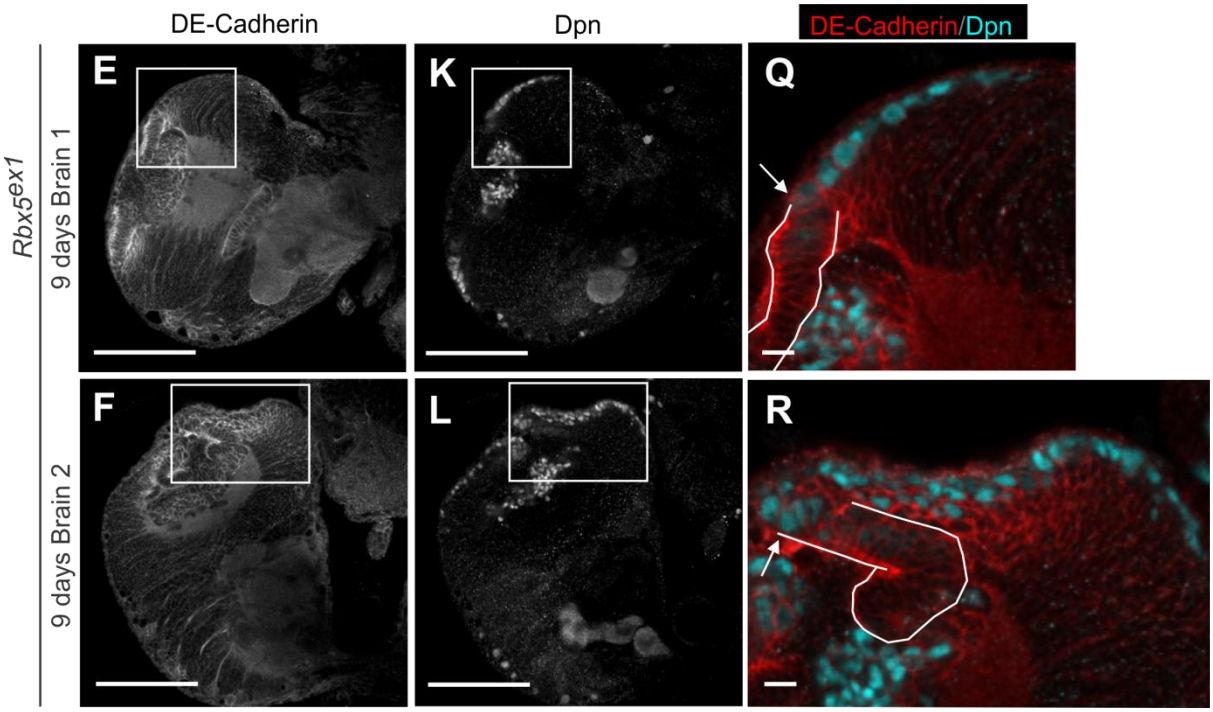

Figure 4.9. Abnormal optic lobe development in *Rbx5*^{ex1} larvae. (A-F) Brain hemispheres of control and *Rbx5*^{ex1} mutant larvae were immunostained using antibodies against DE-Cadherin to allow the visualization of the optic lobe structure, in particular the neuroepithelium (NE). (G-L) Dpn staining was used for the visualization of neuroblasts (NB). Boxed regions in (A-L) are magnified in panels (M-R) to show DE-cadherin staining in red, Dpn staining in cyan, the NE-NB transition zone (white arrow) and outlined NE (white lines). (A/G boxed regions; and M) Control brain at 5 days showed a relatively small neuroepithelial region (outlined) and ~10 neuroblasts (cyan). (B/H boxed regions; and N) Five-day-old mutant NE was capable of transitioning into NB, but notice the increased NE thickness. (C/I and D/J boxed regions; and O-P) Mutant brains at 7 and 8 days of age showed a thick NE and many NB. (E/K and F/L boxed regions; and Q-R) Brains from two 9-day-old larvae showed high variability in NB and NE numbers. Scale bars represent 100 µm (A-L) or 10 µm (M-R).

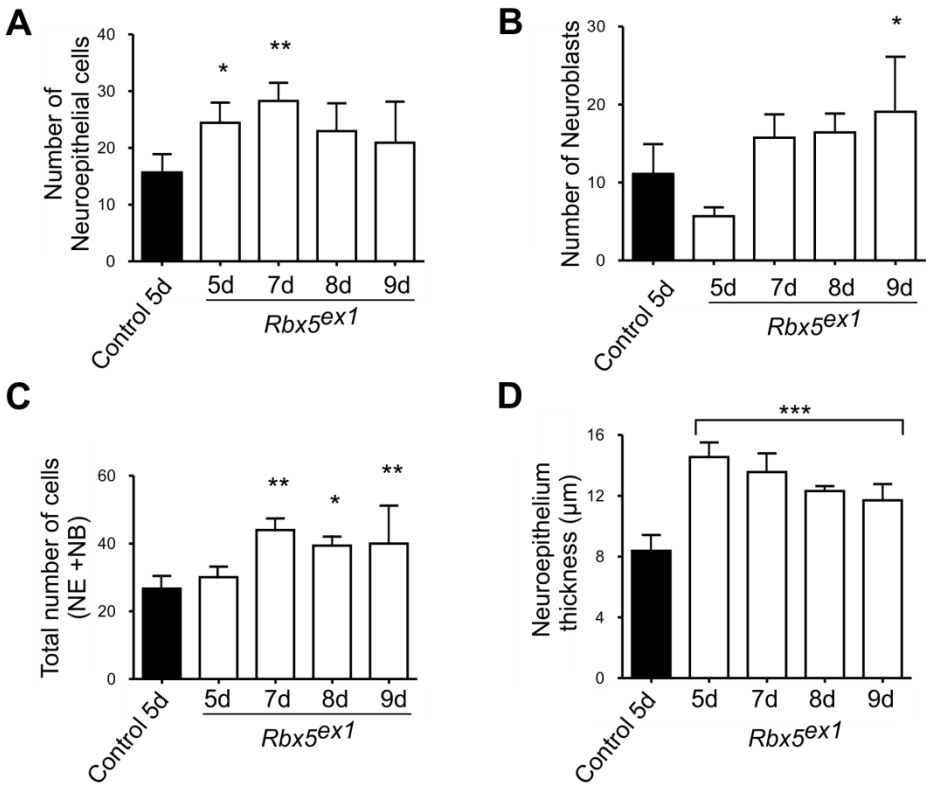

Figure 4.10. *Rbx5*^{ex1} mutant larvae have abnormal number of neuroepithelial cells and neuroblasts in the optic lobe. (A) Quantification of neuroepithelial (NE) cells, (B) neuroblasts (NB), (C) NE+NB and (D) neuroepithelium thickness from two separate cross-section per brain of 5-day-old (5d) control larvae (N =5), 5d *Rbx5*^{ex1} (N =5), 7-day-old (7d) *Rbx5*^{ex1} (N =4), 8-day-old (8d) *Rbx5*^{ex1} (N =5) and 9-day-old (9d) *Rbx5*^{ex1} (N =5).Bars represent Mean ± SD. One-way ANOVA followed by Dunnett's test comparing each mutant to control: * $P < 0.05$, ** $P < 0.01$ and *** $P < 0.001$.

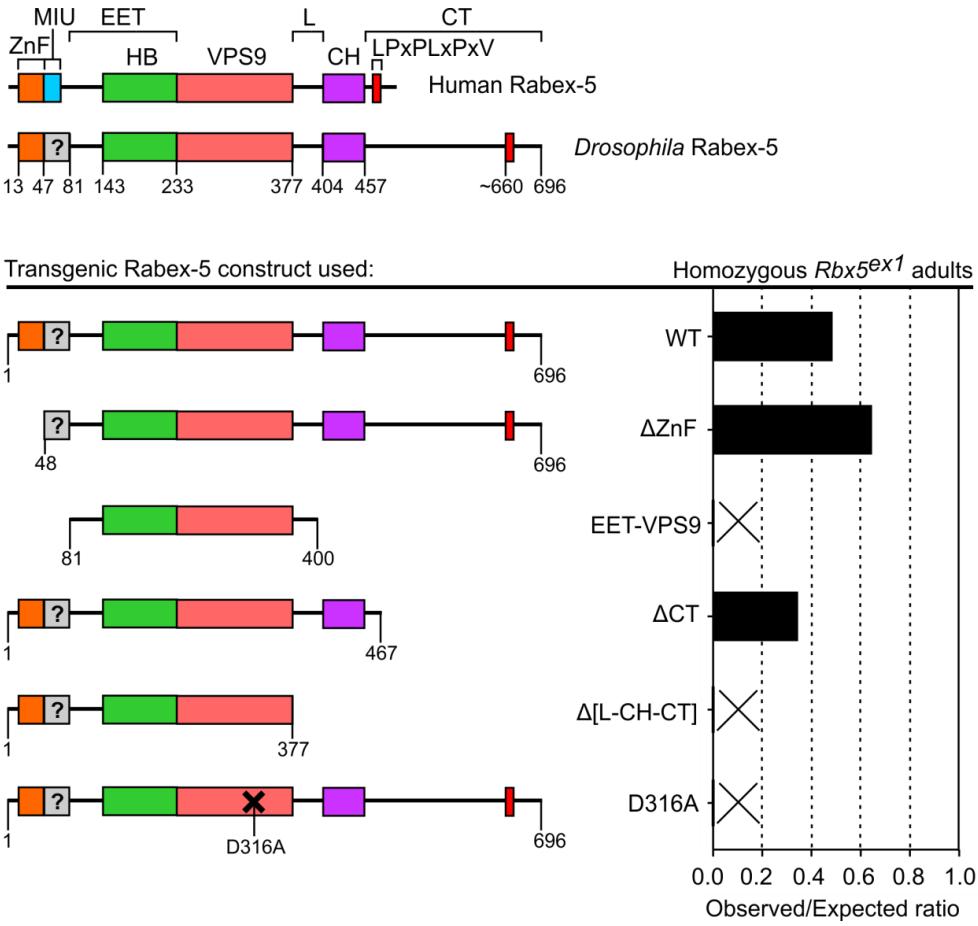

Figure 4.11. Lethality of *Rbx5*^{ex1} flies is likely due to impaired Rab5-activating function of Rabex-5. (Top) Schematic representation of human and *Drosophila* Rabex-5 proteins. Domain names are based on the human protein after amino acid sequence alignment. (Bottom) Transgenic Rabex-5 constructs, inserted at the same position of chromosome 2, were generated to express wild type Rabex-5 (WT), truncated forms (ΔZnF, EET-VPS9, ΔCT and Δ[L-CH-CT]); and a catalytically dead Rabex-5 with substitution of aspartic acid 316 to alanine (D316A). The ability of these constructs to rescue the lethality of homozygous *Rbx5*^{ex1} flies was tested upon driving their expression ubiquitously using the *Ub-Gal4* driver. Plotted is the observed/expected ratio of a genetic cross designed to yield 33.3% of homozygous *Rbx5*^{ex1} flies. WT (n = 1255), ΔZnF (n = 940) and ΔCT (n =1095) transgenic expression was able to rescue adult lethality. Whereas the expression of EET-VPS9 (n = 585), Δ[L-CH-CT] (n = 647) and D316A (n = 717) did not rescue (represented by an X). n represents the total number of adult flies counted.

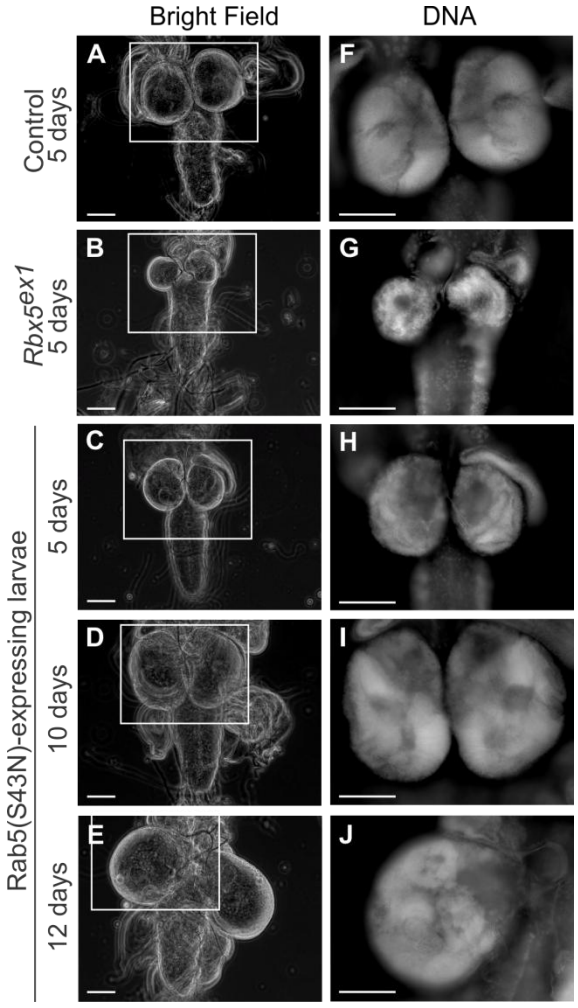

Figure 4.12. Larvae expressing a Rab5 dominant-negative construct displayed brain abnormalities similar to those of *Rbx5*^{ex1} homozygotes. (A-J) Brains from staged larvae with the indicated genotypes were stained with Hoechst to visualize DNA. Bright-field and fluorescence images were taken on whole-mount brains. (A-B, F-G) Images of control and *Rbx5*^{ex1} brains, shown in Figure 4.8, are shown again for comparison since they were obtained in the same experiment as those shown in the rest of the panels. (C) A 5-day-old larvae ubiquitously expressing the Rab5(S43N)-dominant-negative transgene had a slightly smaller brain compared to an age-matched control brain. (D-E) Brains from 10- and 12-day-old Rab5(S43N)-expressing larvae were bigger than control brains. (F-J) Higher magnification of the boxed region in (A-E) stained with DNA shows the structure of the brain hemispheres. Scale bars represent 100 µm.

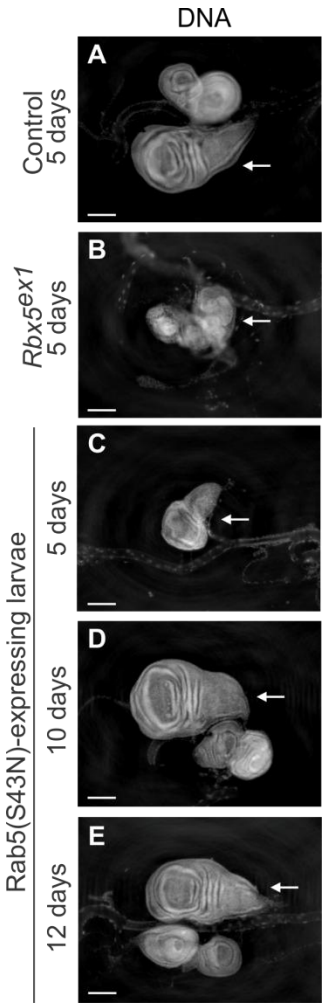

Figure 4.13. Larvae expressing a Rab5 dominant-negative construct displayed normal wing imaginal disc morphology. (A-E) Wing imaginal discs from staged-larvae with the indicated genotype were stained with Hoechst to visualize DNA. Fluorescence images were taken on whole-mount tissues. Arrows in panels point at wing discs. (A and B) Morphology of the wing imaginal disc from control (A) and a Rabex-5 mutant (B). (C) Five-day-old transgenic larvae ubiquitously expressing Rab5(S43N driven by *Ub-Gal4*, had a smaller but normally shaped wing discs as compared to an age-matched control. (D-E) Wing discs from 10- and 12-day-old Rab5-DN transgenic larvae had normal morphology. Scale bars represent 100 µm.

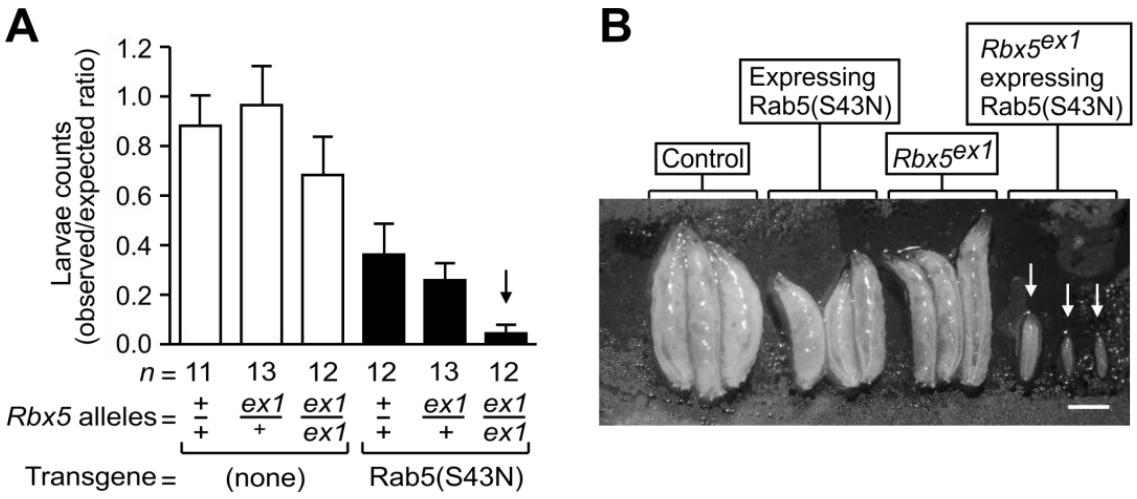

Figure 4.14. Synthetic lethal interaction in *Rbx5^{ex1}* flies overexpressing a dominant-negative Rab5 transgene. (A) Six parental crosses were designed to obtain offspring carrying a copy of the ubiquitous Gal4 driver (*Ub-Gal4*) and the additional combination of alleles: none, one or two copies of *Rbx5^{ex1}*, and with or without one copy of a Rab5(S43N)-dominant-negative transgene. Offspring were staged side-by-side, and the number of larvae at day 1 and 4 was quantified. *n* = number of individual plates counted. At day 1, each cross generated an average of 1,421± 253 larvae. Bars represent the mean ±SD of the observed/expected ratio of the number of larvae (not carrying TM6) at day 4 relative to the total observed at day 1. Notice the reduced viability of larvae overexpressing Rab5-(S43N) construct in a homozygous *Rbx5^{ex1}* background (black arrow). Statistical analysis by two-way ANOVA are described in the *Results* section. (B) Groups of 5-day-old larvae with the indicated genotypes. Notice the strikingly small size of larvae ubiquitously expressing a Rab5(S43N)-dominant-negative with two copies of *Rbx5^{ex1}* (white arrows). Scale bar represents 1 mm.

REFERENCES

1. Scita G, Di Fiore PP (2010) The endocytic matrix. Nature 463: 464-473.

2. Miaczynska M, Pelkmans L, Zerial M (2004) Not just a sink: endosomes in control of signal transduction. Curr Opin Cell Biol 16: 400-406.

3. Lanzetti L, Di Fiore PP (2008) Endocytosis and cancer: an 'insider' network with dangerous liaisons. Traffic 9: 2011-2021.

4. Sorkin A, von Zastrow M (2009) Endocytosis and signalling: intertwining molecular networks. Nat Rev Mol Cell Biol 10: 609-622.

5. Stenmark H (2009) Rab GTPases as coordinators of vesicle traffic. Nat Rev Mol Cell Biol 10: 513-525.

6. Zhang J, Schulze KL, Hiesinger PR, Suyama K, Wang S, et al. (2007) Thirty-one flavors of Drosophila rab proteins. Genetics 176: 1307-1322.

7. Zeigerer A, Gilleron J, Bogorad RL, Marsico G, Nonaka H, et al. (2012) Rab5 is necessary for the biogenesis of the endolysosomal system in vivo. Nature 485: 465-470.

8. Carney DS, Davies BA, Horazdovsky BF (2006) Vps9 domain-containing proteins: activators of Rab5 GTPases from yeast to neurons. Trends Cell Biol 16: 27-35.

9. Wucherpfennig T, Wilsch-Brauninger M, Gonzalez-Gaitan M (2003) Role of Drosophila Rab5 during endosomal trafficking at the synapse and evoked neurotransmitter release. J Cell Biol 161: 609-624.

10. Lu H, Bilder D (2005) Endocytic control of epithelial polarity and proliferation in Drosophila. Nat Cell Biol 7: 1232-1239.

11. Horiuchi H, Lippe R, McBride HM, Rubino M, Woodman P, et al. (1997) A novel Rab5 GDP/GTP exchange factor complexed to Rabaptin-5 links nucleotide exchange to effector recruitment and function. Cell 90: 1149-1159.

12. McBride HM, Rybin V, Murphy C, Giner A, Teasdale R, et al. (1999) Oligomeric complexes link Rab5 effectors with NSF and drive membrane fusion via interactions between EEA1 and syntaxin 13. Cell 98: 377-386.

13. Mattera R, Tsai YC, Weissman AM, Bonifacino JS (2006) The Rab5 guanine nucleotide exchange factor Rabex-5 binds ubiquitin (Ub) and functions as a Ub ligase through an atypical Ub-interacting motif and a zinc finger domain. J Biol Chem 281: 6874-6883.

14. Greenspan RJ (1997) Fly pushing: the theory and practice of *Drosophila* genetics. New York: Cold Spring Harbor Laboratory Press.

15. Robertson HM, Preston CR, Phillis RW, Johnson-Schlitz DM, Benz WK, et al. (1988) A stable genomic source of P element transposase in Drosophila melanogaster. Genetics 118: 461-470.

16. Falcon-Perez JM, Romero-Calderon R, Brooks ES, Krantz DE, Dell'Angelica EC (2007) The Drosophila pigmentation gene pink (p) encodes a homologue of human Hermansky-Pudlak syndrome 5 (HPS5). Traffic 8: 154-168.

17. Page-McCaw A, Serano J, Sante JM, Rubin GM (2003) Drosophila matrix metalloproteinases are required for tissue remodeling, but not embryonic development. Dev Cell 4: 95-106.

18. Brand AH, Perrimon N (1993) Targeted gene expression as a means of altering cell fates and generating dominant phenotypes. Development 118: 401-415.

19. Hariharan IK, Bilder D (2006) Regulation of imaginal disc growth by tumor-suppressor genes in Drosophila. Annu Rev Genet 40: 335-361.

20. Bilder D (2004) Epithelial polarity and proliferation control: links from the Drosophila neoplastic tumor suppressors. Genes Dev 18: 1909-1925.

21. Martin FA, Morata G (2006) Compartments and the control of growth in the Drosophila wing imaginal disc. Development 133: 4421-4426.

22. Menut L, Vaccari T, Dionne H, Hill J, Wu G, et al. (2007) A mosaic genetic screen for Drosophila neoplastic tumor suppressor genes based on defective pupation. Genetics 177: 1667-1677.

23. Egger B, Gold KS, Brand AH (2011) Regulating the balance between symmetric and asymmetric stem cell division in the developing brain. Fly (Austin) 5: 237-241.

24. Ngo KT, Wang J, Junker M, Kriz S, Vo G, et al. (2010) Concomitant requirement for Notch and Jak/Stat signaling during neuro-epithelial differentiation in the Drosophila optic lobe. Dev Biol 346: 284-295.

25. Yasugi T, Umetsu D, Murakami S, Sato M, Tabata T (2008) Drosophila optic lobe neuroblasts triggered by a wave of proneural gene expression that is negatively regulated by JAK/STAT. Development 135: 1471-1480.

26. Zhu H, Zhu G, Liu J, Liang Z, Zhang XC, et al. (2007) Rabaptin-5-independent membrane targeting and Rab5 activation by Rabex-5 in the cell. Mol Biol Cell 18: 4119-4128.

27. Bischof J, Maeda RK, Hediger M, Karch F, Basler K (2007) An optimized transgenesis system for Drosophila using germ-line-specific phiC31 integrases. Proc Natl Acad Sci U S A 104: 3312-3317.

28. Morrison HA, Dionne H, Rusten TE, Brech A, Fisher WW, et al. (2008) Regulation of early endosomal entry by the Drosophila tumor suppressors Rabenosyn and Vps45. Mol Biol Cell 19: 4167-4176.

29. Gateff E, Schneiderman HA (1967) Developmental studies of a new mutant of *Drosophila melanogaster*: Lethal malignant brain tumor (l(2)gl 4. Am Zool 7.

30. Yan H, Jahanshahi M, Horvath EA, Liu HY, Pfleger CM (2010) Rabex-5 ubiquitin ligase activity restricts Ras signaling to establish pathway homeostasis in Drosophila. Curr Biol 20: 1378-1382.

31. Xu L, Lubkov V, Taylor LJ, Bar-Sagi D (2010) Feedback regulation of Ras signaling by Rabex-5-mediated ubiquitination. Curr Biol 20: 1372-1377.

32. Jekely G, Sung HH, Luque CM, Rorth P (2005) Regulators of endocytosis maintain localized receptor tyrosine kinase signaling in guided migration. Dev Cell 9: 197-207.

33. Yang Y, Hentati A, Deng HX, Dabbagh O, Sasaki T, et al. (2001) The gene encoding alsin, a protein with three guanine-nucleotide exchange factor domains, is mutated in a form of recessive amyotrophic lateral sclerosis. Nat Genet 29: 160-165.

34. Lee CY, Robinson KJ, Doe CQ (2006) Lgl, Pins and aPKC regulate neuroblast self-renewal versus differentiation. Nature 439: 594-598.

35. Betschinger J, Mechtler K, Knoblich JA (2003) The Par complex directs asymmetric cell division by phosphorylating the cytoskeletal protein Lgl. Nature 422: 326-330.

36. Egger B, Gold KS, Brand AH (2010) Notch regulates the switch from symmetric to asymmetric neural stem cell division in the Drosophila optic lobe. Development 137: 2981-2987.

37. Wang W, Li Y, Zhou L, Yue H, Luo H (2011) Role of JAK/STAT signaling in neuroepithelial stem cell maintenance and proliferation in the Drosophila optic lobe. Biochem Biophys Res Commun 410: 714-720.

38. Kawamori H, Tai M, Sato M, Yasugi T, Tabata T (2011) Fat/Hippo pathway regulates the progress of neural differentiation signaling in the Drosophila optic lobe. Dev Growth Differ 53: 653-667.

39. Reddy BV, Rauskolb C, Irvine KD (2010) Influence of fat-hippo and notch signaling on the proliferation and differentiation of Drosophila optic neuroepithelia. Development 137: 2397-2408.

40. Richter C, Oktaba K, Steinmann J, Muller J, Knoblich JA (2011) The tumour suppressor L(3)mbt inhibits neuroepithelial proliferation and acts on insulator elements. Nat Cell Biol 13: 1029-1039.

CHAPTER 5

CONCLUSIONS

In eukaryotic cells, endosomal protein trafficking is a highly complex and regulated process. Absence of proteins such as BLOC-1 and AP-3, results in hypopigmentation and prolonged bleeding. In some cases, altering normal trafficking routes have implications in cell proliferation and tissue growth. The overall goal of this dissertation was to identify genetic interactions involving components of the endosomal protein trafficking machinery. Two chapters focus on BLOC-1 and AP-3, which have important roles in the biogenesis of LROs, and another chapter is devoted to characterizing the Rab5 GEF protein, Rabex-5.

The data-mining approach discussed in Chapter 2, turned out to be an efficient method to prioritize candidate binding partners for both human and fly BLOC-1. This approach takes advantage of the availability of data derivedfrom large-scale studies of protein-protein interactions. I found a way to efficiently gather high-quality information about each candidate and to represent this information in a friendly and manageable manner. The top candidate in the ranking of binding partners of BLOC-1 was found to be the RabGTPase Rab11. Rab11 has been found to be associated to recycling endosomes and to have important roles in development. Prior evidence coming from the study of *lightoid*, the fly ortholog of Rab38 and Rab32, Rab32 (which are involved in the biogenesis of melanosomes [1]), suggested that due to its relatively "mild" pigmentation defect additional Rabs could be implicated in the biogenesis of LROs [2]. Therefore, the fact that Rab11 ranked at the top of the BLOC-1 ranking was exciting. Experiments using flies carrying mutations in the orthologs of Rab11 and Rab32/38, the later encoded by the *lightoid* gene, uncovered a synthetic lethal genetic interaction [3]. This unexpected finding suggests that *lightoid* may have a general role in development in addition to its specific role in LROs biogenesis.

In the ranked table of binding partners for human BLOC-1, three genes encoding exocyst subunits, *EXOC7, EXOC3,* and *EXOC4,* ranked #4, #9 and #11, respectively. Similarly, ranking #7 in the table of binding partners for *Drosophila* BLOC-1 was the *CG2095*, which is the ortholog of *EXOC4*. Recently Gokhale *et al*. used a combination of proteomic approaches that resulted in the identification of various BLOC-1 binding partners, including two exocyst subunits [4]. This data validates my data-mining approach as a good strategy to select for follow-up experiments, "real" binding partners of BLOC-1. Another advantage provided by this approach is that is a customizable method, which can be potentially applied to other types of "omics" data.

Since the publication of the reprint shown in Chapter 2, at least six scientific papers have been published that describe different approaches to curate, rank or annotate large-scale data of protein-protein interactions [5,6,7,8,9,10]. Due to the difficulty presented at the moment of searching for protein-protein interactions, efforts have been made to develop tools to facilitate this process [11] [12].

Chapter 3 focuses on using a genetic screening strategy to identify genetic modifiers of the function of AP-3 in flies. Validation and fine-mapping identified four genomic regions that partially suppressed the g^2 eye color phenotype. Two interesting candidate genes, *Gap69C* and *Atg2* localized within two separate genomic regions were further investigated, and were shown to be genetic modifiers of AP-3.

Gap69C encodes the *Drosophila* ortholog of the human ARF GAP 1, encoded by the *ARFGAP1* gene [13]. ARF GAP 1 activates ARF1,which has been shown to regulate the recruitment of AP-3 to membranes and other adaptor complexes, and to bind GGAs (Golgi-localized, γ ear-containing, ARF-binding proteins) [14]. GGAs are another type of adaptors with

homology to the AP subunit domains and capable of binding clathrin. My findings describing a partial suppression of the g^2 eye color phenotype by removing a copy of *Gap69C*, suggests several possibilities that will be worth explaining in the future. Is the conversion between active and inactive Arf1 important for the trafficking of specific cargo to the pigment granule? Is this through the interaction with other adaptor complexes such as GGAs or AP-1? Or is the suppression effect on g^2 is results from the mislocalization of AP-3?

Another modifier of AP-3 arising from the screening is *Atg2*, a gene encoding an autophagy protein. Thus far, only one scientific article has been published linking AP-3 and BLOC-1 to autophagy [15]. In this article, Marino *et al*. showed that AP-3 and BLOC-1 levels in autophagy mutant mice are reduced. The mice displayed a sense of balance problem that was attributed to abnormal development of the otoconia in the inner ear. Abnormalities in the inner ear otoliths have also been noted in mocha, muted and pallid [16].Therefore, they suggested that autophagy could be related to a potential role of AP-3 and BLOC-1 in the development of this structure [15]. My results provide another piece of evidence linking autophagy to AP-3 function.

Chapter 4 demonstrates that *Drosophila Rabex-5* is a tumor suppressor gene. *Rabex-5* null mutations resulted in lethality before reading adulthood. Inspection of larval tissue revealed growth abnormalities in the brain and wing imaginal discs. Lethality and abnormal brain development was due to affecting normal Rab5 function. Particularly interesting is the phenotype observed in the optic lobe of $Rabex\text{-}5^{ex1}$ mutant larvae. The fact that the neuroepithelial cells and neuroblasts in the optic lobe, and not those in the central brain, were affected is interesting and deserves attention.

Rabex-5 contains a VPS9 domain providing the catalytic activity necessary for Rab5 activation, a ZnF domain that contains ubiquitin ligase activity and binds ubiquitin and other domains that are important for the interaction with other proteins such as Rabaptin-5 [17,18,19]. Rescue experiments presented here, suggest that at least for adult viability the ZnF domain is dispensable, while the GEF domain is necessary. Yan *et al*. reported that abnormal growth in eye, wings and body size in *Rabex-5* knockdown mutants were due to the ZnF domain and not the GEF domain [20]. The fact that the ubiquitous expression of Rab5(S43N)-transgene affects brain size suggest that Rab5 function is important for brain growth. On the contrary, wing imaginal discs seemed unaffected in flies overexpressing Rab5(S43N). Thus, data presented here and from other laboratories [20,21], suggest that Rabex-5 may have tissue-specific function, and at least in the brain depends on Rab5 function.

The synthetic lethal interaction observed for homozygous $Rbx5^{ex1}$ flies overexpressing Rab5(S43N), suggest that additional Rab5 GEFs may be functionally compensating Rabex-5. Based on published results by Xu *et al*. showing that RIN1 was needed for Ras ubiquitination by Rabex-5; RIN1 (another Rab5 GEF) emerges as a potential candidate to have redundant function with Rabex-5 [21]. In flies, sprint is the only fly counterpart for human RIN1, RIN2, RIN3 and RINL. Loss-of-function mutants for sprint are viable and fertile with a mild phenotype only when EGFR is overexpressed [22]. Therefore, a possibility could be that sprint has redundant roles with Rabex-5 in some tissues, while in others Rabex-5 is essential. However, the role in tissue growth and viability of the others VPS9-domain-containing proteins, encoded by the genes *CG1657* and *CG7158* remains to be elucidated. Overall, these findings provide additional evidence regarding the role of the endosomal protein trafficking pathway in tissue growth and cell signaling [23].

REFERENCES

1. Wasmeier C, Romao M, Plowright L, Bennett DC, Raposo G, et al. (2006) Rab38 and Rab32 control post-Golgi trafficking of melanogenic enzymes. J Cell Biol 175: 271-281.
2. Ma J, Plesken H, Treisman JE, Edelman-Novemsky I, Ren M (2004) Lightoid and Claret: a rab GTPase and its putative guanine nucleotide exchange factor in biogenesis of Drosophila eye pigment granules. Proc Natl Acad Sci U S A 101: 11652-11657.
3. Rodriguez-Fernandez IA, Dell'Angelica EC (2009) A data-mining approach to rank candidate protein-binding partners-The case of biogenesis of lysosome-related organelles complex-1 (BLOC-1). J Inherit Metab Dis 32: 190-203.
4. Gokhale A, Larimore J, Werner E, So L, Moreno-De-Luca A, et al. (2012) Quantitative proteomic and genetic analyses of the schizophrenia susceptibility factor dysbindin identify novel roles of the biogenesis of lysosome-related organelles complex 1. J Neurosci 32: 3697-3711.
5. Braun P, Tasan M, Dreze M, Barrios-Rodiles M, Lemmens I, et al. (2009) An experimentally derived confidence score for binary protein-protein interactions. Nat Methods 6: 91-97.
6. Aranda B, Blankenburg H, Kerrien S, Brinkman FS, Ceol A, et al. (2011) PSICQUIC and PSISCORE: accessing and scoring molecular interactions. Nat Methods 8: 528-529.
7. Orchard S, Kerrien S, Abbani S, Aranda B, Bhate J, et al. (2012) Protein interaction data curation: the International Molecular Exchange (IMEx) consortium. Nat Methods 9: 345-350.
8. Mathivanan S, Periaswamy B, Gandhi TK, Kandasamy K, Suresh S, et al. (2006) An evaluation of human protein-protein interaction data in the public domain. BMC Bioinformatics 7 Suppl 5: S19.

9. Li D, Liu W, Liu Z, Wang J, Liu Q, et al. (2008) PRINCESS, a protein interaction confidence evaluation system with multiple data sources. Mol Cell Proteomics 7: 1043-1052.

10. Patil A, Nakamura H (2005) Filtering high-throughput protein-protein interaction data using a combination of genomic features. BMC Bioinformatics 6: 100.

11. Lee SA, Chan CH, Chen TC, Yang CY, Huang KC, et al. (2009) POINeT: protein interactome with sub-network analysis and hub prioritization. BMC Bioinformatics 10: 114.

12. He M, Wang Y, Li W (2009) PPI finder: a mining tool for human protein-protein interactions. PLoS One 4: e4554.

13. Frolov MV, Alatortsev VE (2001) Molecular analysis of novel Drosophila gene, Gap69C, encoding a homolog of ADP-ribosylation factor GTPase-activating protein. DNA Cell Biol 20: 107-113.

14. Robinson MS, Bonifacino JS (2001) Adaptor-related proteins. Curr Opin Cell Biol 13: 444-453.

15. Marino G, Fernandez AF, Cabrera S, Lundberg YW, Cabanillas R, et al. (2010) Autophagy is essential for mouse sense of balance. J Clin Invest 120: 2331-2344.

16. Li W, Rusiniak ME, Chintala S, Gautam R, Novak EK, et al. (2004) Murine Hermansky-Pudlak syndrome genes: regulators of lysosome-related organelles. Bioessays 26: 616-628.

17. Mattera R, Tsai YC, Weissman AM, Bonifacino JS (2006) The Rab5 guanine nucleotide exchange factor Rabex-5 binds ubiquitin (Ub) and functions as a Ub ligase through an atypical Ub-interacting motif and a zinc finger domain. J Biol Chem 281: 6874-6883.

18. Zhu H, Zhu G, Liu J, Liang Z, Zhang XC, et al. (2007) Rabaptin-5-independent membrane targeting and Rab5 activation by Rabex-5 in the cell. Mol Biol Cell 18: 4119-4128.

19. Lippe R, Miaczynska M, Rybin V, Runge A, Zerial M (2001) Functional synergy between Rab5 effector Rabaptin-5 and exchange factor Rabex-5 when physically associated in a complex. Mol Biol Cell 12: 2219-2228.

20. Yan H, Jahanshahi M, Horvath EA, Liu HY, Pfleger CM (2010) Rabex-5 ubiquitin ligase activity restricts Ras signaling to establish pathway homeostasis in Drosophila. Curr Biol 20: 1378-1382.

21. Xu L, Lubkov V, Taylor LJ, Bar-Sagi D (2010) Feedback regulation of Ras signaling by Rabex-5-mediated ubiquitination. Curr Biol 20: 1372-1377.

22. Jekely G, Sung HH, Luque CM, Rorth P (2005) Regulators of endocytosis maintain localized receptor tyrosine kinase signaling in guided migration. Dev Cell 9: 197-207.

23. Lanzetti L, Di Fiore PP (2008) Endocytosis and cancer: an 'insider' network with dangerous liaisons. Traffic 9: 2011-2021.